



Recent Complex Massive Sulfide Mineralizations (Black Smokers) from the Southern Part of the East Pacific Rise

By WERNER TUFAR*)

With 88 Figures and 7 Tables

*Ostpazifischer Rücken
Rezente hydrothermale Aktivität
„Schwarze Raucher“
Komplexmassivsulfiderze*

Contents

Zusammenfassung	109
Abstract	109
1. Introduction	110
2. Sample Location and Setting, Sampling Technique	110
3. Hydrothermal Complex Massive Sulfide Ores – Black Smokers	113
3.1. Mineral Paragenesis of the Complex Massive Sulfide Ores	114
4. Mineralized Basalts	139
5. Process Mineralogical Aspects	140
6. Conclusions and Future Prospects	141
References	143

Rezente hydrothermale Komplexmassivsulfiderze („Schwarze Raucher“) aus dem Südteil des Ostpazifischen Rückens

Zusammenfassung

Proben rezenter hydrothermaler Komplexmassivsulfiderze („Schwarze Raucher“) wurden von sechs Fundpunkten am Ozeanboden des südlichen Ostpazifischen Rückens aus Wassertiefen zwischen etwa 2600 m bis 2800 m während der deutschen Forschungsfahrt Geometep 4 geborgen. Die Komplexmassivsulfiderze zeigen beträchtliche Schwankungen in der chemischen und mineralogischen Zusammensetzung, häufig auf Grund von Zonarbau. Die Mineralparagenese setzt sich vor allem aus Eisen-, Kupfer- und Zinksulfiden sowie beibrechender Gangart (z.B. Opal) zusammen, mit erheblichen Variationen in den jeweiligen Mengenverhältnissen. Bleimineralien (Bleiglanz) fehlt fast völlig. Stellenweise zeichnen sich die Komplexmassivsulfiderze durch hohe Spurengehalte an Silber aus, wobei die Zinksulfide die Hauptsilberträger darstellen. Weit verbreitet sind Kolloidal- bzw. Gelgefüge, z.B. mit Pyrit, Markasit, Melnikovitpyrit und Schalenblende, die in enger Verwachsung mit Hochtemperatur-Sulfiden (Chalkopyrrhotin, Hochtemperatur-Kupferkies) auftreten und ebenfalls ersehen lassen, daß sich ein chemisches Gleichgewicht nicht eingestellt hat. Eingebettet im Komplexmassivsulfiderz finden sich Röhren von Polychaeten, Vertreter einer typischen, hydrothermalen Fauna. Diese ist an die Quellaustritte der hydrothermalen Lösungen gebunden. Auflichtmikroskopische, prozeßmineralogisch orientierte Untersuchungen der Komplexmassivsulfiderze lassen ersehen, daß deren Erzqualität durchaus jener von bekannten („fossilen“) Buntmetall-Lagerstätten auf den Kontinenten vergleichbar ist und zeigen darüber hinaus bereits eine Reihe von wichtigen aufbereitungstechnischen und metallurgischen Informationen und Kenngrößen auf.

Abstract

Portions from recent hydrothermal complex massive sulfide mineralizations (black smokers) could be recovered from six locations at water depths between about 2,600 m and 2,800 m at the southern part of the East Pacific Rise during the German Geometep 4 Research Cruise. These sulfide ore samples show a considerable variety in their chemical composition, as well as in the mineralogical composition. Zoning is obvious. The paragenesis consists mainly of sulfides of iron, copper, zinc and some gangue material (e.g. opaline silica), exhibiting a wide range of variations. Also typical is an almost total lack of lead (galena). Widespread are sulfides occurring in colloidal and/or gel textures (e.g. marcasite, melnikovite-pyrite, schalenblende), often in close association with high-temperature sulfides (e.g. chalcopyrrhotite, high-temperature chalcopyrite), revealing non-equilibrium conditions of mineralization. A further characteristic is substantial traces of silver with the zinc sulfides as the major mineralogical residence of silver. Inclusions of worm tubes (polychaetes) embedded and preserved in the black smoker fragments are characterized by the occurrence of typical vent communities connected with the mineralizing hydrothermal solutions. The ore grades are comparable to those of ancient ("fossil") base metal deposits found on the continents. Furthermore, process mineralogical information of these black smoker samples based on ore microscopy yields critical parameters for beneficiation and metallurgical treatment.

*) Author's address: Prof. Dr. WERNER TUFAR, Fachbereich Geowissenschaften der Philipps-Universität Marburg, Hans-Meerwein-Straße, D-35032 Marburg/Lahn, Germany.

1. Introduction

The East Pacific Rise delineates a divergent plate margin between the Pacific Plate and the Cocos and Nazca Plates where new oceanic crust is being created. Such actively spreading plate margins (Fig. 1) are zones of mantle upwelling and may be associated with locally developed but intense hydrothermal activity and sulfide ore deposition (black smokers).

Following its discovery a few years ago (e.g. J. FRANCHE-TEAU et al., 1978, 1979), recent hydrothermal activity along the East Pacific Rise and also along the adjacent Galápagos Rift has received international attention. It is the subject of numerous investigations by French, American, German, and other research teams (e.g. J.L. BISCHOFF et al., 1983; J.B. CORLISS et al., 1979; J.M. EDMOND et al., 1982; Y. FOUQUET et al., 1988; M.S. GOLDFARB et al., 1983; R.M. HAYMON & M. KASTNER, 1981; R. HEKINIAN et al., 1978, 1980; R.A. KOSKI, D.A. CLAGUE & E. OUDIN, 1984; V. RENARD et al., 1985; A. MALAHOFF et al., 1983; E. OUDIN 1983; P.A. RONA, 1983; F.N. SPIESS et al., 1980; M.M. STYRT et al., 1981; R.A. ZIERENBERG, W.C. SHANKS III & J.L. BISCHOFF, 1984).

German contributions to the investigation of modern sulfide formation were carried out with the German Research Vessel *Sonne* on the East Pacific Rise and on the Galápagos Rift (e.g. H. BÄCKER et al., 1985; H. GUNDLACH, V. MARCHIG & H. BÄCKER, 1983; J. LANGE, 1985; J. LANGE & U. PROBST, 1986; V. MARCHIG, 1991; V. MARCHIG & H. RÖSCH, 1987; V. MARCHIG et al., 1988 a, 1988 b; W. TUFAR 1986, 1987, 1988, 1989, 1991; W. TUFAR, H. GUNDLACH & V. MARCHIG, 1984, 1985; W. TUFAR & H. JULLMANN, 1991; W. TUFAR, E. TUFAR & J. LANGE, 1986 a, 1986 b, 1986 c).

The mineralizing hydrothermal solutions originate in magmatic (i.e. volcanic) activity in the oceanic crust of the East Pacific Rise. Identical processes have been observed on the Galápagos Rift and other mid-ocean ridges. The solutions are certainly of hydrothermal origin.

The fundamental nature of the processes resulting in the origin of hydrothermal solutions related to seafloor spreading centers could also be clarified over the last few years (e.g. J.L. BISCHOFF & F.W. DICKSON, 1975; J.L. BISCHOFF & R.J. ROSENBAUER, 1983; J.L. BISCHOFF & W.E. SEYFRIED, 1978; J.B. CORLISS, 1971; M.J. MOTTI, 1983; M.J. MOTTI & H.D. HOLLAND, 1978; M.J. MOTTI, H.D. HOLLAND & J.R. CORR, 1979; M.J. MOTTI & W.E. SEYFRIED, 1980; R.J. ROSENBAUER & J.L. BISCHOFF, 1983; W.E. SEYFRIED, 1977).

The geothermal gradient within the oceanic crust at divergent plate margins is very high. While hot magma (up to 1200°C) supplies heat at depth, the surface of the oceanic crust is in contact with cold seawater (temperature about 2°C). Seawater that penetrates to lower crustal levels along fissures, cracks, faults, etc. is heated eventually resulting in the formation of convective cells and/or convective flows. The seawater is chemically modified during the heating processes, resulting in a hydrothermal solution. The pH of the seawater (slightly alkaline, pH approximately 8) is reduced considerably, to about 3.6 in the new hydrothermal solution. This acidic fluid is strongly enriched in silica, potassium, calcium, hydrogen sulfide, iron, manganese, copper, zinc, and barium leached from basaltic oceanic crust. Free oxygen is absent and magnesium and sulfate are strongly depleted. Non-ferrous metals are enriched to 10⁸ times their concentration in ordinary seawater.

It is typical of the recent formation of hydrothermal ore deposits that sulfides with low solubility are primarily precipitated from the hydrothermal fluids emerging from the ocean floor along the central graben, when in contact with seawater. In many cases rapidly growing cone-like ore bodies ("chimneys") accumulate around the fluid outlets. The ascending solutions deposit sulfides in veins and networks in the fractured altered basalt host rock. The modern sulfide chimneys (black smokers) contain complex massive sulfide ores. Their extremely limited areal extent is particularly important in prospecting ore deposits of this type.

The entire sulfur content of the hydrothermal solution is immediately deposited at the fluid outlet, forming metal sulfide ores (e.g. pyrite, pyrrhotite, marcasite, sphalerite, wurtzite, schalenblende, chalcopyrite, chalcopyrrhotite). The overall amount of sulfide deposited is limited by the initial amount of reduced sulfate in the original seawater. A small contribution comes from sulfur and sulfide in the oceanic crust. The typical complex massive sulfide ores (black smokers), precipitated at the ocean floor in the immediate vicinity of the hydrothermal springs, represent only a tiny portion of all metal ions transported by the venting hydrothermal solutions.

Most of the metal ions dissolved in the hydrothermal solution are subsequently precipitated as hydroxides. These deposits occur in enormous quantities and are widespread around the hydrothermal vents, extending for distances up to hundreds of kilometers. They are dominated by the oxides and hydroxides of iron and manganese and constitute the so called "hydrothermal sedimentary oxides" or "oxide ore muds". If not diluted by other sediments, they may dominate vast areas of the ocean floor. In many cases, the oxides define an asymmetric halo around the fluid outlets, which depends on submarine currents.

2. Sample Location and Setting, Sampling Technique

During the German Geometep 4 Research Cruise (**Geothermal Metallogensis East Pacific**) six massive sulfide ore samples were retrieved. All six were obtained using an electrohydraulic TV grab during Leg 3 (December 1985 and January 1986) of the cruise in the neovolcanic zone between 18° 25.2' S and 21° 28.9' S on the East Pacific Rise (Fig. 2, Table 1).

The complex massive sulfide ores commonly occur in areas of basaltic lava (tholeiite) talus. The characteristic chimney-like ore bodies are up to several meters high (Fig. 3) and arranged in groups consisting of many separate chimneys. In addition, low sulfide mounds with preeminent areal extent are present. Around the ore bodies,

Table 1.
Designation, coordinates, and water depths of sulfide ore sampling locations.

Station	Latitude	Longitude	Water Depth
SO 40 - 149 G	21° 28.854' S	114° 16.606' W	2825 m
SO 40 - 152 G	21° 26.386' S	114° 16.811' W	2800 m
SO 40 - 153 G	21° 25.693' S	114° 16.939' W	2778 m
SO 40 - 182 G	18° 31.173' S	113° 24.920' W	2642 m
SO 40 - 199 G	18° 25.369' S	113° 23.296' W	2627 m
SO 40 - 200 G	18° 25.239' S	113° 23.105' W	2663 m

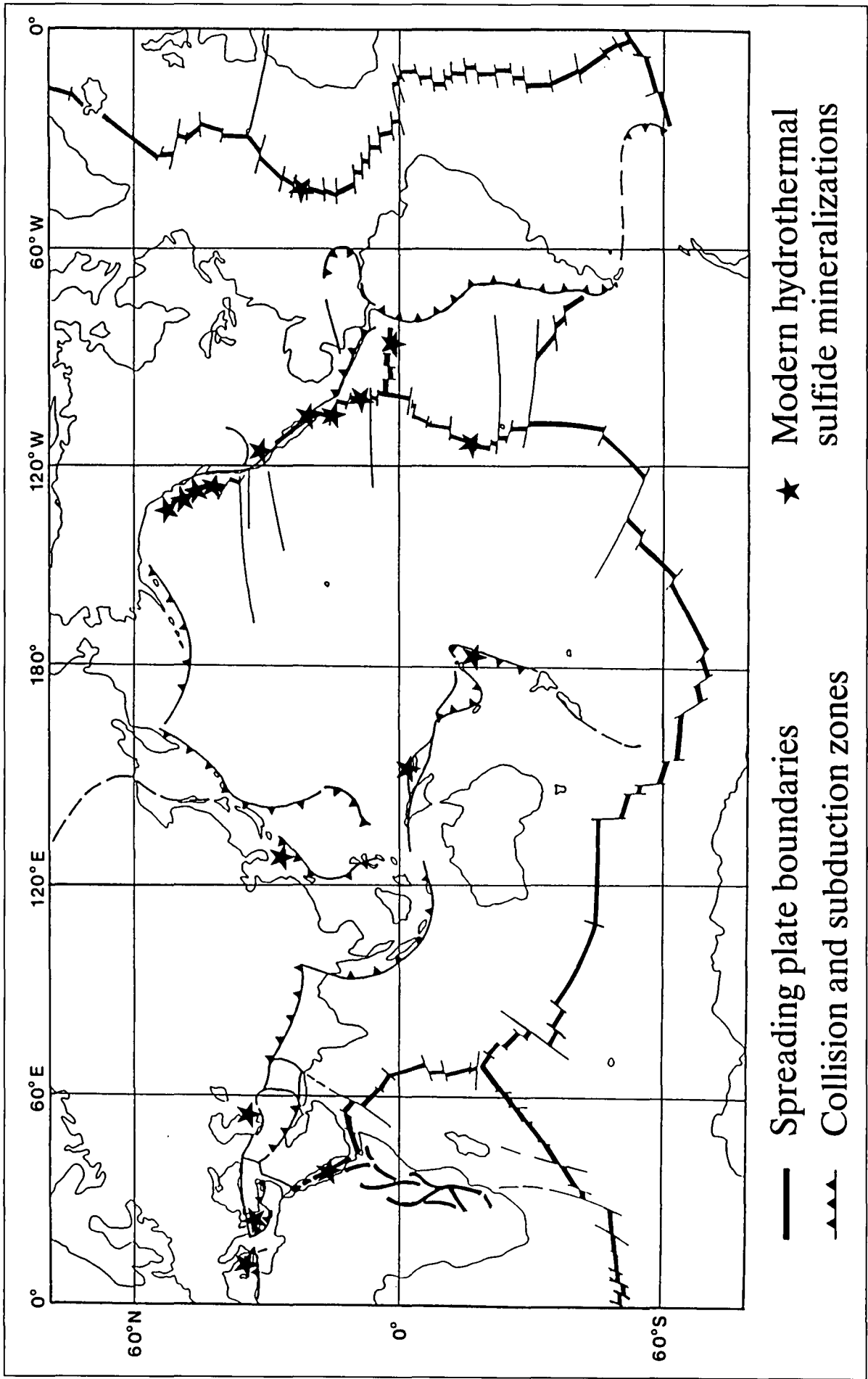


Fig. 1. World map depicting plate boundaries and occurrences of recent and modern hydrothermal sulfide formations (black stars).

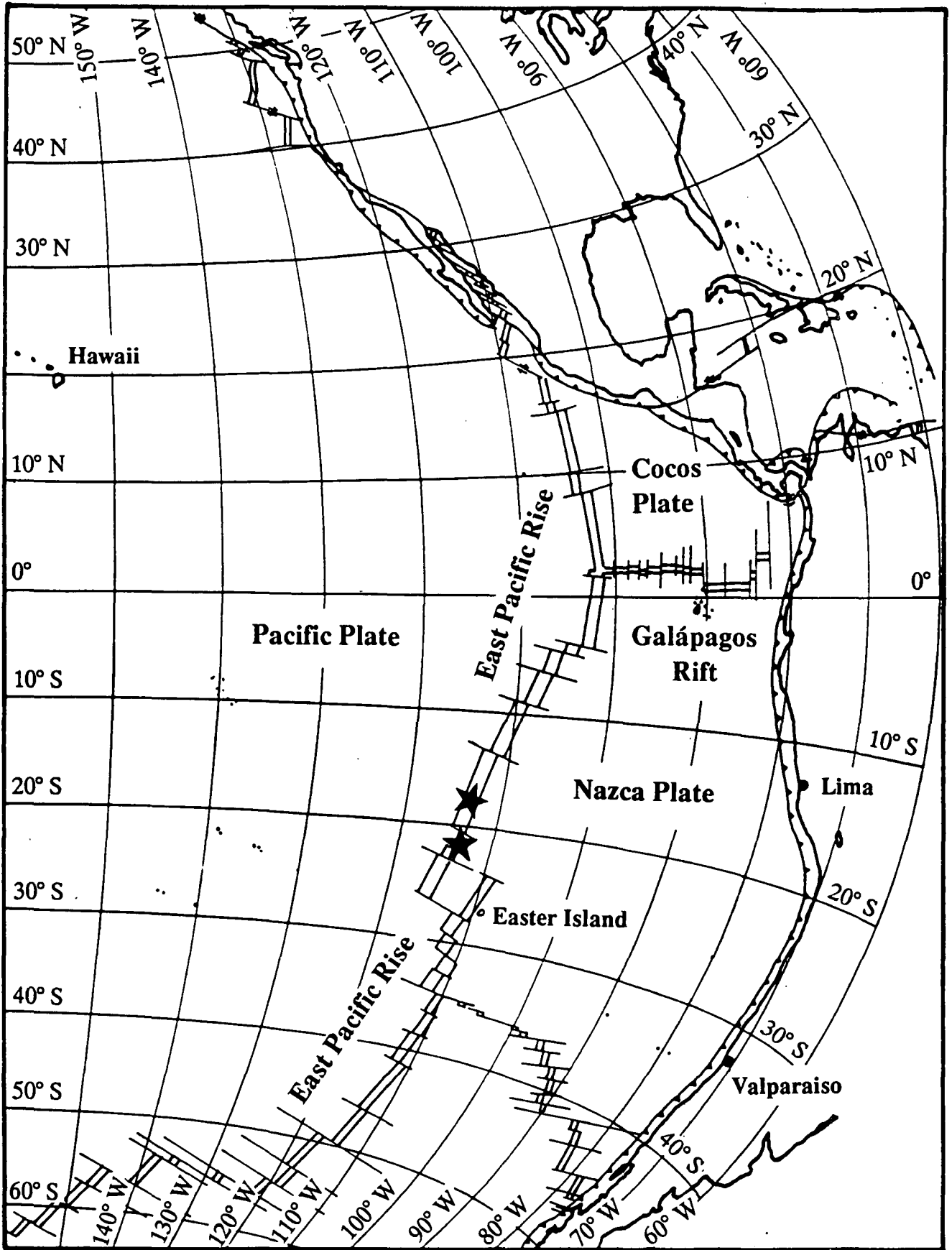


Fig. 2. Map of the East Pacific Rise showing the sampling locations (black stars) of the complex massive sulfide mineralizations.

Fig. 3.
Leg 3, Station 144. East Pacific Rise,
18°24' S, 113°24' W, water depth about
2650 m.

Cluster of complex massive sulfide chimneys (inactive black smokers) partly overgrown by organisms. The ocean floor and part of the chimneys are covered with sediment, consisting mainly of hydrothermal components.

the ocean floor is mainly covered with hydrothermal sediment and, locally, by clasts which have broken away from nearby chimneys.

No active outlets discharging hydrothermal solutions from the massive sulfide ore bodies were found, and the growth of the chimneys has ceased. This conclusion is supported by the mineralogy of sulfide samples, which show alteration to limonite due to halmyrolysis (submarine weathering).

Although the venting of hydrothermal solutions from chimneys was not directly observed in the area studied, there are clear signs of recent hydrothermal activity. In particular, there are numerous organisms (e.g. tube worms, bivalves, crustaceans, fish; Fig. 4) in a faunal association that is atypical of the deep ocean floor, but comparable with vent communities found at active hydrothermal vents elsewhere on the East Pacific Rise (Figs. 5–6). Furthermore, black smokers emanating hydrothermal jets have been recorded nearby (J. LANGE, 1985, V. RENARD et al., 1985).

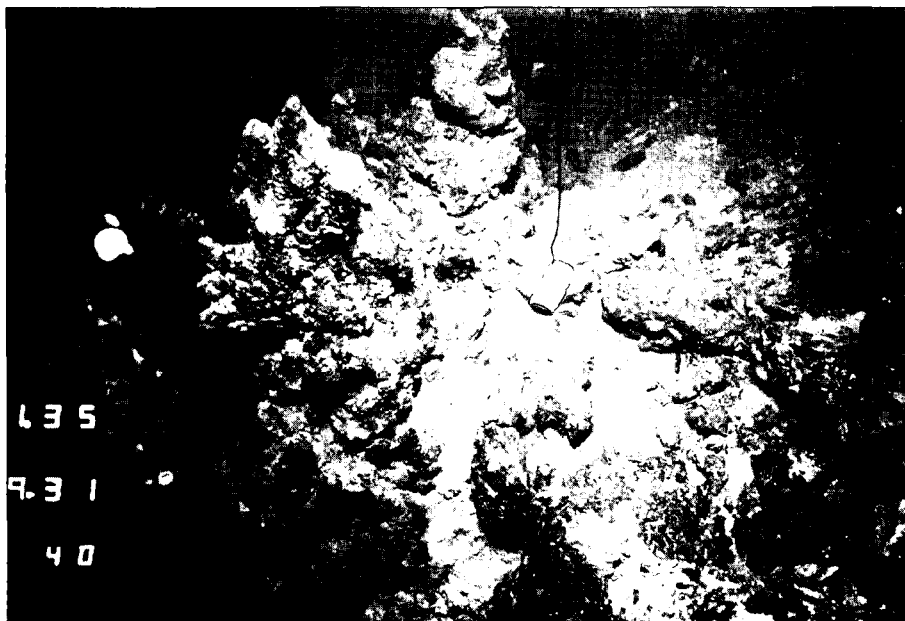
3. Hydrothermal Complex Massive Sulfide Ores – Black Smokers

The six samples of complex massive sulfide ore are fragments of black smoker chimneys (Figs. 7–10). All but one (sample SO 40–199 G) are very friable. Fragility and porosity are at least partly due to halmyrolysis.

Macroscopic features of the fragments (Figs. 7–10) are very high porosity and concentric-conchoidal textures. Zoning involving iron, copper, and zinc sulfides is evident locally.

Fig. 4.
Leg 3, Station 174. East Pacific Rise,
18°49,21' S, 113°26,56' W, water depth
about 2780 m.

Deep-sea vent community characterized by tube worms, actinians, crinoids, bythograeid crabs, and a fish around a hydrothermal vent on the basaltic ocean floor.



In places, the feeder channel of the hydrothermal solutions is encountered in the fragments (Figs. 9–10), while a branching in side- and subchannels may occur in addition (sample SO 40–199 G).

Numerous tubes of polychaetes are embedded in the samples (Figs. 7–10) providing impressive evidence of a fauna that flourished alongside the formerly active black smokers. The tubes are up to more than 1 cm in diameter and commonly lined or filled with chalcopyrite, wurtzite, sphalerite, schalenblende, and pyrite.

Chemical analyses of the samples (Table 2) show that SO 40–149 G has a high zinc content. Relatively high concentrations of copper were found locally in SO 40–152 and SO 40–153 G. In places, these are also rich in zinc. Analyses of SO 40–182 G show the dominance of copper and to a certain extent of zinc. In SO 40–199 G zinc is more abundant, whereas SO 40–200 G consists of fragments some of which have higher zinc contents and others of which have abundant copper.

Gangue material, mainly X-ray amorphous silica (opaline silica), is present in widely variable amounts. Sulfide

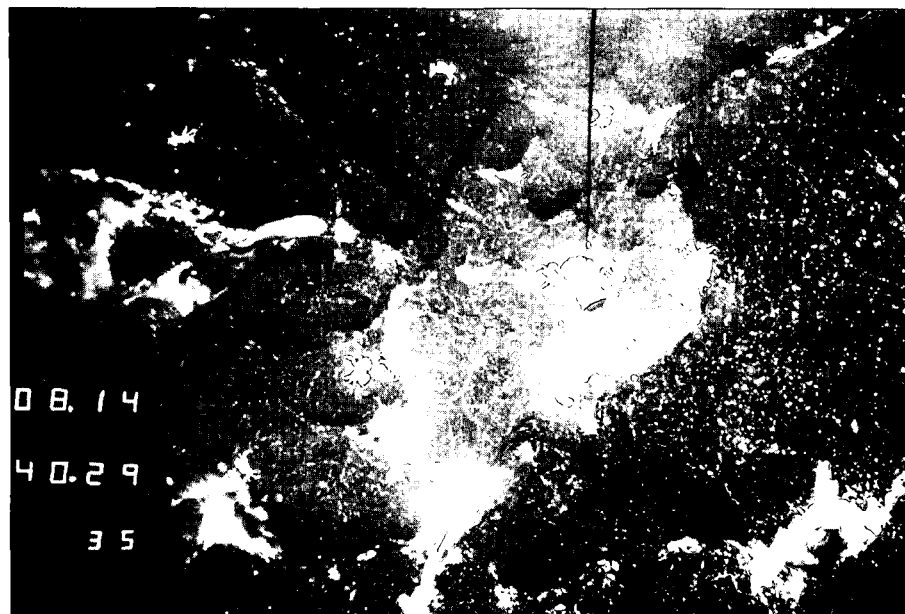


Table 2.
Chemical composition of complex massive sulfide ores (in wt. %).

Sample	Fe	Cu	Zn	SiO ₂
SO 40 - 149 G	27.0	0.1	13.6	14.5
SO 40 - 152 G/1	30.3	16.6	0.6	0.5
SO 40 - 152 G/2	34.1	0.1	1.2	0.3
SO 40 - 153 G/1	31.0	16.6	0.2	0.1
SO 40 - 153 G/2	44.4	5.4	0.8	3.3
SO 40 - 182 G/1	30.9	13.1	0.4	0.1
SO 40 - 182 G/2	16.3	0.2	35.0	4.0
SO 40 - 199 G/1	26.0	0.2	16.1	6.1
SO 40 - 199 G/2	27.6	0.6	1.1	30.9
SO 40 - 199 G/3	0.7	1.6	4.0	93.3
SO 40 - 200 G/1	1.1	0.1	19.8	77.5
SO 40 - 200 G/2	36.5	2.5	2.0	1.0

samples with high proportions of opaline silica gangue material (SO 40–199 G and parts of SO 40–200 G) are relatively strong and stable. Sample SO 40–200 G includes fragments composed almost exclusively of opaline silica, in which extremely fine sulfide grains are disseminated.

Fragments of any given sample reveal significant variations in their mineralogical and chemical composition, partly owing to zoning. Considering the setting and the unknown extent of the six mineralizations, sampling was far from representative with only one sample from each locality. Nor are the samples truly representative of the respective chimneys from which they were obtained. The dimensions and overall compositions of the six massive sulfide ore occurrences are not clear.

3.1. Mineral Paragenesis of the Complex Massive Sulfide Ores

Ore microscopy is a particularly well suited technique for revealing the identity of the ore minerals, their textural relationships, and their genesis. Furthermore, the results have important implications for any proposals on future



Fig. 5.
East Pacific Rise 12°47.0' N, 103°56.2' W, water depth 2620 m (Geometep 2). Active black smokers jetting out hot hydrothermal solutions which precipitate sulfides (dark "stain") on coming into contact with seawater. Organisms (e. g. galatheid crabs on the right edge of the photo) are encountered, even in the immediate vicinity of active black smokers.

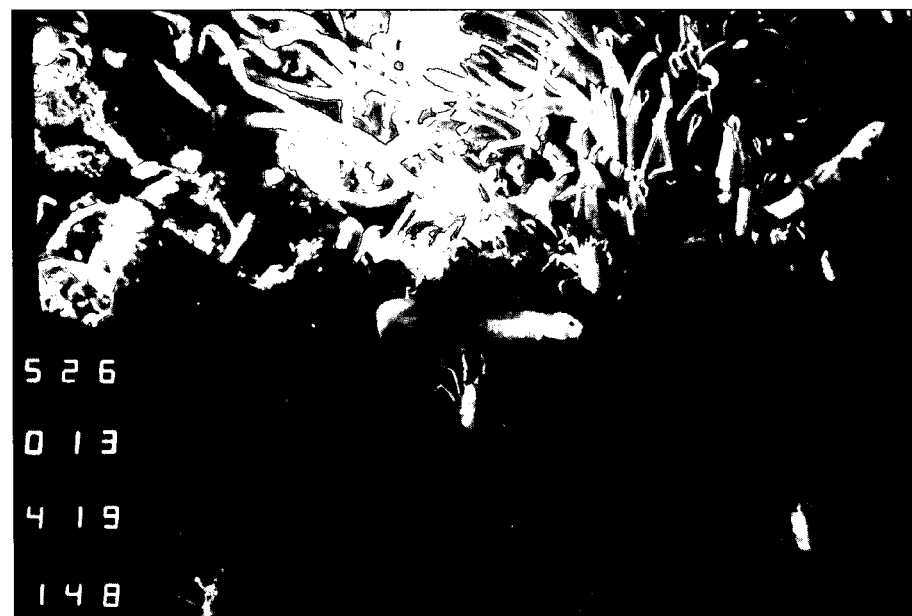


Fig. 6.
East Pacific Rise 12°49.1' N, 103°56.7' W, water depth 2630 m (Geometep 2). Typical deep-sea vent community comprising a bouquet of tube worms, some galatheid crabs, and fish on the ocean floor around active black smokers.



Fig. 7.
Sample SO 40-149 G.
a) Zinc-rich porous black smoker chimney fragment embedding numerous tubes of polychaetes. In places, the tubes are rimmed and partly filled with fine-grained euhedral wurtzite, sphalerite, and schalenblende, while traces of limonite frequently occur. A larger worm tube encloses a smaller one in Fig. 7 b (left side, above the center).
b) Detail from Fig. 7 a.

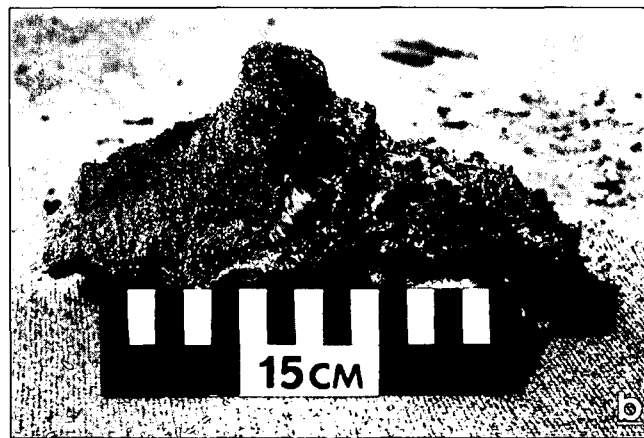
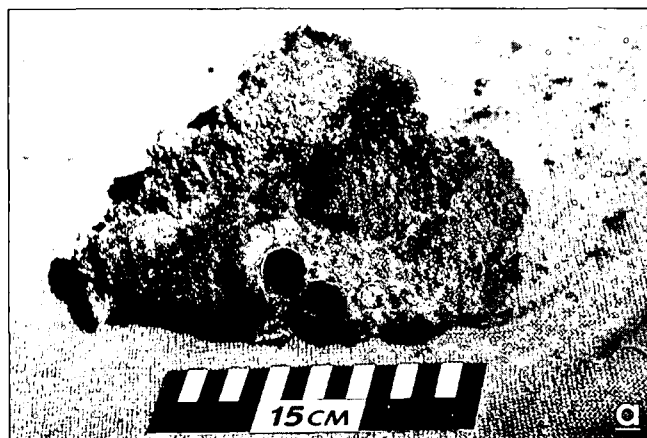


Fig. 8.
Sample SO 40-152 G.
Numerous small crystal aggregates of chalcopyrite and pyrite are discernible in a black smoker fragment containing tubes of polychaetes.



Fig. 9.
Sample SO 40-182 G.
Fragment of a black smoker chimney exhibiting the feeder channel of the hydrothermal solution and zoning. The feeder channel is rimmed with chalcopyrite. Chalcopyrite predominates in the copper-rich zone around the feeder channel, followed by a zinc-rich zone (sphalerite, wurtzite and schalenblende) which contains numerous tubes of polychaetes.

Fig. 10.
Sample SO 40-199 G.
Comparatively large fragment of a black smoker chimney displaying a central feeder channel of the hydrothermal solution (lying horizontal; middle right of photo). The periphery of the black smoker chimney exhibits its tubes of polychaetes and coatings of limonite.

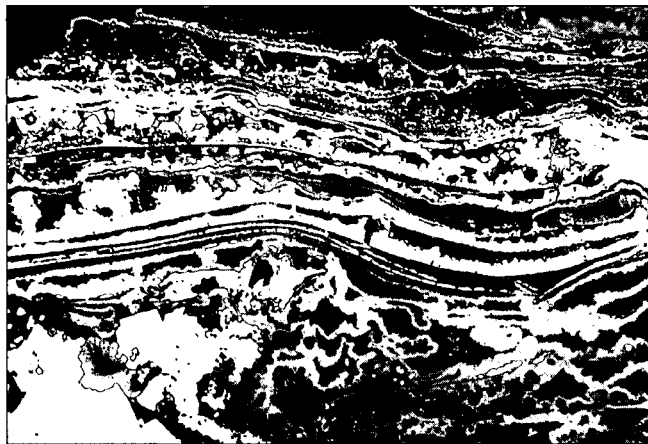


Fig. 11.
Sample SO 40-152 G.
Rhythmic, colloidal masses containing crusty-layered to botryoidal-reniform pyrite (light gray, almost white) alternating with melnikovite-pyrite (light gray to medium gray), some "intermediate product" (medium gray to dark gray), marcasite (likewise light gray, almost white), and rhythmic, botryoidal-reniform to layered-conchoidal schalenblende (light dark gray). Covellite (dark gray) occurs in larger areas dominated by schalenblende (lower right of photomicrograph). In places pyrite develops crystal aggregates. Marginal replacement of sulfides by limonite (likewise dark gray) also occurs (upper edge of photomicrograph). Natural cavities and pores, minor gangue material (all dark gray, almost black).
Polished section, $\times 15$.

exploitation and mineral processing of the sulfides by the mining industry.

As on the macroscopic scale, the porous and concentric-conchoidal textures of the fragments are also characteristic on the microscopic scale.

All samples consist of complex massive sulfide assemblages. The major constituents are pyrite, melnikovite-pyrite, marcasite, chalcopyrite, sphalerite, wurtzite, and schalenblende, and in one sample hematite (SO 40-153 G). Relative proportions of these minerals vary widely.

Minor constituents are chalcopyrrhotite, "intermediate product", and pyrrhotite. Accessories are covellite, galena (only in SO 40-199 G), a lead-sulfosalt (probably jor-



Fig. 12.
Sample SO 40-199 G.
Feathery-flowery, dendritic pyrite (light gray, almost white) around a core of opaline silica gangue material, overgrown by schalenblende (dark gray) in places. Marginally, euhedral aggregates of pyrite are locally rimmed by schalenblende. Natural cavities and pores, abundant opaline silica gangue material (all black, in places internal reflections).
Polished section, oil immersion, $\times 140$.

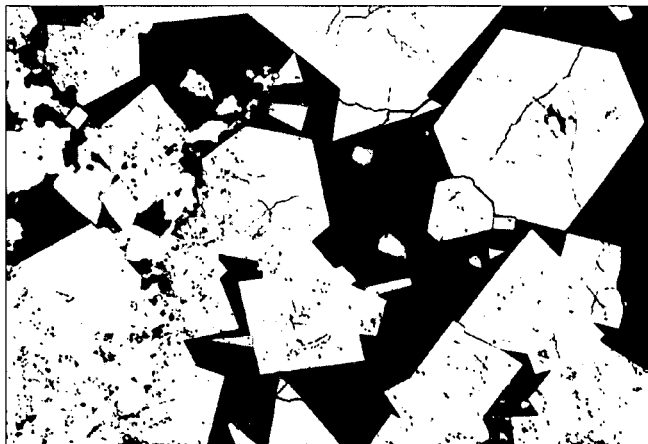


Fig. 13.
Sample SO 40-199 G.
Euhedral pyrite (light gray, almost white) intergrown with chalcopyrite (light medium gray). In places, pyrite contains numerous fine inclusions of chalcopyrite. Schalenblende, opaline silica gangue material, natural cavities and pores (all black).
Polished section, oil immersion, $\times 75$.

danite; only in SO 40-199 G), hematite (only in SO 40-182 G), and neodigenite (only in SO 40-152 G).

The sulfides of iron, copper, and zinc are major constituents and show considerable variations in their relative proportions. This is partly due to zoning. Any one of these sulfides may be highly impoverished locally, and only minor or an accessory, or sufficiently dominant to form an almost monomineralic zone.

This implies that reliable estimates of the mineral content and the chemical composition of the complex massive sulfide deposits, or even of a single black smoker chimney, will not be available until a comprehensive, statistically representative survey is performed.

In all six complex massive sulfide ore samples colloidal and/or gel textures are extremely typical and widespread (Figs. 11-12, 16-21, 27-33, 35-40, 43, 48-53, 55, 57-59, 63-64, 68, 71, 75-78). Rhythmic, colloidal masses (botryoidal to reniform, concentric-conchoidal, concentric layered to spherical-radial) are particularly impressive and distinct in masses of pyrite, melnikovite-pyrite, "intermediate product", marcasite, schalenblende, and the opaline silica gangue material. In places, these textures may be observed in chalcopyrite, hematite, and the accessory phases covellite and galena. Dendrites are also common. In most cases, the dendrites are composed of sphalerite, partially paramorphic to wurtzite, and schalenblende, and subordinately of pyrite. Schalenblende and pyrite exhibit feathery-flowery or bush-like textures. Moreover, tree-like to moss-like aggregates with a distinct transverse segmentation are composed of pyrite accompanied by minor chalcopyrite and chalcopyrrhotite. "Knitted" crystal aggregates and/or skeleton crystals of chalcopyrite and galena occur also.

Pyrite

(Figs. 11-18, 20-23, 25-26, 29-31, 36, 39, 42-44, 46, 48-50, 52, 57-59, 61-65, 67-73, 77) is frequently encountered in rhythmic colloidal, colloform masses. It is often associated there with marcasite, melnikovite-pyrite, schalenblende, and sphalerite, and less frequently with chalcopyrite. Those colloidal and/or gel textures range from botryoidal-reniform, concentric-conchoidal and crusty-layered to concentrically layered. Furthermore,

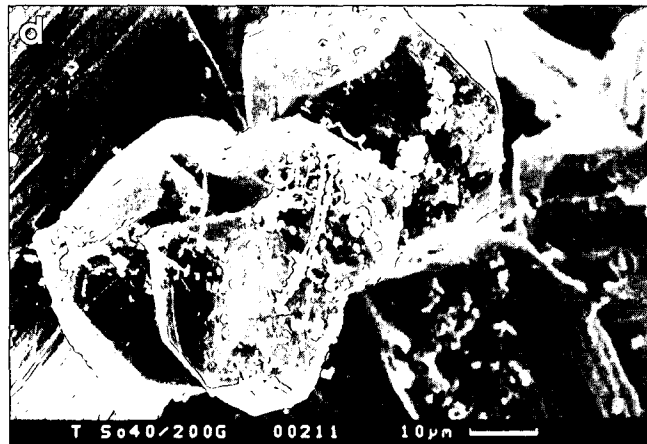
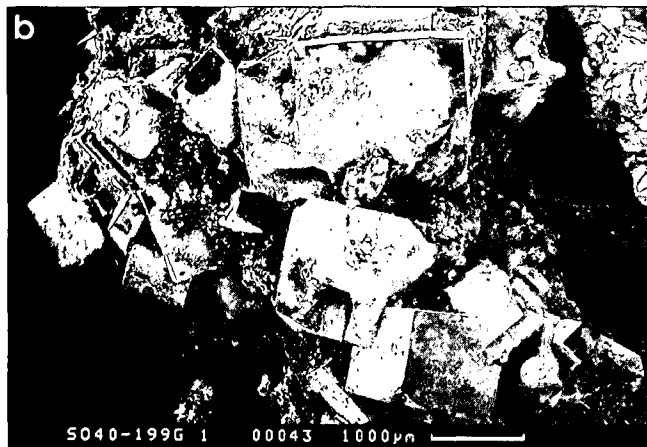
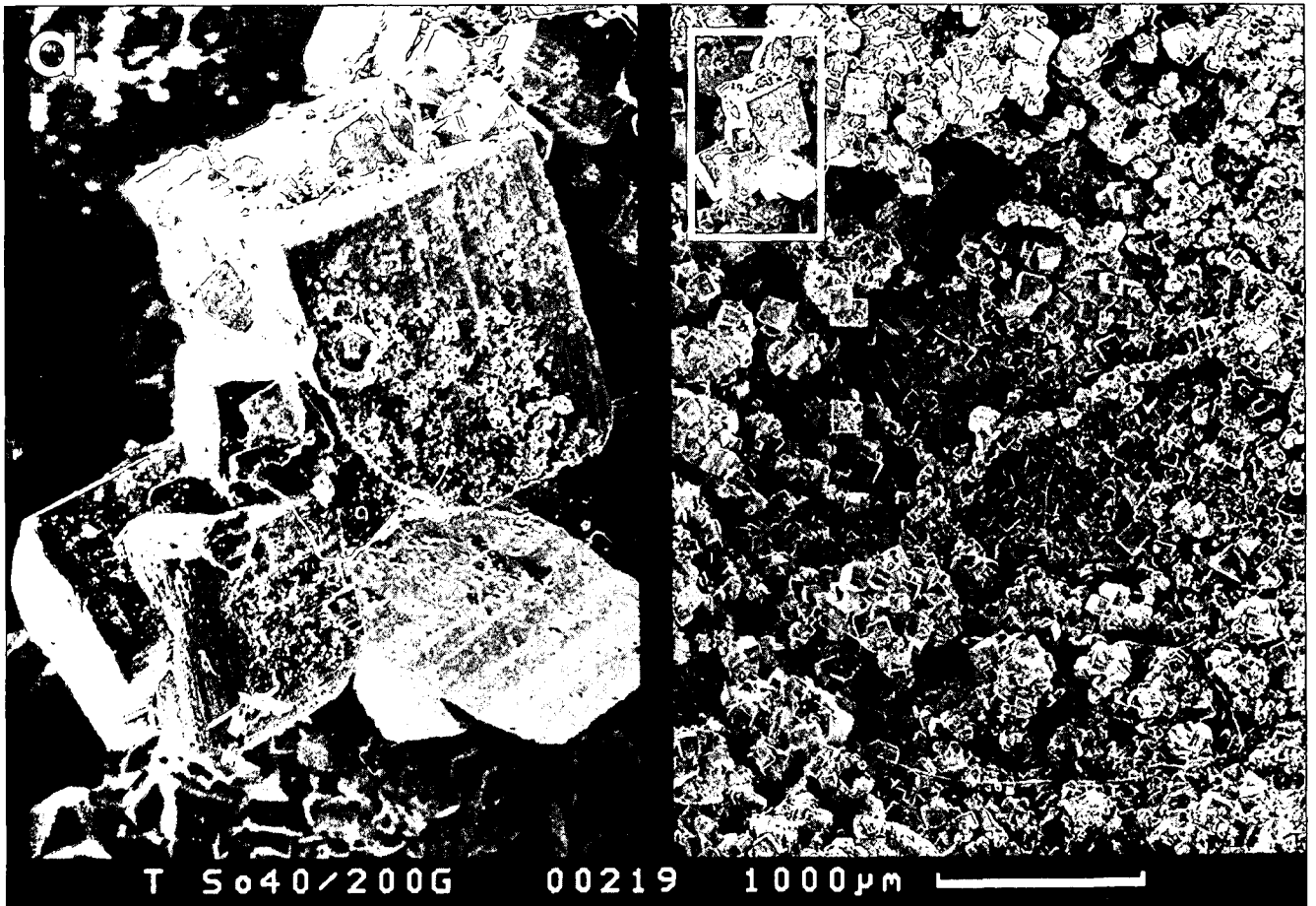


Fig. 14.
Sample S0 40–200 G.
Crystal aggregates of pyrite, chiefly developed after {100} and in places after {201}. Combination twinning is ubiquitous. In places, pyrite exhibits coatings of opaline silica gangue material.
Secondary electron image.

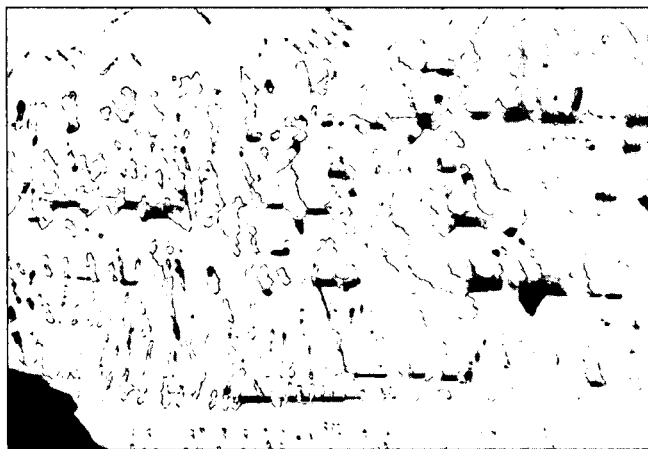


Fig. 15.
Sample SO 40-199 G.
Delicate myrmekitic intergrowth of pyrite (light gray) with chalcopyrite (medium gray). In places, some sphalerite (black) can be observed.
Polished section, oil immersion, $\times 725$.

pyrite exhibits dendritic textures and frequently forms aggregates of euhedral crystals (Figs. 11, 13-14, 17-18, 23, 44, 67, 72) containing zonal inclusions of other sulfides, such as sphalerite or chalcopyrite and hematite. The pyrite cubes may be several millimeters across in extreme cases (sample SO 40-199 G). Pyrite occurs as rims e.g. on chalcopyrite or pyrite crusts with melnikovite-pyrite (Fig. 26) and as inclusions in chalcopyrite and other sulfides. A peculiarity is the delicate myrmekitic intergrowth of pyrite and chalcopyrite (Fig. 15) framing a minor feeder channel in sample SO 40-199 G. Pyrite may be overgrown by sphalerite and schalenblende, in turn rimming both. Spherical- or framboidal pyrite associated with or enclosed in schalenblende (Fig. 50) or in opaline silica gangue material (Fig. 16) was rarely found.

The chemical composition of pyrite is somewhat unusual in that the Co content is high, in some instances exceeding 1 % (Table 3). Locally, Cu and Zn were recorded. Also noteworthy are the trace amounts of TI (0.02 %),

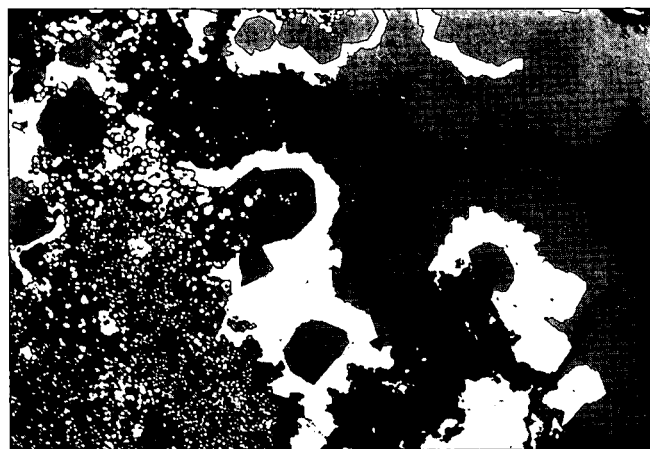


Fig. 16.
Sample SO 40-200 G.
Rhythmic alternation of partly euhedral sphalerite (dark gray), overgrown by pyrite (light gray, almost white) and marcasite (likewise light gray, almost white), which are in turn rimmed by sphalerite within opaline silica gangue material (black). Gangue material, as well as sphalerite, locally exhibit abundant inclusions of pyrite spheroids and/or framboidal pyrite.
Polished section, oil immersion, $\times 75$.

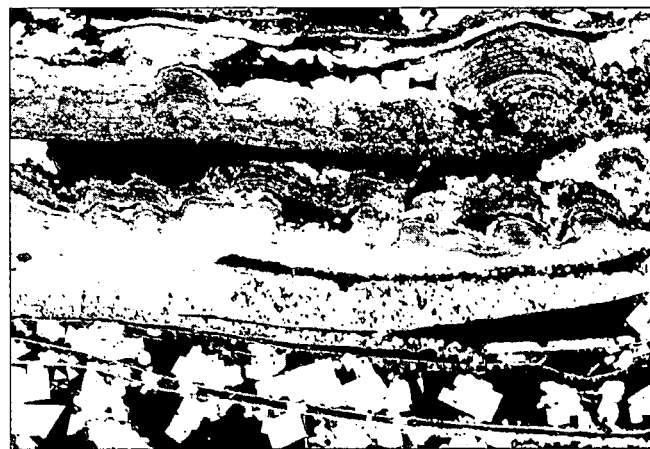


Fig. 17.
Sample SO 40-182 G.
Rhythmically layered crusts of pyrite (light gray in different shades) with melnikovite-pyrite (light gray to medium gray) and some "intermediate product" (medium gray to dark gray). In places, pyrite shows transition to more massive, fine-grained aggregates. In the cavities and pores (both black), this leads to the formation of coarser euhedral aggregates of pyrite (lower edge of photomicrograph), accompanied by interstitial chalcopyrite (likewise light gray). Natural cavities and pores, some gangue material (all black).
Polished section, oil immersion, $\times 60$.

As (317 ppm), and Se (167 ppm) in one sample. Ni occurs only in low concentrations ($\leq 0.01-0.008$ %).

Table 3.
Chemical composition of pyrite (in weight %).

Sample	Fe	S	Co	Cu	Zn	Total
SO 40 - 149 G	45.87	54.04			0.69	100.60
SO 40 - 152 G	46.21	53.67	0.48	0.18		100.54
SO 40 - 152 G	45.57	51.81	0.79	0.37		98.54
SO 40 - 152 G	46.75	53.98	0.09	0.10		100.92
SO 40 - 153 G	46.18	54.21	0.39	0.50		101.28
SO 40 - 153 G	45.28	54.20	1.29			100.77
SO 40 - 153 G	46.02	55.09	0.40			101.51
SO 40 - 153 G	46.04	55.70	0.36	0.16	0.08	102.34
SO 40 - 182 G	45.93	50.53	0.68			97.14
SO 40 - 182 G	45.63	51.97	1.37			98.97
SO 40 - 182 G	46.45	52.85	0.38	0.09		99.77
SO 40 - 182 G	46.19	51.14	0.57	0.07		97.97
SO 40 - 182 G	46.81	54.73	0.02	0.48		102.04
SO 40 - 199 G	45.60	50.08	0.05	0.80		96.53

Melnikovite-pyrite

(Figs. 11, 17-21, 29-31, 48-50, 57-59, 67-68, 71, 79) in places accompanies pyrite and marcasite in the colloidal masses, preponderantly in colloform, rhythmically layered crusts, in concentric-conchoidal, and botryoidal to reniform precipitations to dendritic, feathery-flowery aggregates (Fig. 19). Melnikovite-pyrite may occur together with small amounts of "intermediate product" in colloform masses.

Marcasite

(Figs. 11, 16, 19-22, 25, 31, 39, 48-49, 51, 57, 62, 67, 69, 72, 79) is rarely euhedral (Figs. 19-20). It is primarily found in rhythmic, botryoidal-reniform, concentrically layered, concentric-conchoidal crusts to spherical-radial masses and forms spectacular colloidal and/or gel textures (colloform textures). Coarse to fine polysynthetic twin lamellae

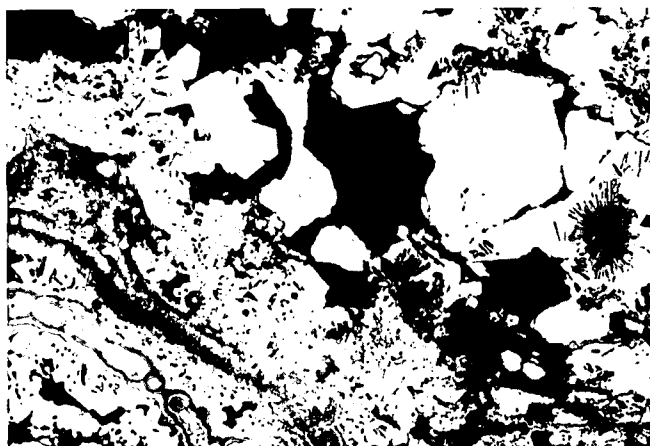


Fig. 18.
Sample SO 40-153 G.
Rhythmic, colloform crusts of concentric to layered-conchoidal melnikovite-pyrite (light gray to medium gray) with some "intermediate product" (medium gray to dark gray) and pyrite (light gray, almost white). On both margins, the latter forms partially euhedral, coarse aggregates embedded in coarse-grained chalcopyrite (light gray). In places, exsolutions of chalcopyrrhotite (light medium gray) and occasional fine tabular aggregates of hematite (dark gray) developed after {0001} are enclosed in chalcopyrite. Hematite is likewise found as inclusions in pyrite. Natural cavities and pores, some gangue material (all black).
Polished section, oil immersion, $\times 75$.

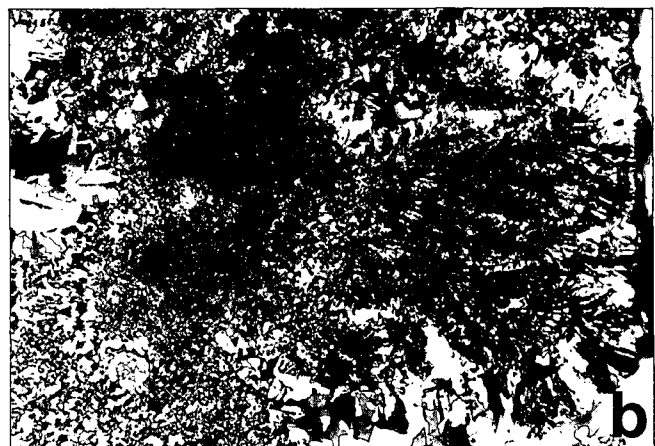
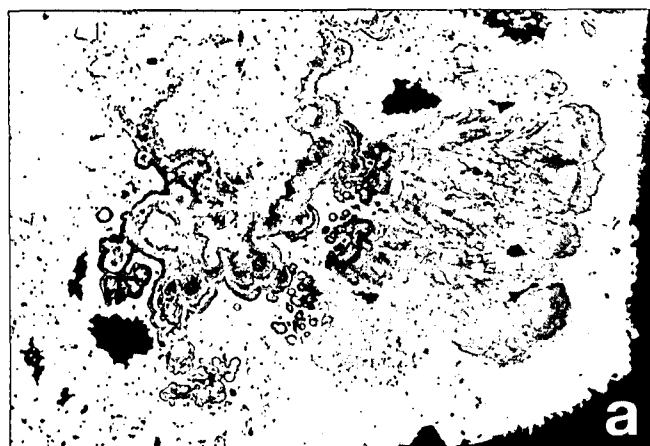


Fig. 19.
Sample SO 40-199 G.
Excellent colloidal masses of rhythmic, concentric-conchoidal to feathery-flowery, dendritic melnikovite-pyrite (medium gray to dark gray) accompanied by some "intermediate product" (medium gray to almost black) and marcasite (light gray in different shades because of weak birefractance). Melnikovite-pyrite and "intermediate product" are embedded in marcasite showing crystal faces along the edges and in pore spaces. In Figure 19 b marcasite, because of its strong anisotropism, very clearly exhibits the different sizes of its grains and the fine-grained textures of the rhythmic masses. Some gangue material (black).
Polished section, oil immersion, $\times 75$.
Fig. 19 a: 1 Pol.,
Fig. 19 b: +Pols.

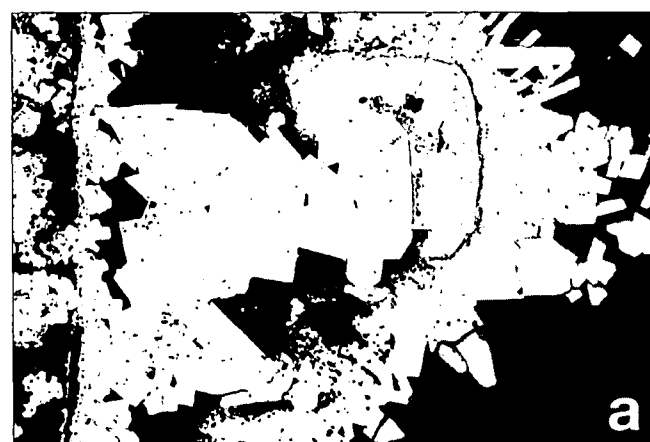


Fig. 20.
Sample SO 40-199 G.
Layered crusts of melnikovite-pyrite (light gray to medium gray) in transition to euhedral, coarse-grained pyrite (light gray), in turn enclosed within fine-grained marcasite (slightly darker light gray in different shades because of weak birefractance). The latter is first rimmed by a thin layer of melnikovite-pyrite and then by coarse-grained, partially euhedral marcasite embedded in opaline silica gangue material. Locally, minor sphalerite (black) is enclosed in pyrite. Internal textures and twin lamellae of marcasite are clearly discernible in Figure 20b due to its strong anisotropism. Opaline silica gangue material is normally black, but often appears light gray to white because of internal reflections.
Polished section, oil immersion, $\times 75$.
Fig. 20 a: 1 Pol.,
Fig. 20 b: +Pols.

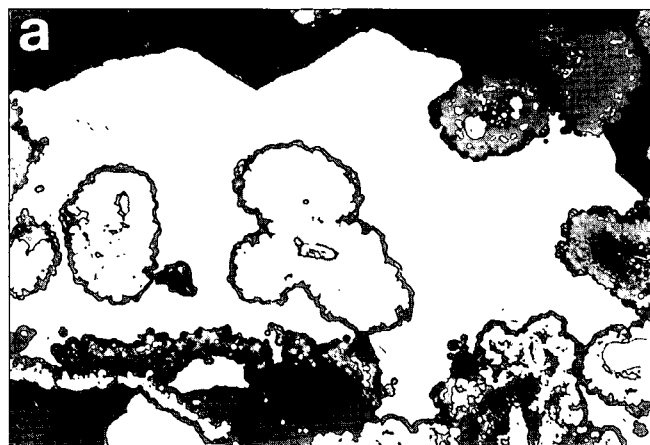


Fig. 21.
Sample SO 40–199 G.
Detail from rhythmic colloidal masses consisting of fine-grained marcasite (light gray, almost white) and some pyrite (likewise light gray, almost white). Both are coated by opaline silica gangue material (black). These colloform masses are contained in coarser grained, partly radiating marcasite also enclosing concentric to layered-conchoidal crusts of schalenblende (dark gray) with minor pyrite and melnikovite-pyrite (light gray to medium gray). The latter two are finely outlined by opaline silica gangue material which may likewise occupy larger areas. In Fig. 21 b opaline silica gangue material and schalenblende are brightened because of internal reflections. The striking anisotropism of marcasite illustrates its twin lamellae and the grain textures of the colloform masses.
Polished section, oil immersion, $\times 110$.
Fig. 21 a: 1 Pol.,

Fig. 21 b: +Pols.

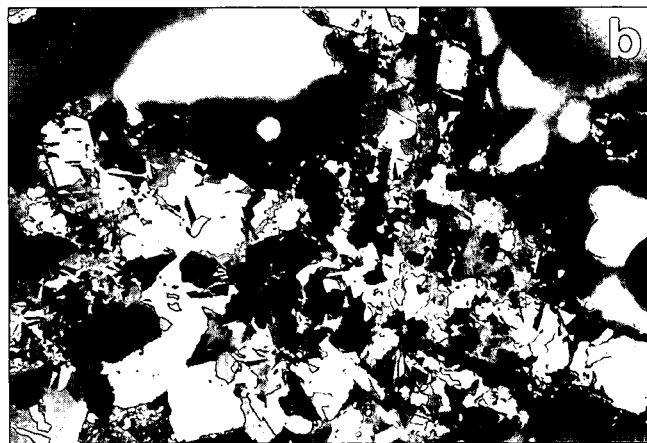


Fig. 22.
Sample SO 40–153 G.
Former euhedral aggregate of tabular pyrrhotite developed after {0001}, entirely replaced and pseudomorphed by marcasite (light gray in different shades because of weak bireflection) and minor pyrite (light gray). Chalcopyrrhotite (medium gray), locally showing exsolution of chalcopyrite (slightly darker light gray), has grown over the original pyrrhotite plates and, as with part of the original pyrrhotite itself, displays a delicate rim of sphalerite (dark gray, almost black) and some schalenblende (likewise dark gray, almost black). In Figure 22 b the strong anisotropism of fine-grained marcasite distinctly documents its replacement of tabular crystals of pyrrhotite and is an impressive record of pseudomorphism. Gangue material, natural cavities and pores are normally black, but appear brightened by internal reflections in Figure 22 b. Locally, sphalerite and schalenblende also reveal internal reflections.
Polished section, oil immersion, $\times 140$.
Fig. 22 a: 1 Pol.,

Fig. 22 b: +Pols.

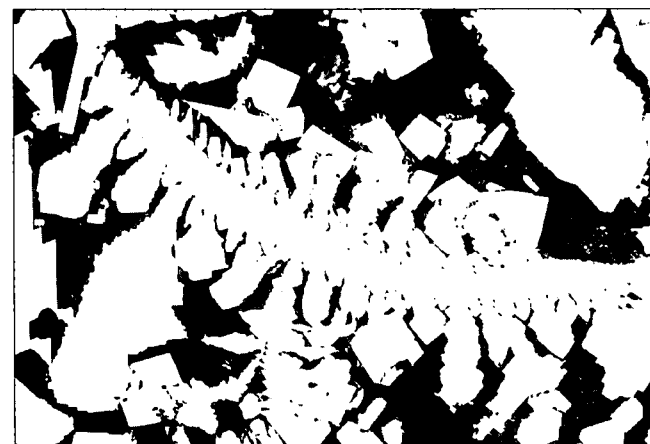


Fig. 23.
Sample SO 40–152 G.
Coarse-grained crystal aggregates of chalcopyrite (light gray, almost white) exhibiting characteristic skeleton crystals. Locally, they are rimmed by sphalerite (black, in photomicrograph barely discernible). Euhedral pyrite (almost white) is overgrown on chalcopyrite and fills interstices. Abundant natural cavities and pores, minor gangue material (all black).
Polished section, oil immersion, $\times 15$.

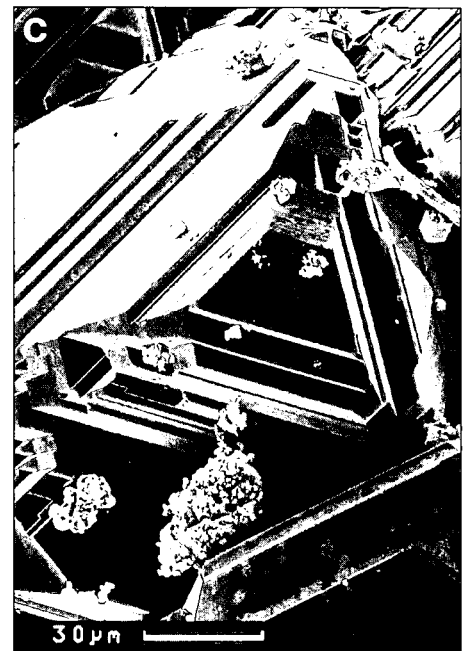
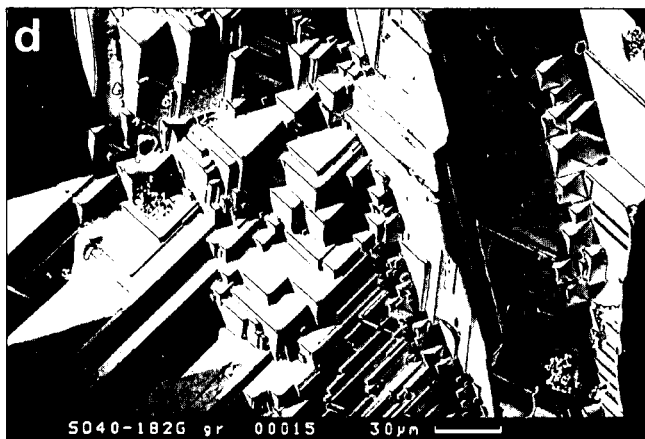


Fig. 24.
Sample S0 40-182 G.
Crystal aggregates of chalcopyrite, partly exhibiting skeleton crystals and also considerable distortion. The pseudotetrahedral and pseudooctahedral development of the crystal aggregates is evident. Twinning, for example after {111}, partly lamellar repetition twinning and combination twinning are frequently encountered, even within the smallest areas. Irregular fractures are occasionally seen. The crystal faces are commonly covered with opaline silica gangue material and locally with small crystal aggregates of sphalerite and pyrite. The latter two are accompanied and sometimes enclosed in opaline silica gangue material. Secondary electron image.

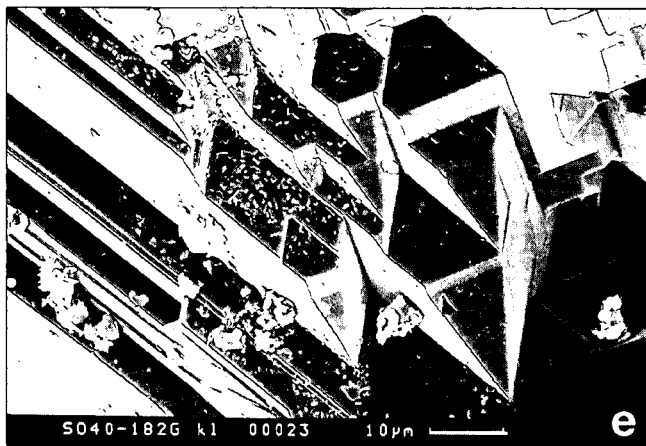


Fig. 24e.
Explanation see p. 121.

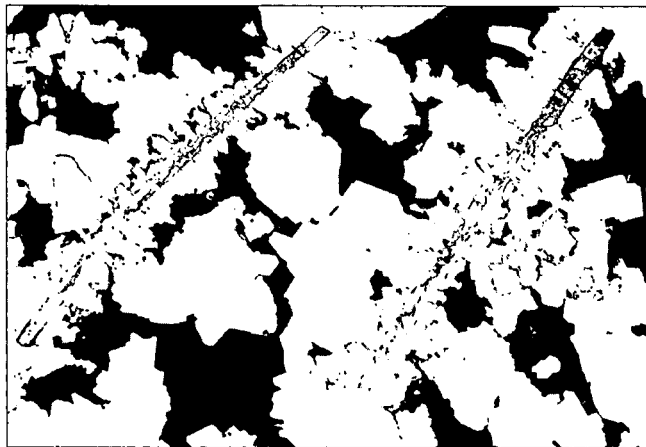


Fig. 25.
Sample SO 40-152 G.
Crystal aggregates of chalcopyrite (light gray), overgrown on euhedral plates of pyrrhotite developed after {0001}. The latter are contained as cores in chalcopyrite. The original pyrrhotite is completely replaced and pseudomorphed, preponderantly by chalcopyrite and, to a lesser extent, by "intermediate product" (medium gray to dark gray) and marcasite (light gray, almost white). The latter two are largely replaced by cellular pyrite (likewise medium gray to dark gray). Chalcopyrite comprises occasional inclusions of euhedral pyrite (likewise light gray, almost white). Natural cavities and pores, minor gangue material (all black). Polished section, oil immersion, $\times 140$.

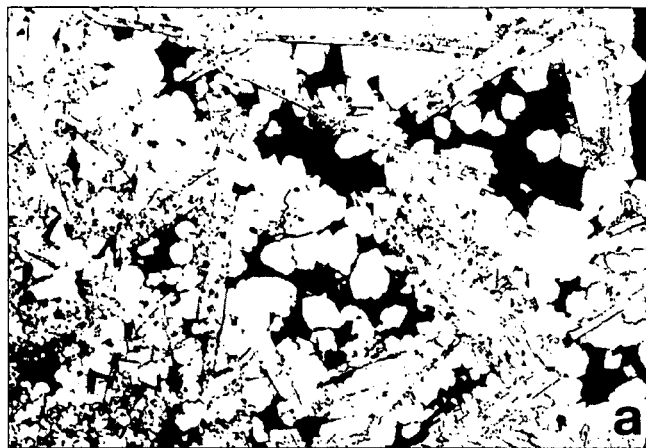


Fig. 26.
Sample SO 40-153 G.
Crystal aggregates of pyrrhotite are completely replaced and pseudomorphed by chalcopyrite (light gray, almost white), which distinctly traces the tabular outlines of the original pyrrhotite. The occurrence of euhedral hematite (dark medium gray in different shades; Fig. 26 b) in these pseudomorphs may simulate replacement of the hematite by chalcopyrite. Locally, euhedral pyrite (likewise light gray, not distinguishable in photomicrograph) occurs. Natural cavities and pores, minor gangue material (all black). Polished sections, oil immersion, $\times 75$.

are clearly detectable in most instances. Marcasite is partially replaced and paramorphed by pyrite and, in turn, is encountered replacing "intermediate product". It is also seen directly replacing and pseudomorphing euhedral pyrrhotite. This replacement texture may easily be mistaken for primary euhedral marcasite (Fig. 22).

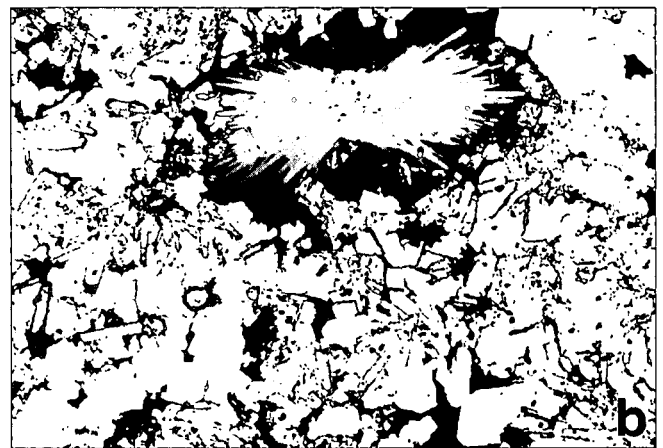
Chalcopyrite

is very common (Figs. 13, 15, 17-18, 22-33, 37-38, 40-42, 45-46, 49, 52-53, 55-57, 59, 61-70, 72-74) and represents the dominant sulfide in some of the fragments. It shows typical tetragonal twinning. The presence of the typical oleander-leaf to lance-like transformation twin lamellae of an initial high-temperature chalcopyrite in two samples (SO 40-153 G, SO 40-182 G) permits an approximate estimate of the sulfide crystallization temperature.

Chalcopyrite often occurs in euhedral grain aggregates, elongated (crystal-) aggregates, and dendritic to skeleton crystals (Fig. 23, 33). These aggregates are particularly numerous where chalcopyrite fills cavities such as pore spaces and tubes of polychaetes. Chalcopyrite crystals frequently exhibit pseudotetragonal or pseudooctahedral habit and may be markedly distorted. The combination of p (112) and p' ($1\bar{1}2$) results in octahedral aggregates, while e (012) and m (110) yield apparent dodecahedra. Striations

Table 4.
Chemical composition of chalcopyrite (in weight %).

Sample	Fe	Cu	S	Co	Zn	Total
SO 40 - 152 G	32.28	32.51	34.59	0.15		99.53
SO 40 - 152 G	32.50	32.40	34.92	0.15		99.97
SO 40 - 152 G	34.60	30.71	34.66	0.17		100.14
SO 40 - 152 G	32.13	33.21	34.35	0.09		99.78
SO 40 - 152 G	31.12	34.30	34.60	0.06		100.08
SO 40 - 152 G	30.86	34.24	34.18	0.08		99.36
SO 40 - 153 G	33.11	31.68	35.56	0.07	0.03	100.45
SO 40 - 153 G	33.17	31.58	35.68	0.08	0.04	100.55
SO 40 - 153 G	33.06	32.15	35.51	0.06		100.78
SO 40 - 153 G	33.33	31.70	35.47	0.08	0.03	100.61
SO 40 - 182 G	32.98	32.26	34.41	0.09	0.02	99.76
SO 40 - 182 G	31.41	33.96	35.97	0.02	0.02	101.38
SO 40 - 182 G	31.76	32.87	37.14	0.06	0.82	102.65
SO 40 - 199 G	30.65	34.31	34.05		0.71	99.72



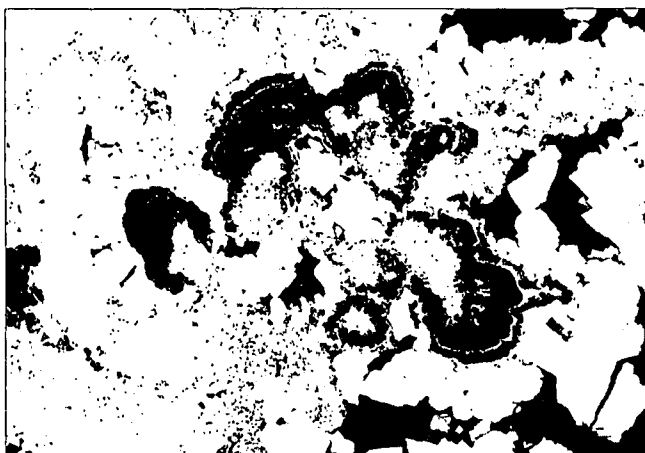


Fig. 27.
Sample SO 40-152 G.
Chalcopyrite (light gray) occurring in rhythmic, concentric-conchoidal intergrowths with schalenblende (dark gray), partially replacing the latter. Natural cavities and pores, minor gangue material (all almost black).
Polished section, oil immersion, $\times 140$.



Fig. 29.
Sample SO 40-152 G.
Layered crusty to tree-like and moss-like pyrite (light gray) and melnikovite-pyrite (light gray to medium gray) are overgrown and enclosed by euhedral pyrite and coarse-grained chalcopyrite (light medium gray). The latter shows marginal replacement by "permanent blue" covellite (black; e.g. lower edge of photomicrograph). Natural cavities and pores, minor gangue material (all likewise black).
Polished section, oil immersion, $\times 190$.

due to repeated combinations, twinning, and parallel intergrowth are observed even on the finest scale. In places, chalcopyrite is rimmed by schalenblende and sphalerite (Figs. 23, 32). To a lesser extent, its euhedral crystals are framed with an oriented overgrowth of sphalerite, which itself is surrounded by fine grained aggregates (colloidal and/or gel textures) of schalenblende, sphalerite, and chalcopyrite. The grain size of the latter increases outwards. In places, tiny exsolution spindles of chalcopyrrhotite are contained in chalcopyrite (Figs. 18, 32, 61, 67, 70) and vice versa (Figs. 32, 61-66, 68, 73-74).

Occasionally, rhythmic, concentric-conchoidal precipitates of chalcopyrite are encountered together with its (crystal-) aggregates (Figs. 27-28).

Chalcopyrite (crystal-) aggregates contain inclusions, for example, of euhedral pyrite and, occasionally, of schalenblende (Fig. 27), wurtzite (Fig. 46), and pyrrhotite

(Figs. 25-26), partially replacing the latter. Chalcopyrite penetrates into and replaces porous, rhythmically layered crusts and colloidal masses mainly composed of melnikovite-pyrite and pyrite (Figs. 29-30). On the other hand, melnikovite-pyrite fills cracks in chalcopyrite and forms rims around it (Fig. 31).

In zinc-rich areas, chalcopyrite frequently accompanied by chalcopyrrhotite occurs in zonal inclusions and complex alternations and sequences within sphalerite and schalenblende (Figs. 32, 37-38, 52, 55-56, 63-64). Locally, extremely complex but rhythmic alternations and precipitations of these mineral phases are evident even on the finest scale. Noteworthy are the occasionally found "knitted" aggregates and skeleton crystals of chalcopyrite, again sometimes accompanied by chalcopyrrhotite (Fig. 33) which are partially paramorphic after wurtzite.

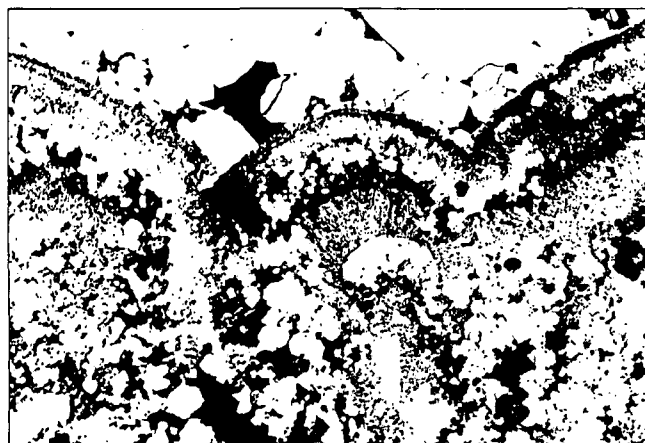


Fig. 28.
Sample SO 40-182 G.
Rhythmic, concentric-conchoidal, occasionally radiating chalcopyrite (light gray, almost white), partly pseudomorphic after schalenblende, displays a peripheral transition into partly euhedral aggregates. The original schalenblende is completely replaced and pseudomorphed by chalcopyrite. Natural cavities and pores, minor gangue material (all black).
Polished section, oil immersion, $\times 140$.



Fig. 30.
Sample SO 40-182 G.
Rhythmically layered crusts to concentric-conchoidal aggregates of pyrite (light gray) and melnikovite-pyrite (light gray to medium gray) exhibiting local overgrowth of euhedral pyrite and penetrated and partially replaced by chalcopyrite (light medium gray). Natural cavities and pores, minor gangue material (all black).
Polished section, oil immersion, $\times 75$.

Fig. 31. ➤
 Sample SO 40–200 G.
 Melnikovite-pyrite (light gray to medium gray) accompanied by some "intermediate product" (medium gray to dark gray) rims euhedral pyrite (light gray) and crystal aggregates of chalcopyrite (light medium gray). Melnikovite-pyrite and "intermediate product", also healing and replacing chalcopyrite along fractures. Colloform masses of pyrite, marcasite (likewise light gray), melnikovite-pyrite, and minor "intermediate product" are encountered along the margins. Natural cavities and pores, opaline silica gangue material (all black).
 Polished section, oil immersion, $\times 140$.

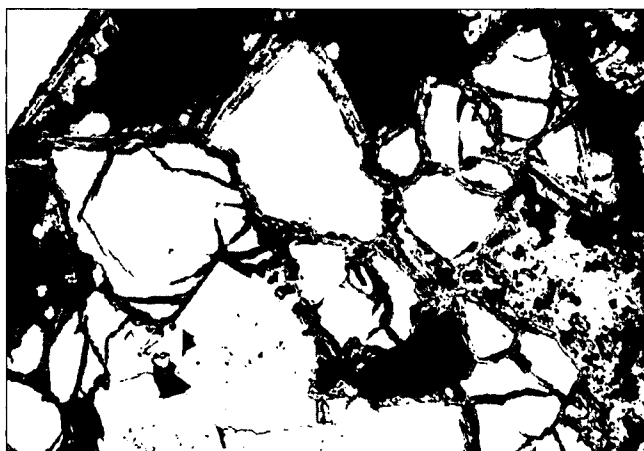


Fig. 32. ➤
 Sample SO 40–152 G.
 Crystal aggregate of chalcopyrite (light gray) showing exsolution of chalcopyrrhotite spindles (slightly darker light gray) and chalcopyrrhotite, exhibiting in turn exsolution of chalcopyrite spindles, both displaying oriented overgrowth of sphalerite (dark gray, almost black). In places, the latter can also be observed as a peripheral rim around chalcopyrite. Natural cavities and pores, minor gangue material (all black).
 Polished section, oil immersion, $\times 235$.

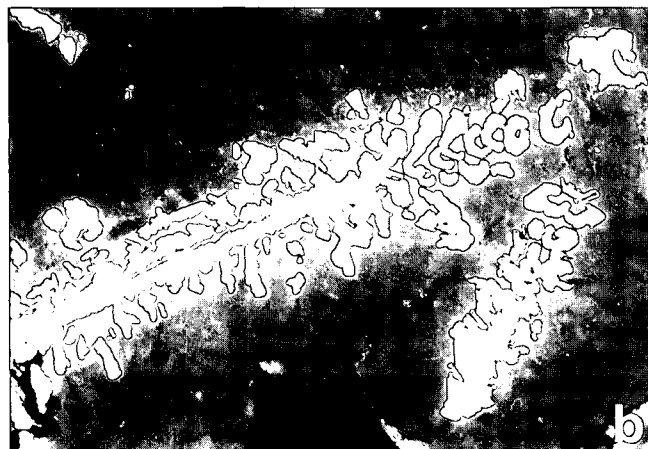
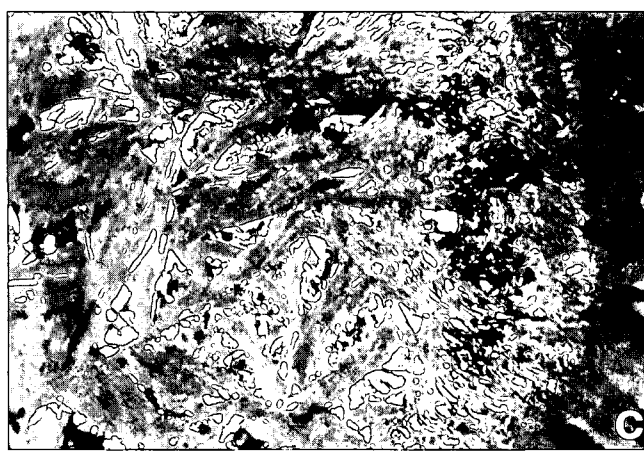
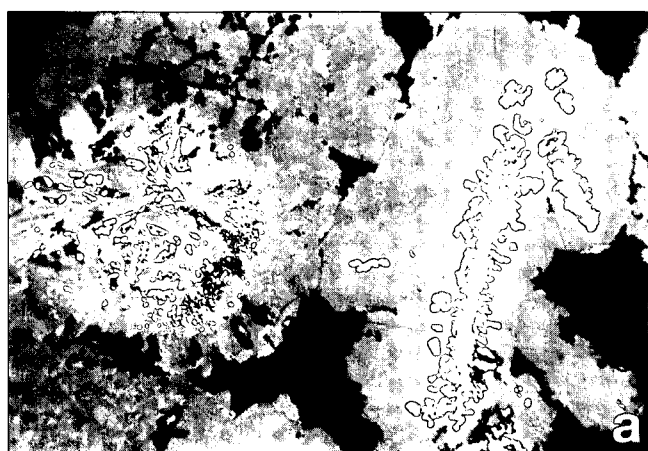


Fig. 33.
 Sample SO 40–152 G.
 Sphalerite dendrites with schalenblende (both dark gray in different shades), partly revealing distinct concentric-conchoidal textures and, marginally, radial textures. "Knitted" aggregates and/or skeleton crystals of chalcopyrite (light gray, almost white) are encountered within the dendrites (right half of photomicrograph). The center of concentric-conchoidal to radiating schalenblende exhibits fine wurtzite crystal aggregates (likewise dark gray) embedded in chalcopyrite ("matrix"). Weak differences in reflectivity indicate zoning of sphalerite and schalenblende. Natural cavities and pores, minor gangue material (all black).
 Polished section, oil immersion,
 Fig. 33 a: $\times 360$.
 Fig. 33 b: (Detail of Fig. 33 a): $\times 915$.
 Fig. 33 c: (Detail of Fig. 33 a): $\times 1125$.

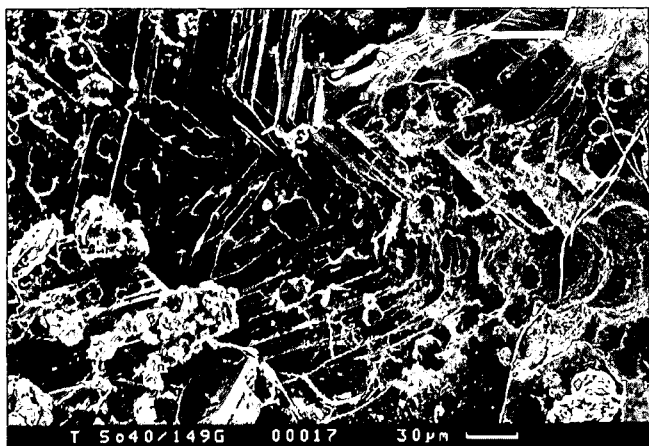


Fig. 34.
Sample SO 40-149 G.
Sphalerite crystals, showing distinct polysynthetic twinning along the [111] axis.
Secondary electron image.

Moreover, chalcopyrite surrounds fine grained, euhedral wurtzite crystals in the center of schalenblende (Fig. 33, 42) and is finely dispersed (close to the limit of optical resolution) in sphalerite (Fig. 56) and schalenblende.

Newly formed "permanent blue" covellite replaces and encloses chalcopyrite (Fig. 72). Limonite is another replacement product. It results from halmyrolysis.

Chalcopyrite may contain some zinc (Table 4) and minor cobalt. An analysis of the trace elements yielded Ni (0.008-0.01 %), Tl (up to 0.02 %), As (22-34 ppm), Se (27-44 ppm), and Ag (<2-40 ppm). Zinc sulfide is another major constituent and locally may be the most abundant sulfide in the black smoker chimney fragments. It occurs as sphalerite, wurtzite, and schalenblende.

Sphalerite

Primary crystallization of sphalerite (Figs. 15-16, 20, 22-24, 32-44, 52, 55-56, 62-67, 73, 75) is reflected by grain shapes in crystal aggregates. Further evidence for a primary origin is provided by characteristic twinning (e.g. polysynthetic twin lamellae; Figs. 34-35, 37-38, 55-56).



Fig. 35.
Sample SO 40-149 G.
Porous schalenblende (dark gray) in transition to euhedral sphalerite (dark gray in different shades). Due to weak differences in reflectivity, the latter exhibits zoning and characteristic twinning such as polysynthetic twin lamellae. Occasionally, sphalerite and schalenblende exhibit internal reflections. Natural cavities and pores, minor gangue material (all black).
Polished section, oil immersion, $\times 360$.

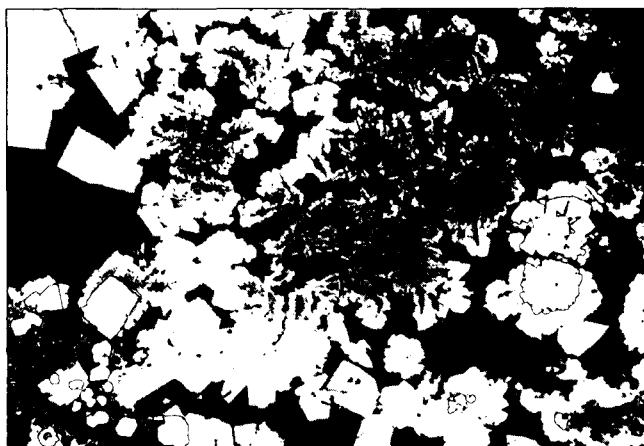


Fig. 36.
Sample SO 40-149 G.
Dendritic, feathery-flowery schalenblende (dark gray in different shades), partly with cores of opaline silica gangue material (black), in transition to crystal aggregates of sphalerite and wurtzite (both dark gray in different shades). Zoning in the zinc sulfides is visible by small differences in the reflectivity. All zinc sulfides are rimmed by opaline silica gangue material. In places, euhedral pyrite can be observed, partially overgrown by schalenblende associated with sphalerite and wurtzite. Natural cavities and pores (both likewise black).
Polished sections, oil immersion, $\times 140$.

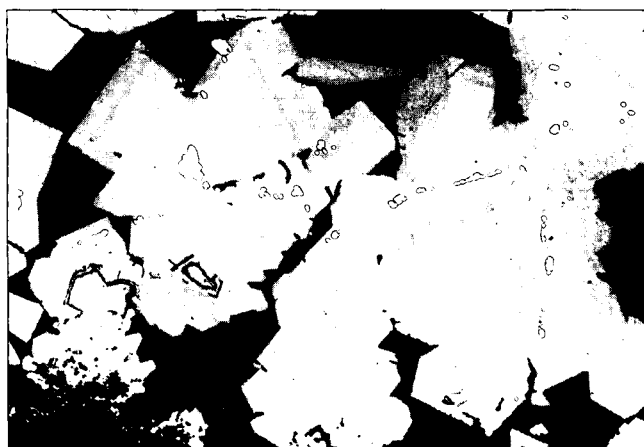


Fig. 37.
Sample SO 40-149 G.
Porous schalenblende (dark gray in different shades) in transition to crystal aggregates of sphalerite and wurtzite (both dark gray to medium gray). Sphalerite and wurtzite display slight differences in reflectivity, which indicate zoning. Furthermore, sphalerite reveals typical twinning. In places, zonal inclusions of chalcopyrite (light gray, almost white) accompanied by chalcopyrite (likewise light gray, almost white), both partially replaced by gangue material (black) can be observed within the zinc sulfides. Natural cavities and pores, some gangue material (all black).
Polished section, oil immersion, $\times 140$.

Sphalerite is encountered as crystals and as dendritic to "knitted" aggregates, partially being paramorphic after wurtzite. The feeder channel of the hydrothermal solutions in two samples (SO 40-182 G, SO 40-199 G) is lined by dendritic aggregates of sphalerite, which are partially paramorphic after wurtzite and accompanied by schalenblende.

In one of these samples sphalerite aggregates contain fine skeleton crystals of chalcopyrite overgrown on pyrite. Distinct but subtle differences in reflectivity denote strong variations in the iron content. Internal textures and zoning of the aggregates are hence readily detected (Figs. 33, 35-38, 40, 42, 55-56, 64).



Fig. 38.
Sample SO 40-200 G.
Porous schalenblende (dark gray in different shades), partly in transition to concentric-conchoidal sphalerite (likewise dark gray in different shades), which in turn contains peripheral zonal inclusions of chalcopyrrhotite with chalcopyrite (both light gray, almost white). Along the margins, sphalerite exhibits coarser aggregates, in part wurtzite (likewise dark gray in different shades). The crystal aggregates of sphalerite and wurtzite display a variable reflectivity due to zoning, with sphalerite twinning as well. Natural cavities and pores, minor gangue material (all black).
Polished section, oil immersion, $\times 360$.

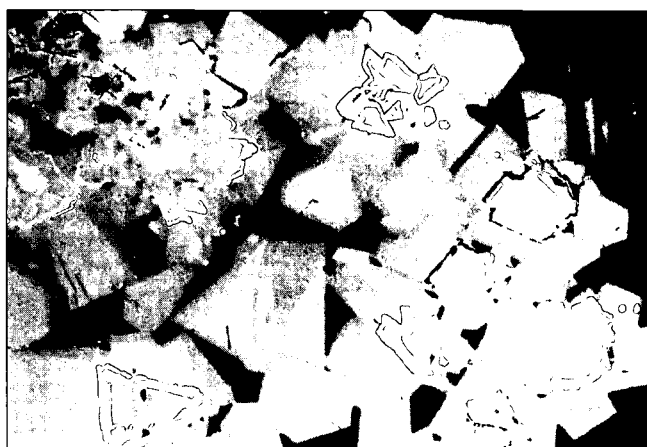


Fig. 40.
Sample SO 40-149 G.
Dendritic schalenblende (dark gray in different shades), with cores of opaline silica gangue material (black) in transition to crystal aggregates of sphalerite and minor wurtzite (likewise dark gray in different shades). The crystal aggregates display internal reflections and zoning manifested by slight variations in the reflectivity. Moreover, there are rhythmic alternations and zones of fine inclusions of chalcopyrite associated with chalcopyrrhotite (both light gray). The latter are replaced by the gangue material to some extent. Natural cavities and pores, minor gangue material (all likewise black).
Polished section, oil immersion, $\times 140$.

Wurtzite

(Figs. 33, 36-38, 40, 42-47) shows euhedral plates after {0001}, although its crystals may be subhedral in places. Cleavage parallel to {0001} is occasionally observed. Differences in the reflectivity are also peculiar to wurtzite. Again, these may be accounted for by variations in the iron content and indicate zoning (Figs. 37-38, 43, 45).

Schalenblende

(Figs. 11-13, 21-22, 27-28, 33, 35-40, 43-44, 48-55, 63-64, 71, 75-79) displays brilliant colloidal and/or gel textures. It occurs in excellent colloform, rhythmically layered crusts, botryoidal-reniform to concentric-conchoidal textures. The feathery-flowery to moss-like textures (Figs. 12, 36, 39-40, 51-52) are commonly arranged

around a gangue material core or else locally around a core of chalcopyrite or chalcopyrrhotite. Schalenblende may reveal peripheral transition to sphalerite or wurtzite in the above cases. The rhythmic-conchoidal textures are distinctly defined by small differences in the reflectivity which, again, are due to considerable variations in the iron content across the aggregates. Schalenblende is frequently associated with pyrite, melnikovite-pyrite, marcasite, and sometimes with "intermediate product", chalcopyrite, and chalcopyrrhotite.

Schalenblende and sphalerite display extremely complex alternating successions and intergrowths with other sulfides, principally with chalcopyrite and chalcopyrrhotite, but also with pyrite, melnikovite-pyrite, marcasite and, in places, with the opaline silica gangue material.

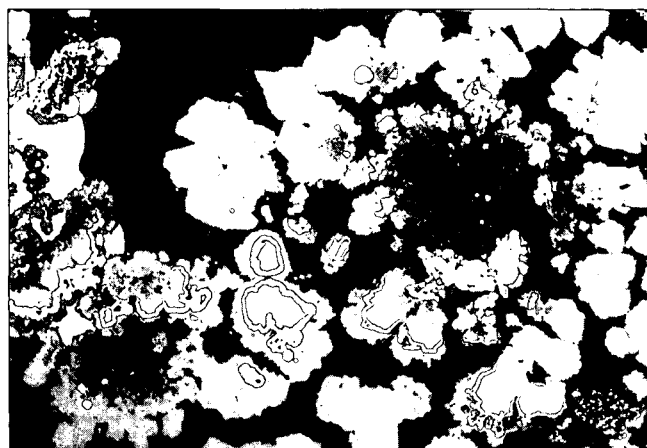


Fig. 39.
Sample SO 40-149 G.
Dendritic, feathery-flowery schalenblende (dark gray) in transition to sphalerite (likewise dark gray). The latter exhibits rhythmic alternation with pyrite (light gray, almost white). Schalenblende and sphalerite are finely coated by opaline silica gangue material (black). Locally, accretions of marcasite (likewise light gray, almost white) fill interstices. Natural cavities and pores (both likewise black).
Polished section, $\times 140$.

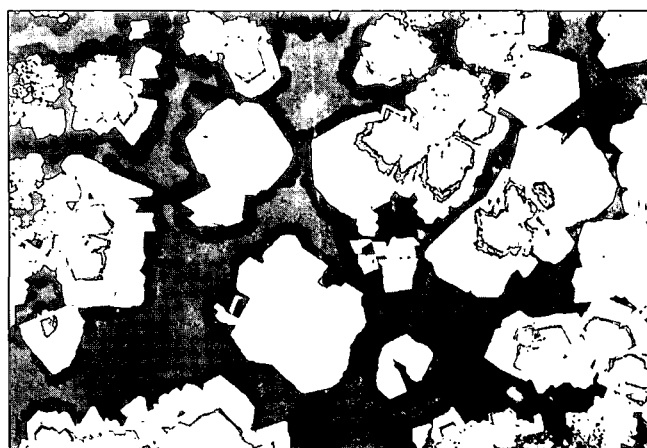


Fig. 41.
Sample SO 40-149 G.
Zoned sphalerite crystal aggregates (medium gray), rimmed by opaline silica gangue material (dark gray, almost black). Chalcopyrite and chalcopyrrhotite were originally contained as rhythmic alternations and inclusion zones within sphalerite, but are now completely replaced by the gangue material. Natural cavities and pores occupy considerable areas (dark gray).
Polished section, $\times 140$.

Rhythmic alternations and sequences of sphalerite and schalenblende with chalcopyrite and chalcopyrrhotite are observed even on a small scale. The copper sulfides are normally at the center of these complex aggregates.

Comparable textures exist in the association of sphalerite and schalenblende with pyrite. In crystal aggregates of sphalerite and wurtzite, inclusions of chalcopyrite and chalcopyrrhotite, as well as pyrite, are arranged in zones relating to different growth stages (Figs. 39–41, 55). This zoning may be extremely delicate and approach the limit of resolution of the ordinary light microscope. The same holds true for finely dispersed zonal inclusions of chalcopyrite and chalcopyrrhotite, mainly in sphalerite (Figs. 55–56).

Skeleton crystals of chalcopyrite which are occasionally associated with chalcopyrrhotite display delicate development when found in dendritic aggregates of schalenblende and sphalerite partially paramorphic after wurtzite (Fig. 33).

There are slight variations in the color of sphalerite, wurtzite and schalenblende in reflected light. The number, intensity, and color of the internal reflections vary distinctly within one sample. This variation together with slight, but common, differences in the reflectivity indicates highly variable iron contents in all three zinc sulfides. Wide variation occurs even within a small area, in adjoining grains, or in a single aggregate. The presence of non-equilibrium conditions of mineralization is thus apparent.

Comparison of the chemical analyses of sphalerite, wurtzite, and schalenblende (Table 5) confirms considerable small-scale variations in the iron content. In places, the zinc sulfides are very rich in iron ("marmatite" and

Table 5.
Chemical composition of sphalerite (Sp), wurtzite (W), and schalenblende (S) (in weight %).

Sample	Ore	Zn	Fe	S	Cu	Co	Total
SO 40 - 149 G	Sp	56.27	9.94	33.95	0.19		100.35
SO 40 - 149 G	W	49.79	15.93	34.45	0.08		100.25
SO 40 - 149 G	W	53.62	11.83	34.23	0.07		99.75
SO 40 - 149 G	W	51.54	14.77	33.82	0.07		100.20
SO 40 - 149 G	S	53.83	10.91	33.49	0.29		98.52
SO 40 - 152 G	S	59.38	6.33	33.37	1.14	0.09	100.31
SO 40 - 152 G	S	57.61	8.05	33.36	1.59	0.09	100.70
SO 40 - 153 G	Sp	57.15	8.08	33.89	0.53	0.09	99.74
SO 40 - 153 G	Sp	60.03	6.25	33.45	0.44	0.07	100.24
SO 40 - 153 G	Sp	56.06	9.98	38.58	0.46	0.09	100.17
SO 40 - 153 G	Sp	57.05	8.09	34.11	0.44	0.10	99.79
SO 40 - 182 G	Sp	63.52	3.11	32.96	0.13	0.06	99.78
SO 40 - 182 G	Sp	64.29	2.48	32.85	0.16	0.04	99.82
SO 40 - 182 G	Sp	58.93	6.83	34.12	0.91	0.19	100.98
SO 40 - 182 G	Sp	50.50	14.05	34.98	0.96	0.40	100.89
SO 40 - 182 G	Sp	53.66	12.12	35.09	0.34	0.24	101.45
SO 40 - 182 G	Sp	61.81	4.85	34.44	0.40	0.16	101.66
SO 40 - 182 G	S	52.99	11.75	33.60	0.87	0.21	99.42
SO 40 - 182 G	S	43.94	19.93	33.93	0.95	0.39	99.14
SO 40 - 182 G	S	63.21	1.05	33.36	0.13		97.75
SO 40 - 182 G	S	62.42	1.17	33.16	0.05	0.01	96.81
SO 40 - 182 G	S	57.86	1.46	30.10	0.04	0.27	89.73
SO 40 - 182 G	S	58.21	7.09	33.66	0.31	0.12	99.39
SO 40 - 199 G	Sp	62.61	4.00	32.56	0.13		99.30
SO 40 - 199 G	Sp	60.00	6.64	32.88	0.22		99.74
SO 40 - 199 G	S	61.64	3.54	34.54	0.35		100.07
SO 40 - 199 G	S	60.91	5.40	33.53	0.20	0.01	100.05
SO 40 - 199 G	S	63.03	2.27	32.97	0.82		99.09

"christophite"). Replacement of zinc by iron may be as much as one third. Apart from Cu (< 1.59 %), Co (< 0.4 %), Ni (0.002 %–0.004 %), Tl (up to 0.01 %), and As (31–85 ppm, up to a maximum of 812 ppm) are also signif-



Fig. 42.
Sample SO 40–199 G.
Crystal aggregate of sphalerite (dark gray in different shades), partly paramorphic after wurtzite (likewise dark gray), within pyrite (light gray, almost white). Small variations in reflectivity exhibit zoning and twinning within the sphalerite crystal aggregate, while internal reflections and cores consisting of fine skeleton crystals of chalcopyrite (light gray) are also present. Natural cavities and pores, opaline silica gangue material (all black).
Polished sections, oil immersion, x 1075.

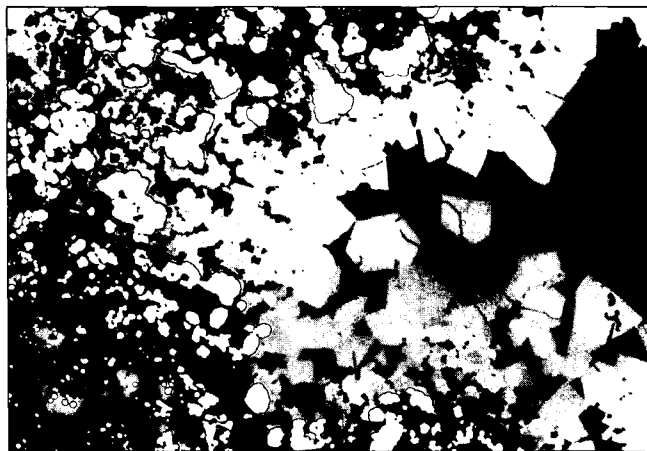


Fig. 43.
Sample SO 40–149 G.
Rhythmic, concentric-conchoidal pyrite (light gray, almost white), overgrown by schalenblende (dark gray in different shades) which is in transition to fine-grained aggregates of sphalerite (likewise dark gray in different shades). The latter is mainly surrounded by euhedral wurtzite (likewise dark gray in different shades) showing tabular development after {0001}. Natural cavities and pores occupy larger areas, minor gangue material (all black).
Polished section, oil immersion, x 85.

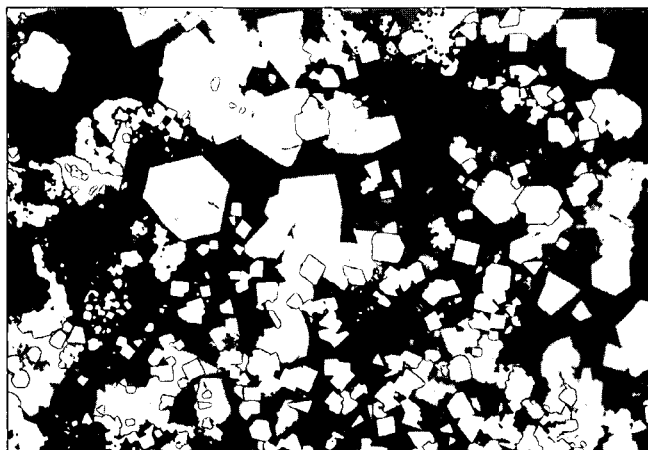


Fig. 44.
Sample SO 40-149 G.
Wurtzite (dark gray), euhedrally developed after {0001}, is associated with some sphalerite, minor schalenblende (both likewise dark gray), and abundant pyrite crystal aggregates (light gray, almost white). All are coated by opaline silica gangue material (black, not discernible in photomicrograph). Natural cavities and pores (both likewise black) occupy larger areas.
Polished section, $\times 140$.

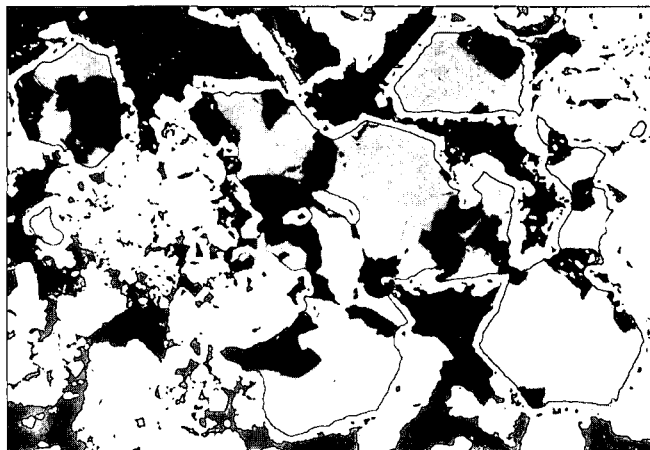


Fig. 46.
Sample SO 40-153 G.
Euhedral wurtzite (dark gray) tabularly developed after {0001} coated and replaced by chalcopyrite (light gray, almost white). Locally, the latter contains crystal aggregates of pyrite (almost white, barely distinguishable in photomicrograph). Natural cavities and pores, some gangue material (all black).
Polished section, oil immersion, $\times 140$.

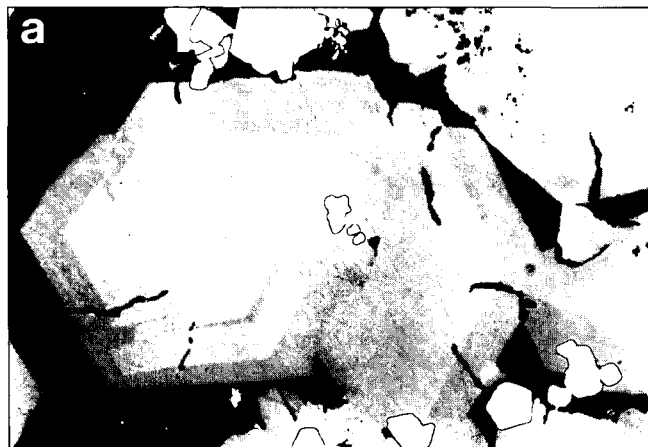


Fig. 45.
Sample SO 40-149 G.
Euhedral plates of wurtzite (dark gray in different shades) developed after {0001}, displaying distinct zoning due to slight differences in reflectivity. Wurtzite contains small inclusions of chalcopyrrhotite with exsolution of chalcopyrite (both light gray, almost white, not distinguishable in photomicrograph). Internal reflections may locally be observed in wurtzite. Natural cavities and pores, gangue material (all black).
Polished section, oil immersion,
Fig. 45 a: $\times 360$,
Fig. 45 b: $\times 235$.

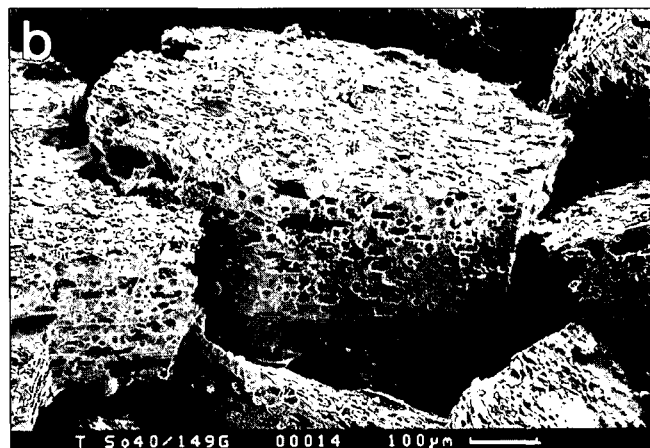
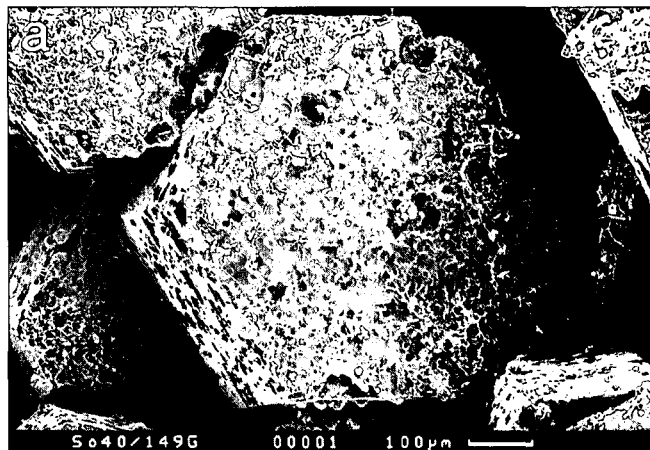


Fig. 47.
Sample SO 40-149 G.
Euhedral plates of wurtzite developed after {0001} and $\{10\bar{1}0\}$ exhibiting numerous small natural cavities and pores which partly delineate fluid inclusions.
Secondary electron image.

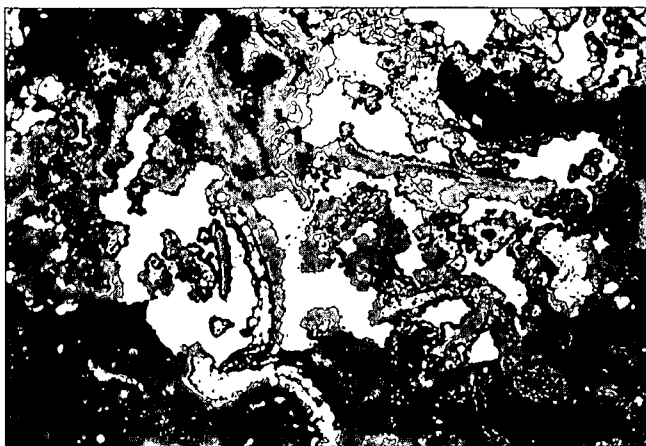


Fig. 48.
Sample SO 40-199 G.
Colloform, rhythmically layered to botryoidal-reniform and concentric-conchoidal masses of melnikovite-pyrite (light gray to medium gray), some "intermediate product" (medium gray to dark gray), pyrite (light gray, almost white), and schalenblende (dark gray) delicately coated by opaline silica gangue material (black) within masses of marcasite (likewise light gray, almost white) and opaline silica gangue material. Polished section, $\times 55$.



Fig. 50.
Sample SO 40-182 G.
Rhythmic, colloidal masses including radiating pyrite (light gray, almost white) and melnikovite-pyrite (light gray to medium gray), partially displaying marginal transition to concentric-conchoidal accretions, in turn followed by rhythmic, concentric-conchoidal and botryoidal-reniform masses of schalenblende (dark gray in different shades) and locally by euhedral pyrite. Pyrite spheroids occur in places. They include radiating pyrite and melnikovite-pyrite, as well as schalenblende. Abundant natural cavities and pores, some opaline silica gangue material (all black). Polished section, oil immersion, $\times 140$.

icant. Of outstanding importance is the locally very high silver concentration (83 ppm-311 ppm-395 ppm). Zinc sulfides thus represent the main silver bearing minerals.

Hematite

(Figs. 18, 26, 57-61) is locally enriched in copper-rich zones, representing a major constituent in SO 40-153 G. Hematite is intergrown with chalcopyrite, pyrite, melnikovite-pyrite, marcasite and chalcopyrrhotite.

Hematite is primarily observed in aggregates of euhedral crystals after {0001}. In addition, hematite delicately intergrown with pyrite and melnikovite-pyrite is frequently present in rhythmic, concentric-conchoidal, layered crusts to colloidal masses. These are embedded in platy aggregates of hematite sprouting on them (Figs. 57-59). Traces of hematite occur in SO 40-182 G, again together with chalcopyrite. The latter is distinctly more abundant in these chimney fragments.

Chalcopyrrhotite

The high-temperature sulfide chalcopyrrhotite ("isocubanite", Figs. 18, 22, 32, 37-38, 40-41, 45, 55-56, 61-68, 70, 73) is a minor constituent in all samples. Its occurrence is an important indicator for the formation temperature of the black smoker chimneys. The presence of chalcopyrrhotite could be easily demonstrated by ore microscopy, as well as by X-ray powder diffraction analysis. Chalcopyrrhotite is equally common in copper-rich and zinc-rich zones, almost invariably associated with chalcopyrite. There is a continuous transition from aggregates of almost pure chalcopyrrhotite with delicate chalcopyrite exsolution spindles to aggregates almost entirely composed of chalcopyrite containing subordinate amounts of exsolved chalcopyrrhotite. This demonstrates a wide chemical variation of the initial high-temperature solid solutions, which mark considerable differences in the $\text{CuFeS}_2 : \text{FeS}$ ratio. Chalcopyrrhotite is frequently

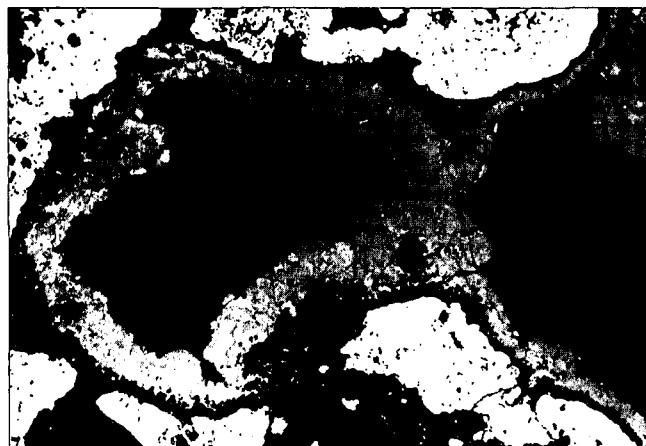


Fig. 49.
Sample SO 40-200 G.
Opaline silica gangue material (black) containing colloidal masses of pyrite (light gray, almost white), associated with minor melnikovite-pyrite, marcasite, and chalcopyrite (all likewise light gray) in places. Spherical, bubble-like cavities are lined with schalenblende. Polished section, oil immersion, $\times 110$.

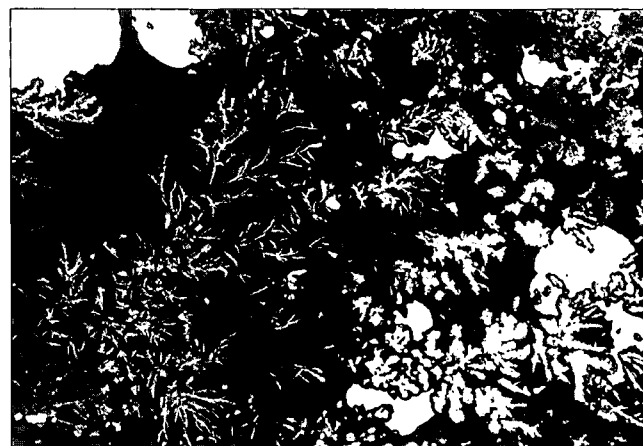


Fig. 51.
Sample SO 40-149 G.
Dendritic, delicately feathery-flowery schalenblende (dark gray in different shades), overgrown by opaline silica gangue material (dark gray, almost black) and locally enclosed by marcasite (light gray, almost white). Abundant natural cavities and pores (both dark gray). Polished section, $\times 140$.

Fig. 52.
Sample SO 40-199 G.
 Fine schalenblende dendrites (dark gray in different shades), containing cores of opaline silica gangue material (black) in transition to massive schalenblende with sphalerite (likewise dark gray in different shades). The latter two include zonal inclusions and rhythmic alternations of chalcopyrite (light gray, almost white) and, at the margins, also euhedral pyrite (likewise light gray, almost white). These are overgrown by sphalerite displaying crystal faces. Abundant natural cavities and pores (likewise black).
 Polished section, oil immersion, $\times 140$.

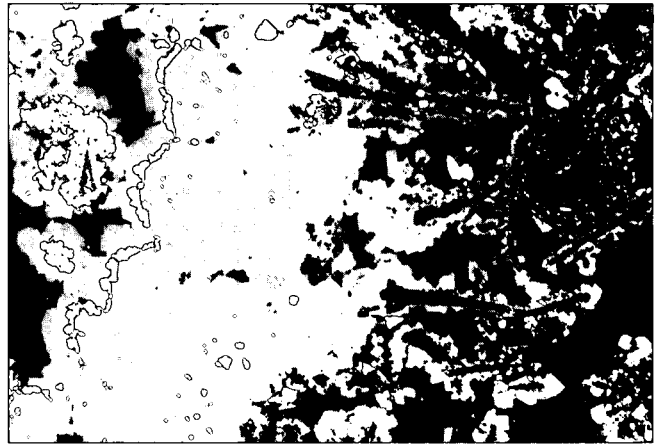


Fig. 53.
Sample SO 40-182 G.
 Excellent rhythmic, concentric-conchoidal, radiating schalenblende (medium gray to dark gray) and few delicate pyrrhotite platelets (light gray, almost white), forming overgrowths on crystal aggregates of chalcopyrite (likewise light gray, almost white). Close to the feeder channel (upper left of photomicrograph), schalenblende is finely coated by chalcopyrite. Schalenblende displays distinct zoning due to differences in reflectivity. Natural cavities and pores, minor gangue material (all black).
 Polished section, oil immersion, $\times 55$.

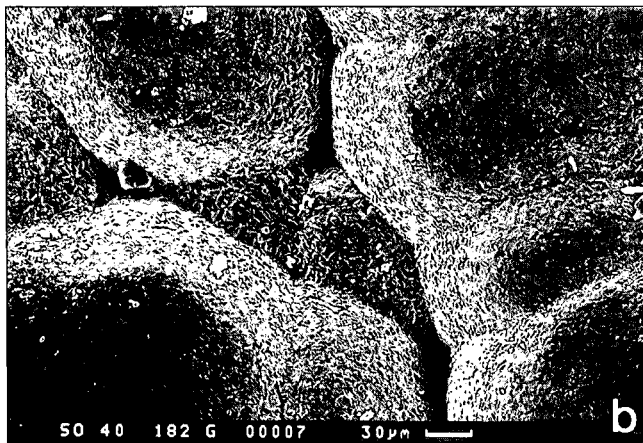
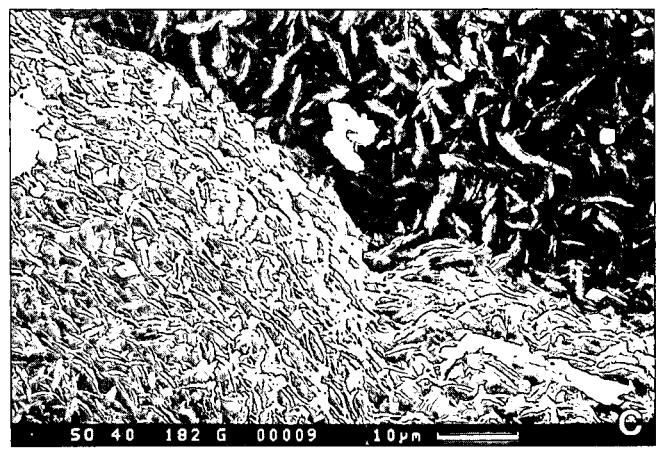
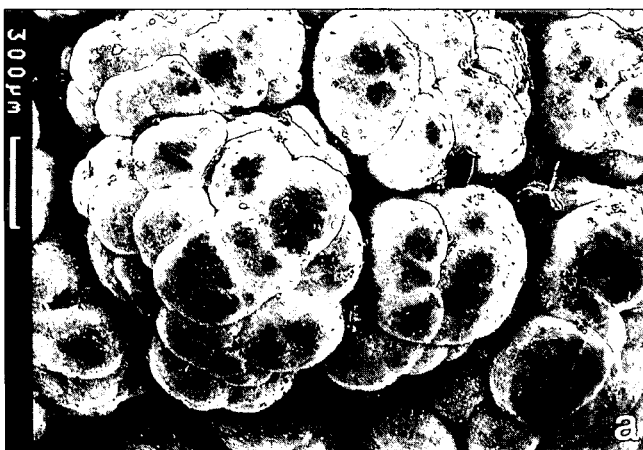
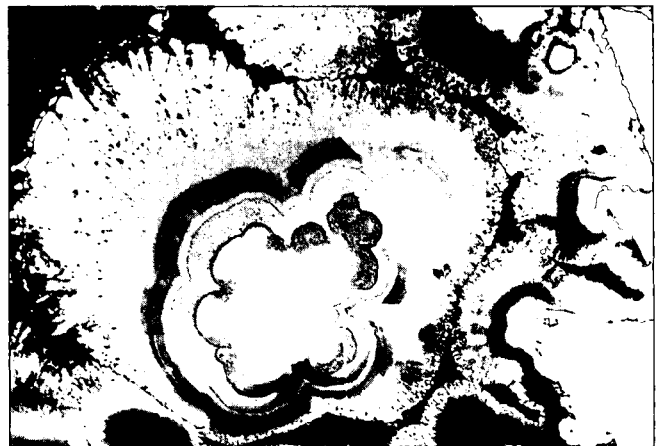


Fig. 54.
Sample SO 40-182 G.
 Well-developed botryoidal-reniform schalenblende, showing distinct laminar to radiating texture (fibrous schalenblende)
 Secondary electron image.

Fig. 55.
Sample SO 40–200 G.
Dendritic sphalerite associated with schalenblende (both dark gray in different shades), exhibiting zoning due to slight variations in reflectivity. The sphalerite also displays twin lamellae. Locally, schalenblende exhibits fine rhythmic alternations with chalcopyrite and chalcopyrrotite (both light gray, almost white). Internal reflections are occasionally observed within sphalerite and schalenblende. Natural cavities and pores, gangue material (all black).
Polished section, oil immersion, $\times 235$.



Fig. 56.
Sample SO 40–200 G.
Sphalerite (dark gray in different shades), exhibiting characteristic twinning and polysynthetic lamellae due to slight differences in reflectivity. The sphalerite contains zonally oriented rhythmic alternations with finely dispersed chalcopyrrotite and chalcopyrite (both light gray). Occasionally, internal reflections are discernible.
Polished section, oil immersion, $\times 915$.

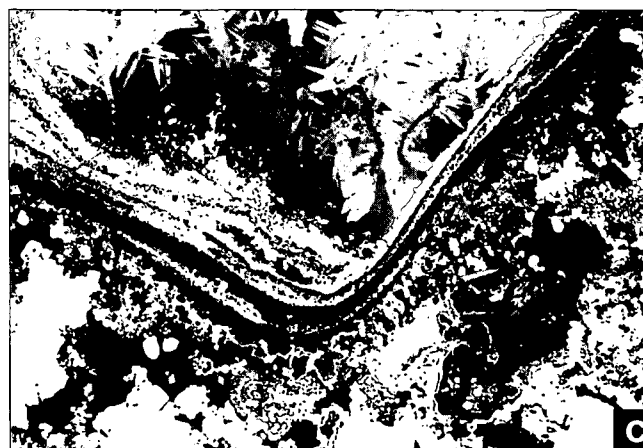


Fig. 57.
Sample SO 40–153 G.
Rhythmically layered to concentric-conchoidal, colloform crusts of pyrite (light gray, almost white), melnikovite-pyrite (light gray to medium gray), some "intermediate product" (medium gray to dark gray, almost black), and marcasite (likewise light gray, almost white) are enclosed in chalcopyrite (likewise light gray, almost white) and crystal aggregates of hematite (medium gray in different shades due to its bireflection) tabular developed after $\{0001\}$, both of which also fill interstices. In places, hematite clearly encloses and replaces the colloidal masses and may contain relics of them. Numerous natural cavities and pores, minor gangue material (all black).
Polished sections, oil immersion.
Fig. 57 a: $\times 60$.
Fig. 57 b–c: $\times 65$.

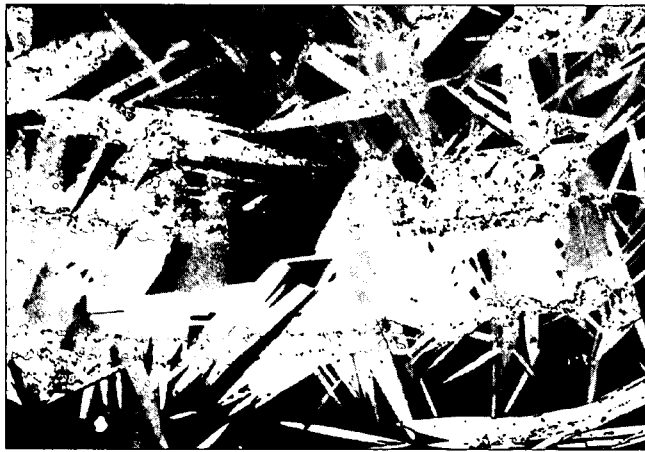


Fig. 58.
Sample SO 40–153 G.
Crystal aggregates of hematite (medium gray in different shades due to its bireflection), tabularly developed after {0001}, contain numerous relics and finely disseminated traces of rhythmically layered crusts to moss-like pyrite (light gray, almost white) with melnikovite-pyrite (light gray to medium gray). Numerous natural cavities and pores, minor gangue material (all black).
Polished section, oil immersion, $\times 140$.

euhedral (Figs. 22, 32, 62, 64–66, 68, 73–74), although dendritic aggregates to skeleton crystals are present as well. Both habits commonly occur in the center of sphalerite or schalenblende aggregates or as overgrowths on pyrrhotite plates which are frequently enclosed in sphalerite or schalenblende themselves. Furthermore, chalcopyrrhotite is encountered in colloform masses, e.g. together with layered crusts to tree- or moss-like aggregates of pyrite, melnikovite-pyrite, and marcasite (Fig. 68). The latter three minerals may be similarly enclosed in chalcopyrrhotite. Chalcopyrrhotite also forms rhythmic, partially very complex sequences and alternations (Figs. 32, 63) with sphalerite and schalenblende, locally developed down to the smallest observable scale (Fig. 55). Extremely fine inclusions of chalcopyrrhotite, again associated with chalcopyrite, occur in particular zones defining growth phases in sphalerite or wurtzite. These and finely dispersed inclusions of chalcopyrrhotite and chalcopyrite, mainly in sphalerite (Fig. 56), may occasionally approach the limit of resolution of the optical microscope.

Replacement of chalcopyrrhotite by “permanent blue” covellite and subordinately by neodigenite (Figs. 73–74) may be attributed to a secondary process of halmyrolysis.

Chalcopyrrhotite (Table 6), now associated with and exsolved in chalcopyrite, has a $\text{CuFeS}_2 : \text{FeS}$ ratio of about

Table 6.
Chemical composition of chalcopyrrhotite (in weight %).

Sample	Cu	Fe	S	Zn	Co	Total
SO 40 - 152 G	23.30	40.22	34.80	0.06	0.39	98.77
SO 40 - 152 G	23.33	40.20	34.98	0.04	0.40	98.95
SO 40 - 152 G	22.55	41.57	35.27	0.03	0.34	99.76
SO 40 - 152 G	23.13	41.04	35.18		0.35	99.70
SO 40 - 153 G	21.74	42.09	35.97	0.26	0.33	100.39
SO 40 - 153 G	22.61	41.54	36.35	0.08	0.30	100.88
SO 40 - 153 G	21.99	42.01	35.15	0.06	0.33	99.54
SO 40 - 153 G	23.74	40.39	35.73	0.05	0.29	100.20
SO 40 - 182 G	22.68	41.53	35.27	0.16	0.51	100.15



Fig. 59.
Sample SO 40–153 G.
Rhythmic, concentric-conchoidal hematite (medium gray in different shades due to its bireflection), accompanied by minor fine-grained pyrite (light gray, almost white) and melnikovite-pyrite (light gray to medium gray), showing peripheral transition to euhedral tabular aggregates developed after {0001}. In places, these enclose and partly replace rhythmically layered crusts of pyrite (Fig. 59 a). Occasionally, the euhedral hematite contains some chalcopyrite (likewise light gray, almost white, Fig. 59 b). Abundant natural cavities and pores, minor gangue material (all black).
Polished sections, oil immersion.
Fig. 59 a: $\times 140$.
Fig. 59 b: $\times 235$.

1 : 1. It approximates the composition CuFeS_3 . Noteworthy are the contents of zinc (up to 0.26 %) and cobalt (up to 0.51 %).

The initial chemical composition of the high-temperature chalcopyrrhotite solid solution is reflected by the relative proportions of chalcopyrite and chalcopyrrhotite now present in the exsolved aggregates. Relative amounts range from chalcopyrite with only few exsolution lamellae of chalcopyrrhotite to chalcopyrrhotite with fine chalcopyrite exsolution spindles amounting to a maximum of 20 %–30 %.

Pyrrhotite

(Figs. 22, 25–26, 53, 62, 67, 69–70, 73) is locally present as a minor constituent. Euhedral crystals after {0001} are predominant. Pyrrhotite is mostly associated with chalcopyrite and chalcopyrrhotite, but also with sphalerite, wurtzite, and schalenblende. Euhedral pyrrhotite together with partially dendritic, coarse-grained chalcopyrite and minor chalcopyrrhotite accompany the dendritic aggregates of sphalerite (partly paramorphic after wurtzite)

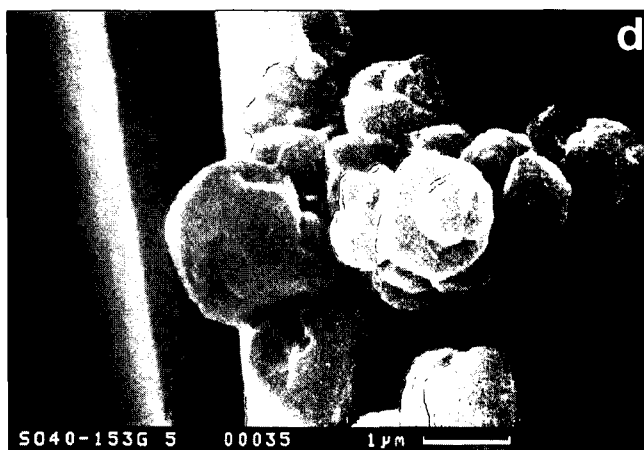
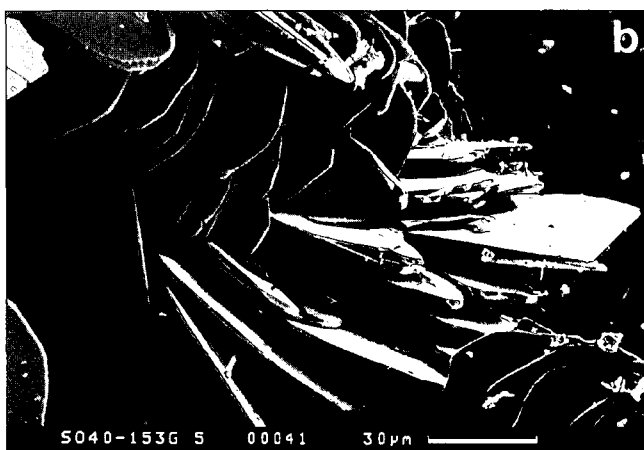
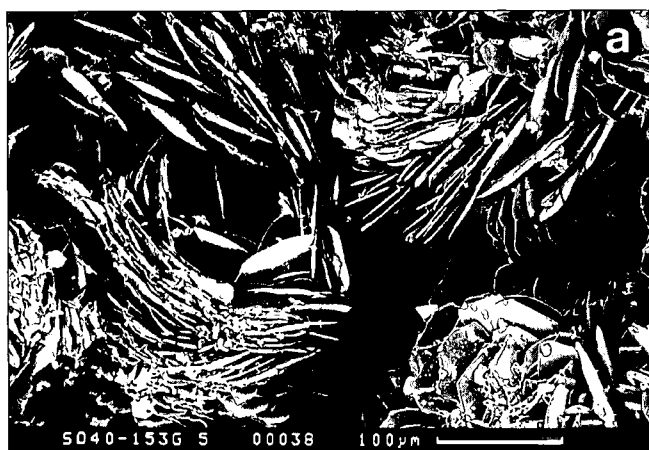


Fig. 60.
Sample SO 40-153 G.
Rosette-like crystal aggregates of hematite developed after {0001}. In places, extremely small crystal aggregates of hematite occur on its euhedral platelets.
Secondary electron image.

which frame the feeder channel of the hydrothermal solution in sample SO 40-182 G.

Chalcopyrrhotite is frequently overgrown on euhedral pyrrhotite plates, moreover locally enclosing and replac-

ing the latter (Figs. 22, 70, 73). The same intergrowth and replacement textures occur with chalcopryrite (Fig. 25). Occasionally, aggregates of pyrrhotite may be completely replaced and pseudomorphed by chalcopryrite (Fig. 26);

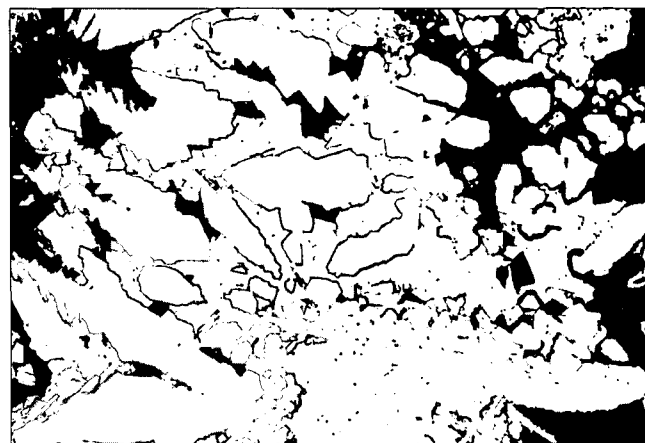
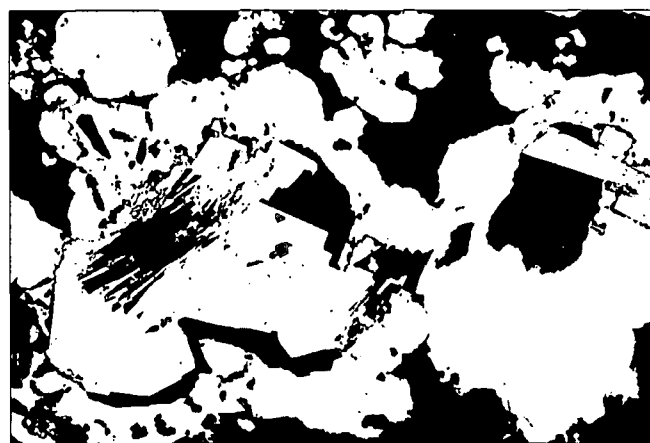


Fig. 61.
Sample SO 40-153 G.
Euhedral pyrite (light gray, almost white), embedded in chalcopyrite (light gray), displaying fine exsolution spindles of chalcopyrrhotite (medium gray). Euhedral hematite (dark gray) is mainly observed in pyrite and less commonly in chalcopyrite with exsolved chalcopyrrhotite. Numerous natural cavities and pores, minor gangue material (all black).
Polished section, oil immersion, $\times 140$.

Fig. 62.
Sample SO 40-153 G.
Marcasite and minor pyrite (both light gray), locally pseudomorphic after pyrrhotite and enclosing crystal aggregates of chalcopyrrhotite (medium gray). The latter are partially skeleton crystals and finely rimmed by sphalerite (dark gray, almost black). In the center of chalcopyrrhotite there may be occasional exsolution spindles of chalcopyrite (slightly darker light gray). Natural cavities and pores, minor gangue material (all black).
Polished section, oil immersion, $\times 75$.

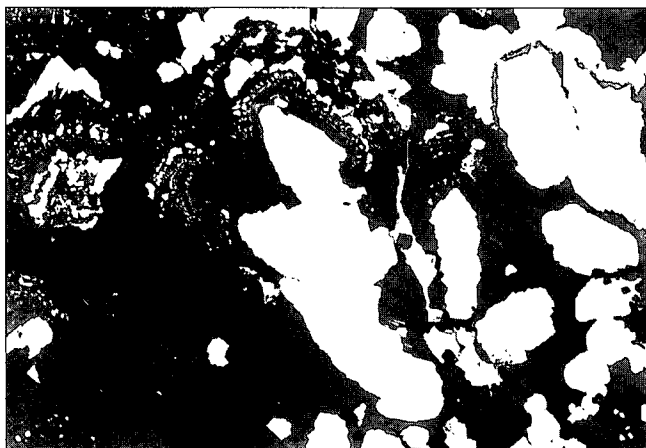


Fig. 63.
Sample SO 40–200 G.
The center of rhythmic dendrites is composed of chalcopyrrhotite (slightly darker light gray), locally with fine exsolution of chalcopyrite (light gray). Chalcopyrrhotite is surrounded by chalcopyrite, locally with zonal alternations of sphalerite and schalenblende (both dark gray), and sometimes with minor exsolved chalcopyrrhotite, followed by rhythmic, concentric-conchoidal alternations of schalenblende, sphalerite and chalcopyrite. Finally, a rim of inclusion-free sphalerite occurs. Locally, pyrite (light gray, almost white) fills interstices. Natural cavities and pores, minor gangue material (all black).
Polished section, oil immersion, $\times 140$.

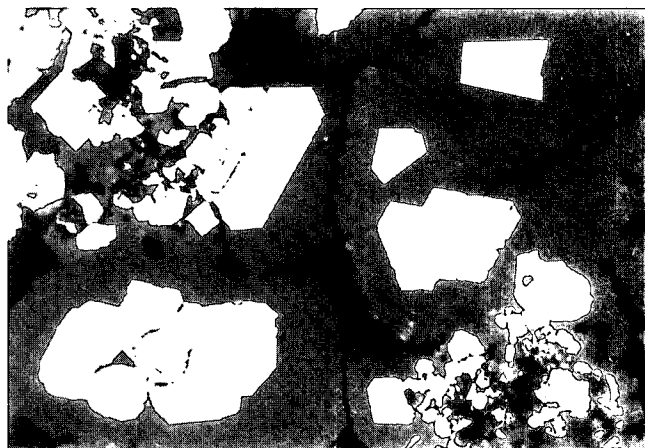


Fig. 65.
Sample SO 40–200 G.
Crystal aggregates of chalcopyrrhotite (medium light gray) with delicate exsolution spindles of chalcopyrite (light gray), oriented overgrown by sphalerite (dark gray). Euhedral pyrite (light gray, almost white) is occasionally found. Internal reflections are visible in sphalerite. Natural cavities and pores, minor gangue material (all black).
Polished section, oil immersion, $\times 365$.

a texture which may be mistaken for replacement of hematite by chalcopyrite in zones where the hematite is present (Fig. 26 b).

Marcasite accompanied by minor pyrite similarly replaces and completely pseudomorphs euhedral plates of pyrrhotite (Fig. 22). Due to halmyrolysis pyrrhotite (Figs. 25, 69–70), in most instances, is largely replaced by “intermediate product” which itself, via secondary halmyrolytic marcasite, is altered to young pyrite (mainly “cellular pyrite”) to a considerable degree. The cellular pyrite in turn is altered to limonite, and both have been dissolved

and left behind holes. Accordingly, pseudomorphs of the secondary minerals after pyrrhotite and holes are dominant. In many instances, pyrrhotite merely occurs in relics and as remnants after incomplete replacement.

Chemical analyses of pyrrhotite (Table 7) from the black smoker chimneys display the common deficiency in iron, but are remarkably high in cobalt (up to 0.79 %).

Table 7.
Chemical composition of pyrrhotite (in weight-%).

Sample	Fe	S	Co	Total
SO 40 - 153 G	59.81	39.82	0.67	100.30
SO 40 - 153 G	59.59	39.86	0.72	100.17
SO 40 - 182 G	59.60	41.12	0.79	101.51

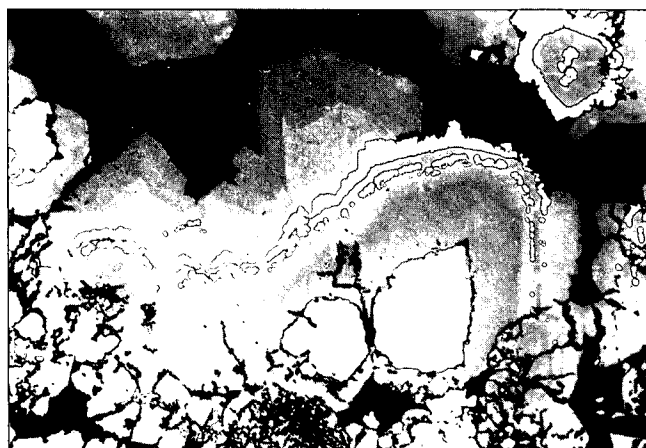


Fig. 64.
Sample SO 40–200 G.
Porous schalenblende (dark gray in different shades, lower edge of photomicrograph) in transition to sphalerite (likewise dark gray in different shades), containing partly euhedral chalcopyrrhotite (light gray, almost white) in its center. The latter shows fine exsolution spindles of chalcopyrite (likewise light gray, almost white, not distinguishable in photomicrograph). Towards the sphalerite margins rhythmic alternations with chalcopyrite are encountered. These are surrounded by partly euhedral, inclusion-free sphalerite. Slight differences in reflectivity of sphalerite delineate zoning and twinning. Natural cavities and pores occupying larger areas, minor gangue material (all black) and pyrite (almost white).
Polished section, oil immersion, $\times 365$.

“Intermediate product”

(Figs. 11, 17–19, 25, 31, 48, 57, 69) is found in colloidal masses of melnikovite-pyrite and as an alteration product of pyrrhotite due to halmyrolysis.

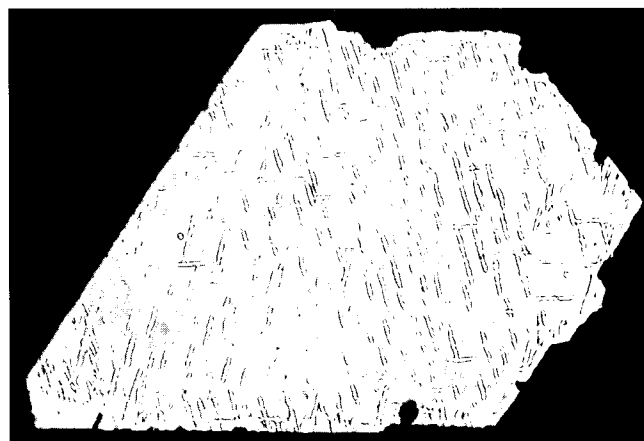


Fig. 66.
Sample SO 40–200 G.
Euhedral chalcopyrrhotite (medium gray) with delicate exsolution spindles of chalcopyrite (light gray), revealing an oriented overgrowth of sphalerite (black).
Polished section, oil immersion, $\times 1020$.

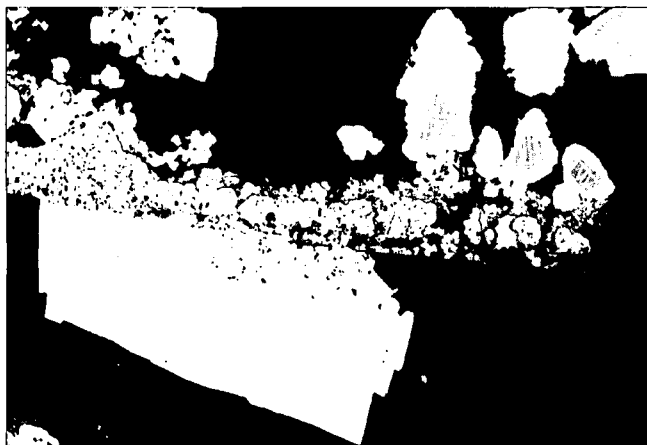


Fig. 67.
Sample SO 40–152 G.
Tree-like to moss-like, partly transverse-segmented and fractured layered crust of pyrite (light gray, almost white) with minor melnikovite-pyrite (light gray to darker light gray) and marcasite (likewise light gray), healed and partly replaced by chalcopyrite (medium gray). The latter also overgrows and coats this crust in coarse-grained to dendritic aggregates. Its dendrites exhibit exsolution of chalcopyrrhotite (dark gray). A few minute inclusions of pyrrhotite (likewise medium gray) occur within a larger euhedral aggregate of pyrite, which is likewise overgrown onto this crust. Sphalerite, abundant natural cavities and pores, minor gangue material (all black).
Polished section, oil immersion, $\times 120$.

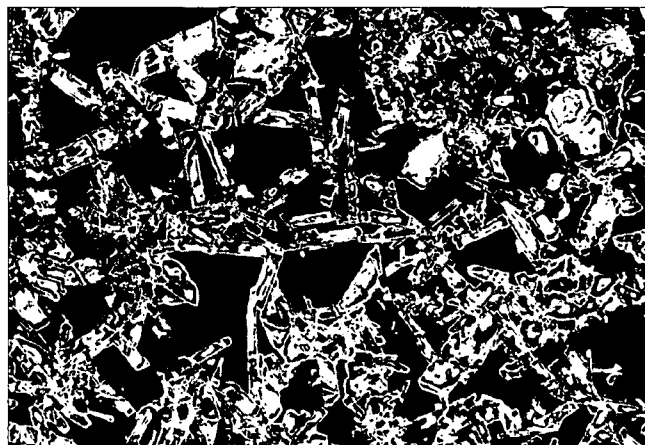


Fig. 69.
Sample SO 40–152 G.
Euhedral aggregates of pyrrhotite (light gray), tabularly developed after {0001}, either largely replaced and pseudomorphed by a halmyrolytic sequence via "intermediate product" and marcasite to cellular pyrite (all light gray to medium gray) or already entirely dissolved. Interstices between pyrrhotite plates are locally filled with chalcopyrite (light gray, almost white). Numerous natural cavities and pores, some gangue material (all black).
Polished section, oil immersion, $\times 75$.

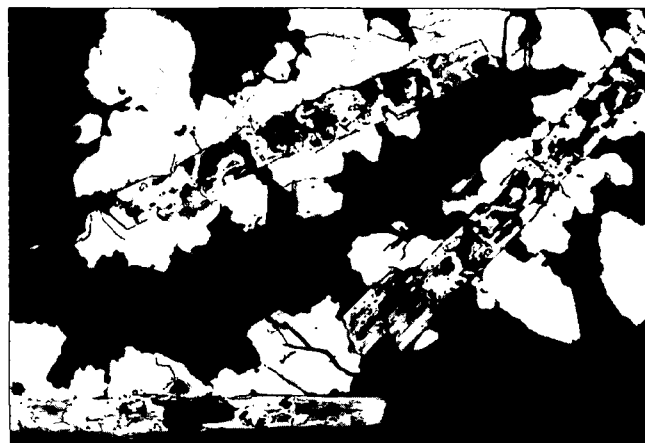


Fig. 70.
Sample SO 40–152 G.
Euhedral plates of pyrrhotite (light gray) developed after {0001}, largely replaced and pseudomorphed by cellular pyrite (light gray to dark gray) as a result of halmyrolysis. Both have been substantially dissolved. The original pyrrhotite plates are overgrown by coarse-grained, dendritic chalcopyrite (likewise light gray). The latter contains a central zone of exsolved chalcopyrrhotite spindles (medium gray). Numerous natural cavities and pores, some gangue material (all black).
Polished section, oil immersion, $\times 365$.

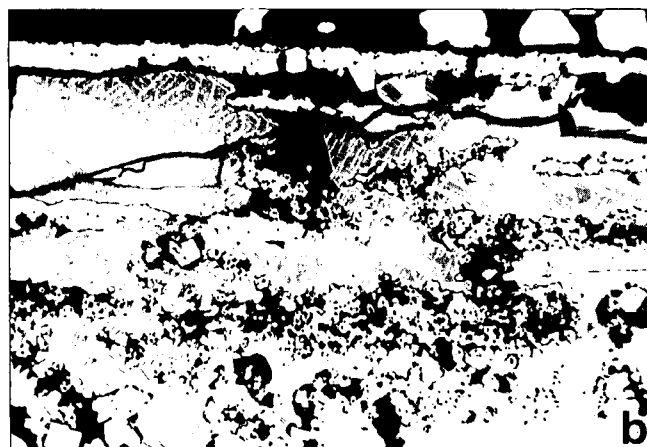


Fig. 68.
Sample SO 40–152 G.
Rhythmically layered crusts to moss-like pyrite (light gray, almost white) with melnikovite-pyrite (light gray to medium gray), enclosed in chalcopyrrhotite (medium gray) with exsolution spindles of chalcopyrite (light gray). A partial replacement of pyrite is encountered in these aggregates. In places, euhedral chalcopyrrhotite and euhedral pyrite are present. Abundant natural cavities and pores, minor gangue material (all black).
Polished sections, oil immersion, $\times 365$.

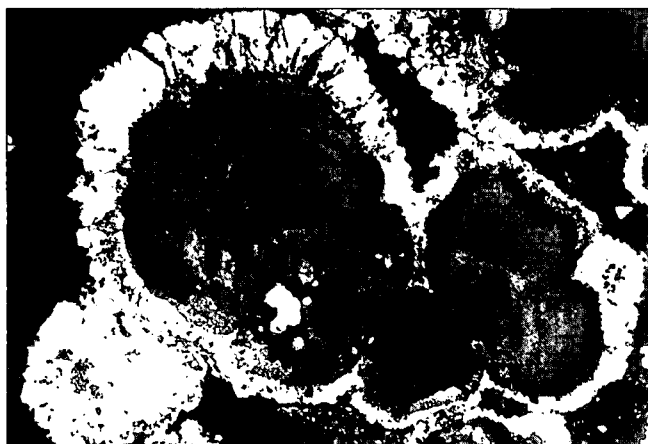


Fig. 71.
Sample SO 40–152 G.
Rhythmic, concentric-conchoidal, largely dissolved colloform masses of "permanent blue" covellite (dark gray to almost black – bireflectance), rimmed by schalenblende (medium gray) associated with minor pyrite and melnikovite-pyrite (both light gray). Locally, small pyrite spheroids may be observed. Natural cavities and pores, minor gangue material (all black).
Polished section, oil immersion, $\times 215$.

Covellite

(Figs. 11, 29, 71–74) is present as an accessory mineral in all samples. It frequently occurs in its "permanent blue" variety. Covellite is observed in small, partially euhedral aggregates together with other sulfides and in rhythmic, colloform, concentric-conchoidal precipitates with schalenblende, in which both display excellent colloidal and/or gel textures (Fig. 71). Late crystals of covellite replace chalcopyrite, sphalerite, wurtzite, schalenblende, and, in association with neodigenite, also chalcopyrrhotite (Figs. 73–74). It is particularly apparent that in replacements of exsolved chalcopyrrhotite-chalcopyrite-aggregates by covellite and neodigenite only the (iron-rich) chalcopyrrhotite host is significantly affected,



Fig. 72.
Sample SO 40–152 G.
Crystal aggregate of pyrite (light gray) containing some marcasite (likewise light gray) and exhibiting delicate myrmekitic intergrowth with chalcopyrite (likewise light gray, hardly distinguishable in photo-micrograph). Replacement rims of "permanent blue" covellite (different shades of dark gray to black) are developed around dendritic aggregates of chalcopyrite overgrown onto pyrite. Natural cavities and pores, minor gangue material (all black).
Polished section, oil immersion, $\times 365$.

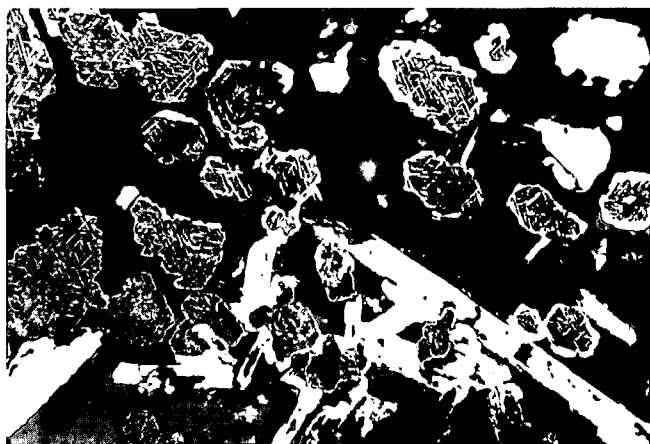


Fig. 73.
Sample SO 40–152 G.
Euhedral pyrrhotite plates (light gray) developed after {0001}, almost entirely replaced and pseudomorphed by cellular pyrite (likewise light gray). In places, the original pyrrhotite plates show rims of sphalerite (dark gray). Crystal aggregates of chalcopyrrhotite (likewise light gray) contain fine exsolution spindles of chalcopyrite (likewise light gray). Chalcopyrrhotite is largely replaced by "permanent blue" covellite and subordinate neodigenite (both dark gray to black). The chalcopyrite spindles are more resistant to this replacement than their host. Abundant natural cavities and pores, minor gangue material (all black).
Polished section, oil immersion, $\times 235$.

while the exsolution spindles of (copper-rich) chalcopyrite remain almost intact. Thus the latter is quite resistant to halmyrolytic alteration, whereas chalcopyrrhotite, an unstable high-temperature sulfide, may be entirely replaced and pseudomorphed by covellite accompanied by neodigenite.

Galena

(Figs. 75–79) is an accessory sulfide mineral in one of the samples (SO 40–200 G). It is locally enclosed in rims of schalenblende around slightly older sphalerite (Fig. 75) or schalenblende (Fig. 76) and in rhythmic, concentric-conchoidal to botryoidal-reniform or crusty-layered colloidal masses primarily consisting of melnikovite-pyrite, pyrite,

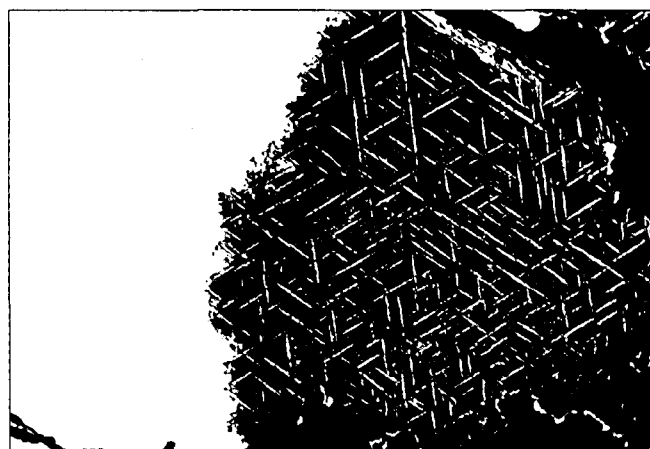


Fig. 74.
Sample SO 40–152 G.
Detail of euhedral chalcopyrrhotite (medium gray) with fine exsolution spindles of chalcopyrite (light gray). "Permanent blue" covellite, accompanied by some neodigenite (both dark gray to almost black), preferentially replacing chalcopyrrhotite. The exsolved chalcopyrite spindles are preserved due to their relative resistance to replacement. Natural cavities and pores, minor gangue material (all black).
Polished sections, oil immersion, $\times 925$.

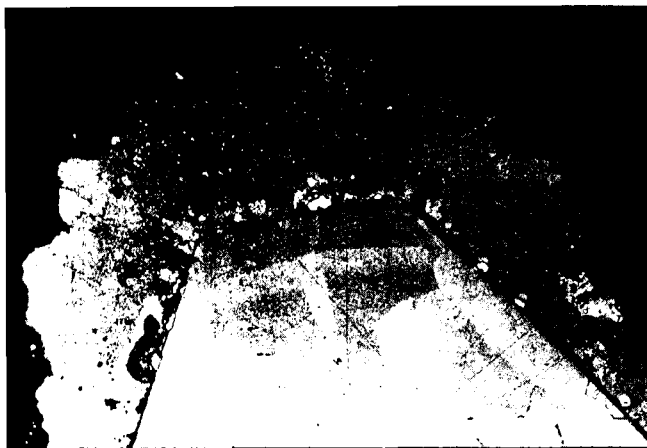


Fig. 75.
Sample SO 40-200 G.
Euhedral sphalerite (dark gray in different shades), thinly coated by opaline silica gangue material (black) and overgrown by schalenblende (likewise dark gray in different shades). Sphalerite and schalenblende display distinct zoning due to slight differences in reflectivity. Minor galena (light gray, almost white) is found at the sphalerite margins. Occasionally, schalenblende exhibits internal reflections. Natural cavities and pores, abundant opaline silica gangue material (all black).
Polished section, oil immersion, $\times 140$.

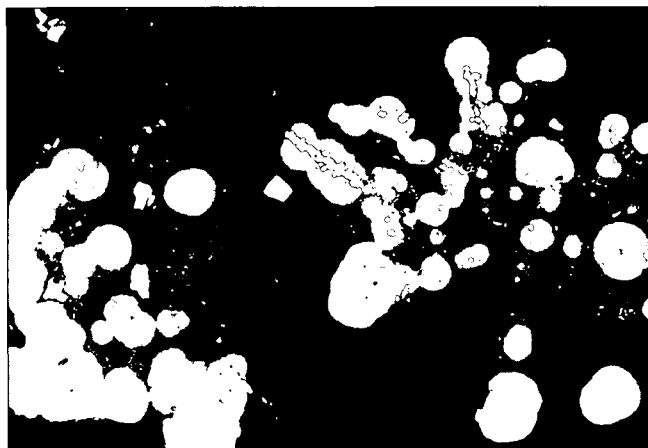


Fig. 77.
Sample SO 40-200 G.
Rhythmic, concentric-conchoidal schalenblende (dark gray) rimmed by opaline silica gangue material (black), both containing small inclusions of galena (light gray). In places, the galena is present in finely "knitted" skeleton crystals within schalenblende and opaline silica gangue material. Pyrite (light gray, almost white) is occasionally found. Abundant natural cavities and pores (dark gray, almost black).
Polished section, $\times 170$.

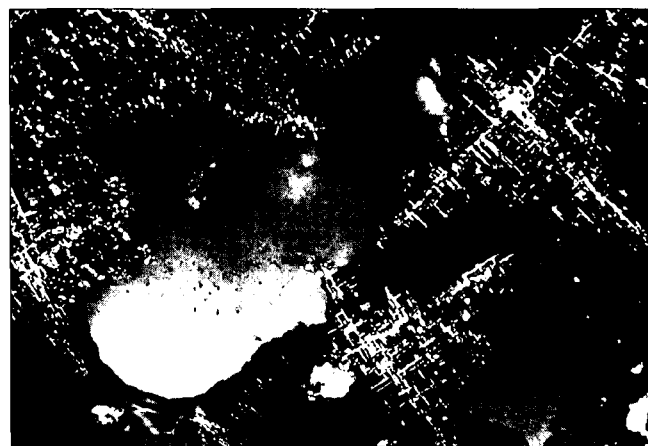
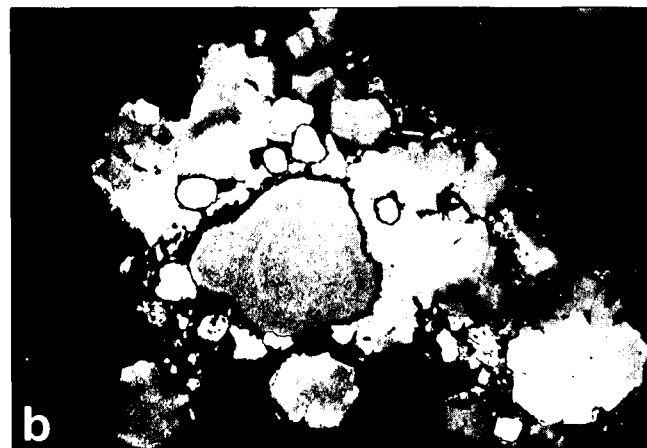
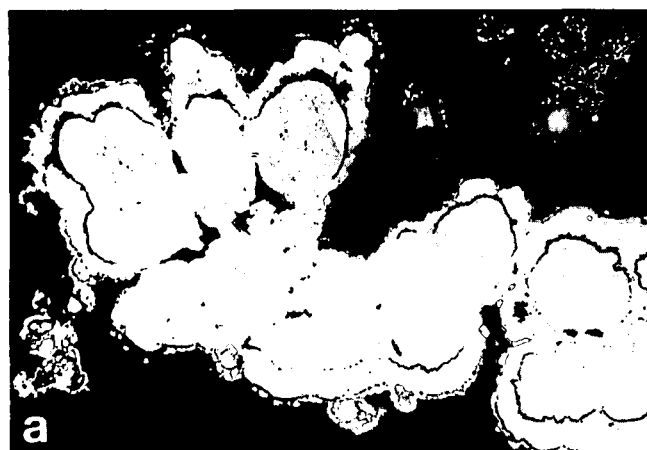


Fig. 78.
Sample SO 40-200 G.
Delicate, "knitted" galena skeleton crystals (light gray, almost white) within schalenblende (dark gray) and in the adjacent opaline silica gangue material (almost black) which partly surrounds schalenblende. The brightness of opaline silica gangue material and schalenblende are locally exaggerated due to internal reflections.
Polished section, oil immersion, $\times 925$.

Fig. 76.
Sample SO 40-200 G.
Rhythmic, concentric, colloform schalenblende (dark gray in different shades) containing thin layers of opaline silica gangue material (black) and partly brightened by internal reflections. Schalenblende exhibits some inclusions of galena in the peripheral layers. Natural cavities and pores, abundant opaline silica gangue material (all black).
Polished sections, oil immersion.
Fig. 76 a: $\times 110$.
Fig. 76 b: $\times 365$.

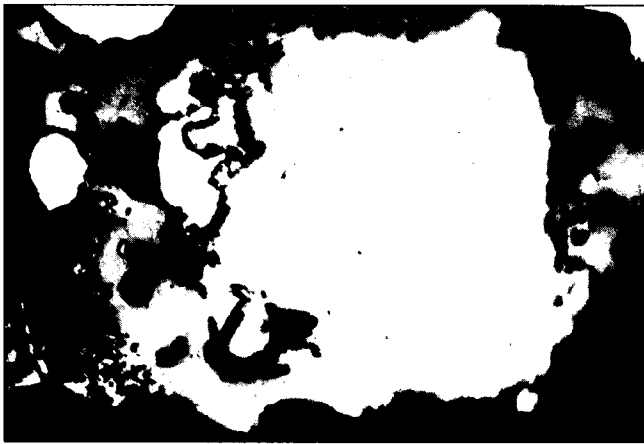


Fig. 79.
Sample SO 40–200 G.
Inclusion of galena (light gray) associated with a lead sulfosalt, probably jordanite (slightly darker light gray) within rhythmic colloform masses of melnikovite-pyrite, pyrite, marcasite (all light gray, almost white), schalenblende (almost black), and opaline silica gangue material (black). Galena occurs in zonal intergrowth with jordanite. Polished section, oil immersion, $\times 2225$.

schalenblende, and marcasite. Like the other sulfides, galena is rimmed by opaline silica gangue material in these colloform masses. Particularly characteristic are “knitted” crystal aggregates and skeleton crystals of galena (Fig. 77–78) in schalenblende and opaline silica gangue material.

A lead sulfosalt often associated with galena is probably jordanite (Fig. 79) as indicated by the color, the weak bireflection, the anisotropism, and the high reflectivity (slightly less than galena). Jordanite is found in delicate intergrowth with galena, partly in zonally arranged aggregates, and often constitutes rims around the lead sulfide. Jordanite occasionally forms discrete crystals void of or with very little galena.

Neodigenite

(Figs. 73–74) occurs as an accessory phase in sample SO 40–152 G, where it accompanies “permanent blue” covellite replacing chalcopyrrotite. Like covellite, it is a product indicating the commencement of halmyrolysis.



Fig. 81.
Sample SO 40–152 G.
Finely “knitted” skeleton crystals of pyrite (light gray, almost white) within glassy basaltic gangue material (dark gray, almost black, partly brightened by internal reflections). Polished section, $\times 365$.

lite replacing chalcopyrrotite. Like covellite, it is a product indicating the commencement of halmyrolysis.

The fragments of the black smoker chimneys are marginally coated by limonite, which may be locally enriched to form crusts. It is apparent from the occurrence of limonite that the black smokers were not active any more at the time of sampling, since submarine weathering (i. e. halmyrolysis) and oxidation in oxygen-rich seawater had already commenced. Limonite replaces and pseudomorphs the primary sulfides. In part, it consists of cryptocrystalline to microcrystalline iron hydroxides (e.g. goethite).

Gangue material

The proportion of the gangue material (e.g. opaline silica, barite, anhydrite) in the fragments is quite variable and may be relatively low. In two samples (SO 40–199 G, SO 40–200 G) X-ray amorphous silica (opaline silica) is

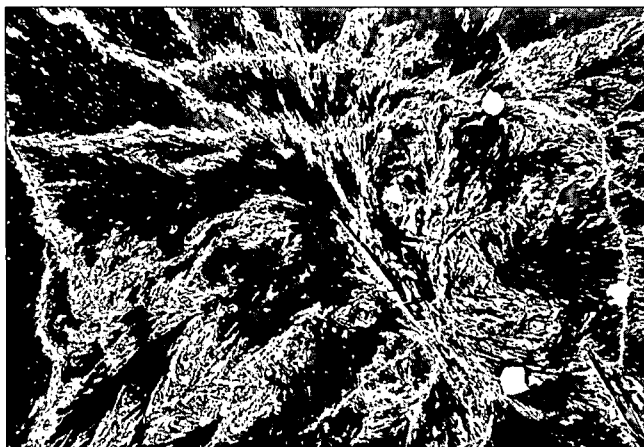


Fig. 80.
Sample SO 40–152 G.
Delicate, net-like to skeleton crystal aggregates of pyrite (light gray, almost white), originating from minute fractures and joints within glassy basaltic gangue material (dark gray, almost black). Locally, pyrite is seen as tiny euhedral aggregates. Polished section, $\times 100$.



Fig. 82.
Sample SO 40–152 G.
Pyrite (light gray, almost white), dispersed through the glassy basaltic gangue material (dark gray, partly brightened by internal reflections) and rimming elongated microlites in which it forms inclusions paralleling their long axis. Polished section, $\times 140$.

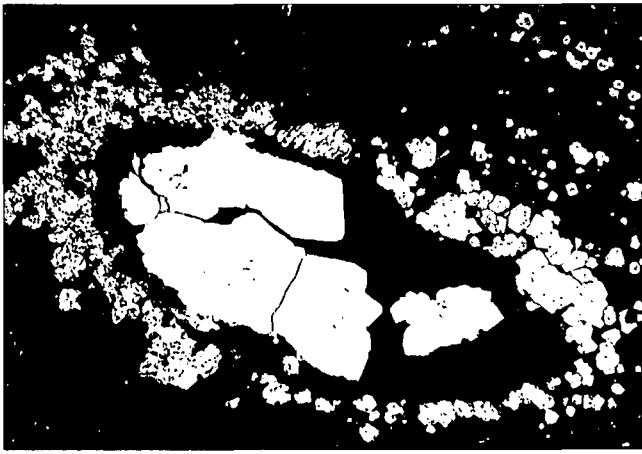


Fig. 83.
Sample SO 40–152 G.
Dendritic, inclusion-rich aggregates of pyrite (light gray, almost white) within the glassy basaltic gangue material (almost black) in transition to partly euhedral aggregates of pyrite poor in or void of inclusions. Polished section, oil immersion, $\times 140$.

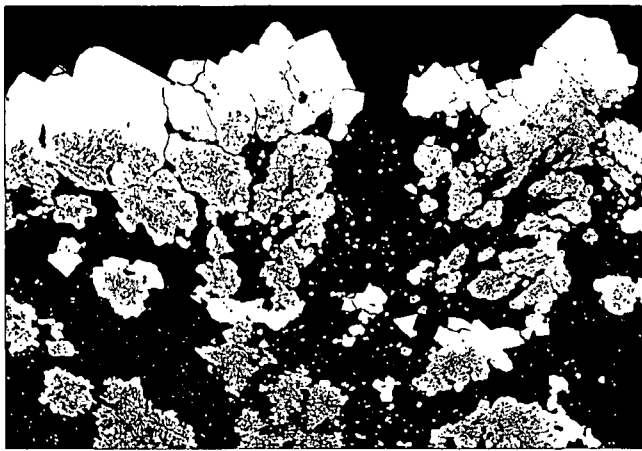


Fig. 84.
Sample SO 40–152 G.
Dendritic feathery-flowery pyrite rich in inclusions, contained within the glassy basaltic gangue material (black). Towards the edges, pyrite is in transition to massive, partly euhedral aggregates of pyrite devoid of inclusions. Locally, fine-grained pyrite is disseminated within the gangue material. Polished section, oil immersion, $\times 140$.

locally present in significant amounts, virtually monomineralic in some areas. At these places, only very subordinate, finely disseminated sulfide minerals (e.g. schalenblende, melnikovite-pyrite, marcasite, pyrite) occur and show the typical colloidal and/or gel textures. Likewise, the opaline silica gangue material (Figs. 12–14, 16, 20–21, 24, 31, 36, 39–42, 44, 48–52, 75–79) displays excellent colloidal and/or gel textures down to the submicroscopic scale. In several fragments, opaline silica locally coats sulfides, mainly sphalerite, wurtzite, and schalenblende. This feature has implications in regard to mineral processing techniques.

4. Mineralized Basalts

At three of the six localities where sulfide fragments were recovered with the TV grab, the samples also contained basaltic rocks (tholeiite). They originate from the ba-

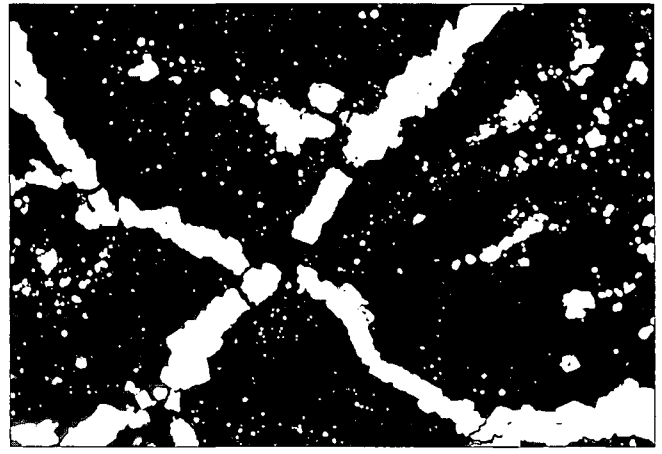


Fig. 85.
Sample SO 40–152 G.
In some zones pyrite (light gray, almost white) is rich in inclusions of the glassy basaltic gangue material (dark gray). Pyrite heals and cements a tight network of fractures and joints ("stockwork") within the glassy basaltic gangue material. In addition, there are finely disseminated aggregates of pyrite within the glassy basaltic gangue material. Locally, traces of sphalerite (medium gray) and chalcocopyrite (likewise light gray, almost white) can be observed. Polished section, $\times 55$.

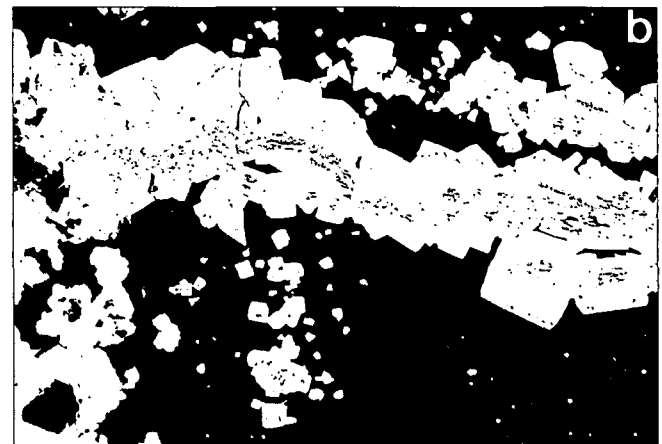
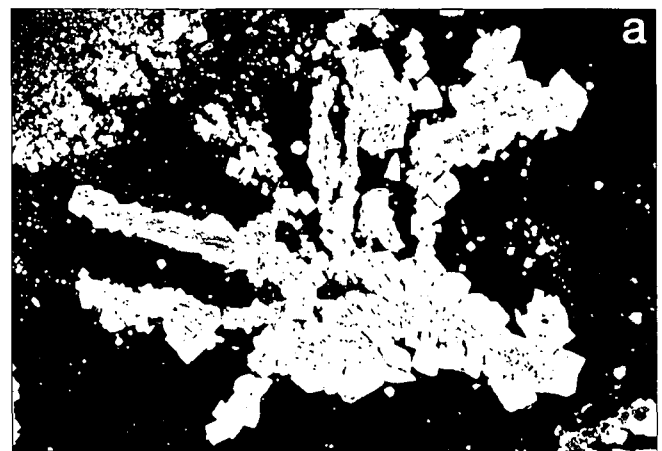


Fig. 86.
Sample SO 40–152 G.
Crystal aggregates of pyrite (light gray, almost white), contained in the glassy basaltic gangue material (black, which itself forms abundant zonal inclusions within pyrite). Locally, chalcocopyrite (light gray) as well as minor sphalerite and wurtzite (both dark gray) occur. Polished sections.
Fig. 86 a: air, $\times 55$,
Fig. 86 b: oil immersion, $\times 140$.

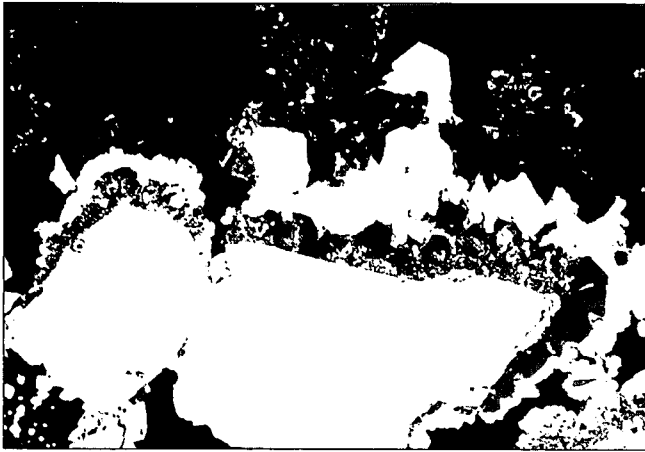


Fig. 87.
Sample SO 40–152 G.
Rhythmic alternation, including coarse-grained chalcopyrite aggregates (light gray) coated by fine-grained pyrite (light gray, almost white) with chalcopyrite, schalenblende (dark gray), and sphalerite (likewise dark gray). The latter three are, in turn, surrounded by coarser grained chalcopyrite, followed by marginal sphalerite, and some pyrite.
Polished section, oil immersion, $\times 55$.

saltic ocean floor on which the black smoker chimneys were precipitated. In two samples (SO 40–149 G, SO 40–152 G) fissures and fractures in the basaltic lava, partly due to chilling, are either filled with sulfides (mainly pyrite) or show traces of sulfides.

More strongly fractured and hydrothermally altered zones are present in SO 40–152 G. This sample includes fragments and small pillows with strong hydrothermal alteration along their margins and exhibits various alteration stages of glass. In contrast, their centers comprise relatively fresh, apparently isotropic glass (“sideromelane”). Locally, the margin of SO 40–152 G contains pyrite (Figs. 80–86) in irregular, net-like, xenomorphic, loose and porous to dendritic and skeleton crystal aggregates. In some zones these are rich in gangue material inclusions.

As a result of its young age and late crystallization the habit of pyrite (Figs. 80–86) is obviously controlled by the preexisting interstices of the glassy matrix and the em-

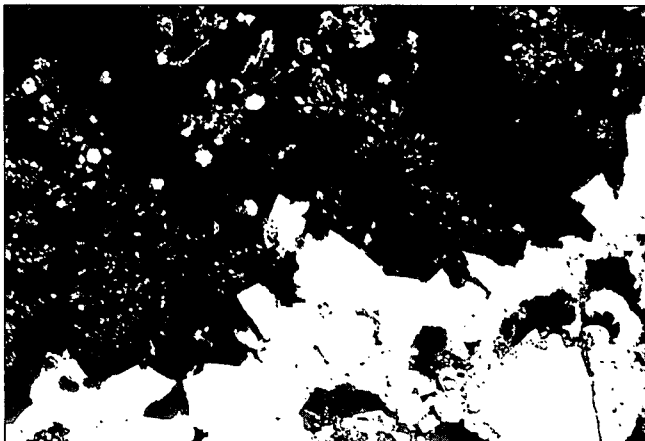


Fig. 88.
Sample SO 40–152 G.
Rhythmic sequence including chalcopyrite (light gray, lower right corner of photomicrograph) coated by gangue material (black), schalenblende (dark gray), and pyrite (light gray, almost white) paramorphic after marcasite. These are surrounded by coarser grained chalcopyrite. The latter is rimmed by tabular, partly euhedral wurtzite and some sphalerite (both likewise dark gray), both containing tiny inclusions of chalcopyrite.
Polished section, oil immersion, $\times 75$.

bedded microlites, as well as by tiny fissures and fractures. Furthermore, small aggregates of pyrite are finely disseminated in the glassy matrix, rim longish microlites and are intimately intergrown with the latter. Pyrite heals fissures in the glassy matrix, which it penetrates in net-like and dendritic to delicate skeleton aggregates, partially originating from the fissures. Small xenomorphic aggregates of pyrite, rich in matrix inclusions, frequently develop into euhedral pyrite crystals containing zonally arranged, locally abundant gangue material inclusions (Figs. 83–86).

The more strongly fractured and brecciated fragments of the sample were subject to more intense hydrothermal alteration. Alteration minerals include montmorillonite, nontronite, and beidellite. These are also found in SO 40–153 G.

Basaltic lava clasts, partially subject to strong hydrothermal alteration, are cemented by sulfide, which thereby forms a “matrix” around them. The network sulfides (“stockwork mineralization”, “network mineralization”) which penetrate and cement the basaltic lava fragments are altogether comparable with the paragenesis of complex massive sulfides in sample SO 40–152 G. Pyrite, melnikovite-pyrite, marcasite, sphalerite, wurtzite (occasionally in very small crystals), schalenblende, chalcopyrite, accessory covellite, and its “permanent blue” variety are similarly present. Sulfides of the non-ferrous metals normally occur in instances where network and veins are not too delicately developed. Again, the typical colloidal and/or gel textures, such as characteristic rhythmic alternations and successions (Figs. 87–88), are frequently observed. Preponderantly pyrite is often disseminated in basaltic lava clasts. In the delicate network penetrating the basalt (“stockwork mineralization”, “network mineralization”) and in the basaltic lava itself, pyrite is repeatedly encountered in typical crystal aggregates (Figs. 85–86) containing zones rich in gangue material. In turn, the sulfides are locally rimmed by opaline silica.

Certain textural differences between the basalt-hosted mineralization and the black smoker sulfide formation, both derived from the same hydrothermal solution, are merely due to differences in the emplacement and/or crystallization of sulfide ores. Crystallization takes place either still in the basalt, providing a “rigid matrix”, or directly in the seawater above the ocean floor.

Limonite, which locally replaces the sulfides of the mineralized basalt samples, arises from incipient submarine weathering (halmyrolysis).

The primary ore content of the basalt has to be clearly distinguished from the younger hydrothermal sulfide mineralization. Primary minerals are preserved in fresh, glassy basaltic lava and consist of small amounts of extremely delicate skeleton crystals of magnetite and traces of sulfides (e.g. pyrite, pyrrhotite, chalcopyrite).

5. Process Mineralogical Aspects

The detailed ore microscopic study of portions from the black smokers not only reveal important information on their paragenesis and formation, but also constitute critical parameters for beneficiation and metallurgical treatment.

The strongly fluctuating sulfide mineral contents observed in six samples showed that for any quantitative assessment (even of a single ore body) the utmost care will

be required during sampling and sample preparation (e.g. blending of representative ore types) in order to establish true average ore grades. The presently available sample material is inadequate for quantitative assessments because of the erratic sampling procedures.

The individual intergrowth features with colloidal textures, high porosity, replacements, complex and intimate intergrowth, fine disseminations of sulfides, large amounts of gangue material/sulfide inclusions, coatings of opaline silica and partially oxidized sulfides, represent important process mineralogical parameters.

The intergrowths indicate that a fine grind will be required for selective or bulk flotation. The vast amounts of gangue material inclusions in sulfides may make it difficult to prepare high-grade Cu and Zn concentrates under economic conditions. Tarnished or partially oxidized sulfides may require Na_2S treatment prior to flotation. Soluble copper in the pulp and collector adsorption on sphalerite, wurtzite or schalenblende may hamper selectivity. Additional problems are anticipated due to the presence of iron-rich zinc sulfides (marmatite/cristophite).

The most frequent sulfides – pyrite, melnikovite-pyrite, marcasite, sphalerite, wurtzite, schalenblende and chalcopyrite – occur with a large range of particle sizes.

It is likely that good Cu and Zn recoveries can only be achieved through a fine grind (70 % <37 microns). Slimy fines formed from fine grinding will be detrimental to the flotation of coarser particles. Primarily iron sulfides, such as melnikovite-pyrite, may cause the formation of -10 micron slimes, which are known to cause selectivity problems in conventional flotation.

Screen analyses were performed to determine the metal distribution as a function of particle size. The preliminary results indicate that the metal concentrations increase in the fine particle sizes (<37 microns).

The continuous mineralogical control of gangue minerals during process testwork is recommended. The presence of clay minerals, limonitic oxidation products and X-ray amorphous opaline silica could explain why substantial sulfide concentrations are carried into the slime fractions. Increased amounts of gangue minerals should be recognized during early examination of feed material prior to the metallurgical testwork.

High amounts of limonite could increase the amounts of iron oxides/hydroxides in the final stages of flotation, which would result in high iron contents in the non-ferrous metal concentrates.

Several trace elements in the black smokers, especially As, but also Co, Ni, and Cd, could be responsible for penalties or loss of metal values. The occurrence of trace elements requires periodic analytical and mineralogical characterization.

In the complex sulfide ores, zinc sulfide is the major mineralogical residence of silver. In addition, the chalcopyrite contains silver values. Since the majority of the silver occurs in the ZnS and will therefore be collected in the Zn concentrate, losses could be encountered during the sale of such a product. During further metallurgical treatment of the Zn flotation concentrates by conventional pyrometallurgical processes such as smelting, it is possible that silver concentrations will not be credited, depending on the type of smelter. Should the Zn concentrates be processed by hydrometallurgical methods, it can be anticipated that the silver values will be credited.

For continued evaluation of the metallurgical treatment options for the black smoker/complex massive sulfide

ores, the following recommendations are made based on the recent mineralogical studies:

- The process mineralogical work should be continued concurrently with the metallurgical work.
- Any meaningful studies of these ores require large amounts of sample material and a more representative sampling program, even in the case of a single black smoker.
- Although the grain sizes observed, intergrowths, and surface characteristics of the sulfides rule out strictly conventional physical separation methods, it is recommended that the applicability of gravity separation and magnetic separation of light gangue material and rock fragments from sulfide minerals on a laboratory scale be further evaluated.
- A selective and collective flotation of the complex massive sulfide ores should be tested. Particularly the impact of slimy fines with regard to the flotation response of the value minerals occurring in the coarser sizes should be studied.
- All flotation products should be examined by ore microscopic and other mineralogical methods.
- It is recommended to investigate the production of bulk flotation concentrates with subsequent hydro/pyrometallurgical treatment. Furthermore, the feasibility of bacterial leaching should be tested.

6. Conclusions and Future Prospects

Fragments of the six black smoker samples under consideration are notable for their complex sulfide ore paragenesis. The main constituents – pyrite, melnikovite-pyrite, marcasite, sphalerite, wurtzite, schalenblende, chalcopyrite, and the gangue material (e.g. opaline silica), as well as hematite in one sample (SO 40–153 G) – display considerable differences in their relative proportions, partially owing to zoning. Consequently, the amounts of the main components (iron, copper, zinc, silica) vary widely.

The paucity of galena and other lead minerals is striking. Locally, galena was recorded from only one sample (SO 40–199 G), in which it is a typical accessory constituent and in places associated with a lead sulfosalt, probably jordanite. The very minor amount of galena in the black smoker fragments is simply a reflection of the low lead concentrations in the basaltic oceanic crust, representing the source rock that was leached by hydrothermal solutions.

In high-grade zinc ore, concentrations of 0.036 % – 0.176 % Pb with a maximum of 0.405 % Pb were obtained, while high-grade copper ores, rich in chalcopyrite, yielded 0.01 % – 0.019 % Pb.

Furthermore, the occurrence of the high-temperature sulfide chalcopyrrhotite as a typical constituent in all six samples is characteristic. Its presence indicates high crystallization temperatures of the black smoker chimneys and correspondingly high temperatures of the venting hydrothermal fluids. Chalcopyrrhotite shows a complete solid solution series with chalcopyrite above approximately 350°C. Below this temperature, exsolution in chalcopyrite and another chalcopyrrhotite solid solution occurs. The composition of the latter relates to temperature. Chalcopyrrhotite in the present samples can be described approximately by the chemical formula CuFe_2S_3 .

Even higher temperatures (above 550°C) are required for the formation of high-temperature chalcopyrite, identified in two samples (SO 40–153 G, SO 40–182 G).

As soon as high-temperature hydrothermal solutions extrude, they are chilled by seawater (temperature approximately 2°C). Diverse fauna, organized in a typical deep-sea association (vent communities), make use of the rich nutrient supply in the immediate vicinity of hydrothermal vents, including high-temperature hydrothermal solutions. Evidence for this is given by the six black smoker fragments by numerous tubes of polychaetes embedded in ore. The conclusions of V. MARCHIG & H. GUNDLACH (1987a, 1987b) that organisms such as crabs and fish living close to hydrothermal outlets are evidence for a low temperature of the venting solutions are inconsistent with the results of this study.

To a considerable degree sulfide minerals in the black smoker samples show intimate intergrowths, are rich in inclusions, and frequently display complex sequences to rhythmic alternations in which opaline silica gangue material is locally incorporated.

Another extremely characteristic feature of the paragenesis is the very abundant, excellent colloidal and/or gel textures. This type of intergrowth is generally attributed to low formation temperatures (e.g. P. RAMDOHR, 1975, 1981).

The presence of the high-temperature sulfide chalcopyrrhotite in the rhythmic precipitates and colloidal masses is of outstanding importance in this context. Its occurrence points to the existence of non-equilibrium conditions of mineralization and telescoping. The existence of non-equilibrium conditions of formation is corroborated by strongly variable iron contents in adjacent grains of sphalerite and within layers of schalenblende.

Studies by V. MARCHIG (1991) and V. MARCHIG & H. RÖSCH (1987) did not recognize all these facts and instead have erroneously distinguished between a "hot" formation (chalcopyrite, pyrite, hematite) rich in copper and a "cold" formation (sphalerite, marcasite) rich in zinc and iron. These far-reaching misinterpretations are primarily based on statistical correlations of chemical analyses and mineralogical studies by X-ray powder diffraction analysis, not realizing that because of the highly heterogeneous composition of the black smokers (e.g. zoning) and the telescoping of different mineralization sequences these chemical analyses can only furnish average values. While such values may be very useful for material balance, they are altogether unsuitable for genetic clarification. In particular, it is not possible to derive crystallization sequences from such data. Furthermore, it is just with such examinations and analyses that detailed and sample-specific ore microscopic examinations cannot be replaced by X-ray powder diffraction analyses – which are totally unsuited for this specific purpose.

Zoning of complex massive sulfide chimneys defines strong variations in the mineralogical and, hence, the chemical composition. This gives evidence for temporal differences in the chemistry of hydrothermal solutions, while precipitating and penetrating through the black smokers. This is supported by the observation of rhythmically layered sulfide minerals of different chemistry and very complex rhythmic alternations and successions of various different sulfide minerals. Even within rhythmic masses of schalenblende extreme variations in the iron content are encountered in neighboring or sequential layers. Further evidence of chemical variation is provided by extended "crystallization waves", mainly of chalcopyrite, which infiltrate and partially replace pre-existing sulfide minerals.

There is a direct link between the formation of black smoker chimneys on the ocean floor and sulfide mineralizations in the underlying basaltic lava. As indicated by the basaltic lava samples, the wall rocks are disintegrated and fractured. Locally they have been strongly altered by the penetration of hydrothermal solutions, whereby alteration minerals such as chlorite have been formed. This too is not particularly astonishing to the economic geologist, nor is the observation that hydrothermal solutions deposit sulfides when forcing their way through the fractured basaltic lava. To denote these ore types the purely descriptive old miner's term "stockwork" ("stockwork deposit", "network deposit") is employed.

It is appropriate here to consider whether recent ophiolites may be observed on the ocean floor as described by V. MARCHIG & H. GUNDLACH (1987 a, 1987 b). First of all, the term "ophiolite" is well defined and collectively applies to geologically ancient ("fossil") oceanic crust. It consists of typically basic to ultrabasic rock sequences which, in the light of plate tectonics, are regarded as remnants of regionally metamorphosed, former – and therefore geologically ancient – oceanic crust which is transposed onto a continent by obduction during orogenesis (e.g. R.L. BATES & J.A. JACKSON, 1980; R. JUBELT & P. SCHREITER, 1982; L. PFEIFFER et al., 1985; H. RAST, 1980; H. WILLIAMS et al., 1982). Well-known examples of ophiolites occur, among other localities, in the Troodos Mountains on Cyprus and in the Eastern Alps. Hydrothermal alteration of basalt, giving rise to processes such as the formation of chlorite on the East Pacific Rise by hydrothermal solutions producing black smokers and network mineralizations in the underlying wall rocks, does not represent ophiolitization and is by no means related to it. The observation of "a recent ophiolite formation in statu nascendi" by V. MARCHIG & H. GUNDLACH (1987 a, 1987 b) in parts of the oceanic crust of the Pacific and in particular in the central graben of the East Pacific Rise is simply inconsistent with the geological setting and represents a far-reaching misinterpretation. The present day oceanic crust is by no means ophiolite and could only become ophiolite through an orogenesis in the future by obduction of the respective oceanic crust onto a continent.

A comparison with the sulfide mineralization discovered during the previous Geometep 3 Research Cruise (W. TUFAR, H. GUNDLACH & V. MARCHIG, 1984, 1985) along the southern flank of the East Pacific Rise reveals certain similarities. In the present collection of black smoker fragments chalcopyrrhotite is less abundant, forming only a minor constituent. In contrast to the previous material the opaline silica gangue material may be present in significant amounts and may locally be almost monomineralic.

Sulfide samples collected from the Galápagos Rift at 85° 51' W and at 85° 55' W (J. LANGE & U. PROBST, 1986; W. TUFAR, E. TUFAR & J. LANGE, 1986 a, 1986 b, 1986 c) also reveal a number of similarities. These include the huge differences in chemical composition, the similar mineral paragenesis with considerable variations of the main constituents, the mineral zonation patterns, the almost entire lack of galena, zinc sulfide as the main silver bearing mineral, the occurrence of characteristic intergrowths and textures (e.g. colloidal and/or gel textures), the high porosity, and the stockwork sulfide mineralization in the underlying wall rocks. An important difference is the only local and very subordinate occurrence of chalcopyrrhotite along the Galápagos Rift. Consequently, high-temperature hydrothermal vents extruded only locally along

the Galápagos Rift to provide conditions favorable for the crystallization of chalcopyrrotite. In places along the Galápagos Rift, opaline silica gangue material is abundant. Furthermore, other new types of hydrothermal mineralizations from this area are smoker chimneys chiefly composed of manganese hydroxide, of limonite, or of iron-rich montmorillonite (iron-rich "protosmectite", nontronite) with limonite and opaline silica. Mineralizations of this type are so far unknown from the East Pacific Rise.

Furthermore some similarities are also obvious with complex massive sulfide mineralizations from the Manus Spreading Center in the Bismarck Sea (W. TUFAR, 1990; W. TUFAR & H. JULLMANN, 1991). There, the black smoker chimneys are mostly rich in zinc and contain only relatively low concentrations of copper. Very striking is the lack of high-temperature sulfides (e.g. chalcopyrrotite). As is the case at the East Pacific Rise, the zinc-rich chimneys at the Manus Spreading Center often contain substantial traces of silver (25–1036 ppm Ag) and in contrast to the East Pacific Rise in places extremely high traces of gold (maximum of 52.5 ppm Au). Furthermore, the complex massive sulfide mineralizations from the Manus Spreading Center exhibit galena and barite as typical paragenetic constituents.

The materials examined in the massive sulfide ores from the Red Sea (Kebrit Deep) and the Tyrrhenian Sea are distinctly different in composition from the East Pacific Rise complex massive sulfides, which may also be indicative of their genetic differences.

The massive sulfide ores from the Red Sea and the Tyrrhenian Sea are locally characterized by considerable amounts of galena. The ore paragenesis in the Kebrit Deep consists basically of three sulfides (i.e. pyrite, schalenblende, galena), and exhibits occasionally diagenetic effects and typically contains inclusions of microfossils in the ore (foraminiferid tests, diatom frustules).

The Tyrrhenian Sea complex massive sulfide mineralization is characterized by the occurrence of chalcopyrite, enargite, tennantite, and major concentrations of galena, barite, pyrite, melnikovite-pyrite, sphalerite, and schalenblende, all of which show effects of diagenesis. Locally, the ore mud exhibits indications of sedimentary slumping.

Considering the large variations of the three major chemical constituents Fe, Cu and Zn in the black smoker samples examined recently, it is evident that six randomly taken samples in such a large area as the East Pacific Rise do not permit any conclusions regarding the extent and composition of one single sulfide ore body.

Urgently needed is a detailed assessment of a complete black smoker deposit with a thorough statistical sampling to determine the form and extent of a particular deposit, as well as the distribution patterns of the ore minerals/valuable metals. Such a study would improve the confidence level of determinations on the ore potential and, hence, would therefore be of essential economic significance.

In conclusion, modern hydrothermal activity along the East Pacific Rise is most strikingly demonstrated by recent complex massive sulfide deposits (black smokers). These offer a unique opportunity to study the precipitation of sulfides from hydrothermal solutions and the formation of complex massive sulfide ore deposits on the ocean floor, thereby yielding important new knowledge in regard to economic geology and mineral exploration. It is a matter of common interest to determine the economic signifi-

cance of recent complex massive sulfides in the light of the world's future supply of raw materials.

Acknowledgements

I wish to express my sincere thanks to the Bundesminister für Forschung und Technologie (BMFT, Bonn) and the Bundesanstalt für Geowissenschaften und Rohstoffe (Hannover) for their support of this study. My thanks are also due to Dr. W. BAUM (Pittsburgh Mineral & Environmental Technology, Inc., New Brighton, Pennsylvania) for his valuable assistance. The critical review of the English manuscript by Dr. J. McMINN (Siemens AG, Erlangen) and Dr. W. BAUM (Pittsburgh Mineral & Environmental Technology, Inc., New Brighton, Pennsylvania) is kindly appreciated.

References

- BÄCKER, H., LANGE, J. & MARCHIG, V.: Hydrothermal activity and sulphide formation in axial valleys of the East Pacific Rise crest between 18° and 20° S. – *Earth Planet. Sci. Lett.*, **72**, 9–22, Amsterdam 1985.
- BATES, R.L. & JACKSON, J.A.: *Glossary of Geology*. – American Geological Institute, Falls Church, Virginia 1980.
- BISCHOFF, J.L. & DICKSON, F.W.: Seawater-basalt interaction at 200°C and 500 bars: Implication for origin of sea-floor heavy metal deposits and regulation of seawater chemistry. – *Earth Planet. Sci. Lett.*, **25**, 385–397, Amsterdam 1975.
- BISCHOFF, J.L. & ROSENBAUER, R.J.: A note on the geochemistry of seawater in the range 350°C–500°C. – *Geochim. Cosmochim. Acta*, **47**, 139–144, Elmsford, New York 1983.
- BISCHOFF, J.L., ROSENBAUER, R.J., ARUSCAVAGE, P.J., BAEDECKER, P.A. & CROCK, J.G.: Sea-Floor Massive Sulfide Deposits from 21° N, East Pacific Rise; Juan de Fuca Ridge; and Galapagos Rift: Bulk Chemical Composition and Economic Implications. – *Econ. Geol.*, **78**, No. 8, 1711–1720, Lancaster, Pennsylvania 1983.
- BISCHOFF, J.L. & SEYFRIED, W.E.: Hydrothermal chemistry of seawater from 25°C to 350°C. – *Amer. Journ. Sci.*, **278**, 838–860, New Haven 1978.
- CORLISS, J.B.: The origin of metal-bearing submarine hydrothermal solutions. – *Journ. Geophys. Research*, **76**, 8128–8138, Washington 1971.
- CORLISS, J.B., DYMOND, J., GORDON, L.I., EDMOND, J.M., HERZEN, R.P. VON, BALLARD, R.D., GREEN, K., WILLIMAS, D., BAINBRIDGE, A., CRANE, K. & ANDEL, T.H. VAN: Submarine Thermal Springs on the Galápagos Rift. – *Science*, **203**, No. 4385, 1073–1083, Washington 1979.
- EDMOND, J.M., DAMM, K.L. VON, MCDUFF R.E. & MEASURES, C.I.: Chemistry of hot springs on the East Pacific Rise and their effluent dispersal. – *Nature*, **297**, 187–191, London 1982.
- FOUQUET, Y., AUCLAIR, G., CAMBON, P. & ETOUBLEAU, J.: Geological setting and mineralogical and geochemical investigations on sulfide deposits near 13° N on the East Pacific Rise. – *Marine Geology*, **84**, 145–178, Amsterdam 1988.
- FRANCHETEAU, J., NEEDHAM, H.D., CHOUKROUNE, P., JUTEAU, T., SÉGURET, M., BALLARD, R.D., FOX, P.J., NORMARK, W., CARRANZA, A., CORDOBA, D., GUERRERO, J., RANGIN, C., BOUGAULT, H., CAMBON, P. & HEKINIAN, R.: Découverte par submersible de sulfures polymétalliques massifs sur la dorsale du pacifique oriental par 21° N. – *C.R. Acad. Sc. Paris*, **287**, Series D, 1365–1368, Paris 1978.
- FRANCHETEAU, J., NEEDHAM, H.D., CHOUKROUNE, P., JUTEAU, T., SÉGURET, M., BALLARD, R.D., FOX, P.J., NORMARK, W., CARRANZA, A., CORDOBA, D., GUERRERO, J., RANGIN, C., BOUGAULT, H., CAMBON, P. & HEKINIAN, R.: Massive deep-sea sulphide deposits discovered on the East Pacific Rise. – *Nature*, **277**, 523–528, London 1979.

- GOLDFARB, M.S., CONVERSE, D.R., HOLLAND, H.D. & EDMOND, J.M.: The Genesis of Hot Spring Deposits on the East Pacific Rise, 21° N. – *Econ. Geol.*, Monograph 5, 184–197, Lancaster, Pennsylvania 1983.
- GUNDLACH, H., MARCHIG, V. & BÄCKER, H.: Neue Erzfundte im Pazifik, "Geometep 3"–Dritte deutsche Forschungsfahrt zu aktiven Plattenrändern im Pazifik. – *Erzmetall*, **36**, 495–500, Weinheim 1983.
- HAYMON, R.M. & KASTNER, M.: Hot spring deposits on the East Pacific Rise at 21° N: preliminary description of mineralogy and genesis. – *Earth Planet. Sci. Lett.*, **53**, 363–381, Amsterdam 1981.
- HEKINIAN, R., ROSENDAHL, B.R., CRONAN, D.S., DIMITRIEV, Y., FODOR, R.V., GOLL, R.M., HOFFERT, M., HUMPHRIS, S.E., MATTEY, D.P., NATLAND, J., PETERSEN, N., ROGGENTHEN, W., SCHRADER, E.L., SRIVASTAVA, R.K. & WARREN, N.: Hydrothermal deposits and associated basement rocks from the Galapagos Spreading Centre. – *Oceanologica Acta*, **1**, No. 4, 473–482, Paris 1978.
- HEKINIAN, R., FEVRIER, M., BISCHOFF, J.L., PICOT, P. & SHANKS, W.C.: Sulfide Deposits from the East Pacific Rise Near 21° N. – *Science*, **207**, 1433–1444, Washington 1980.
- JUBELT, R. & SCHREITER, P.: Gesteinsbestimmungsbuch. – 7th edition, VEB Deutscher Verlag für Grundstoffindustrie, Leipzig 1982.
- KOSKI, R.A., CLAGUE, D.A. & OUDIN, E.: Mineralogy and chemistry of massive sulfide deposits from the Juan de Fuca Ridge. – *Geol. Soc. Amer. Bull.*, **95**, 930–945, Boulder, Colorado 1984.
- LANGE, J.: Schlußbericht Mineralische Rohstoffe – GEOMETEP 3 – Geothermale Metallogene an divergierenden Plattenrändern des Ost-Pazifik. – Preussag AG Meerestechnik, Schlußbericht Bundesminister für Forschung und Technologie, 1–125, Hannover 1985.
- LANGE, J. & PROBST, U.: Schlußbericht Mineralische Rohstoffe – GARIMAS 1 – Galápagos Rift Massivsulfide. – Preussag AG Meerestechnik, Schlußbericht Bundesminister für Forschung und Technologie, 1–202, Hannover 1986.
- MALAHOFF, A., EMBLEY, R. W., CRONAN, D.S. & SKIRROW, R.: The Geological Setting and Chemistry of Hydrothermal Sulfides and Associated Deposits from the Galapagos Rift at 86° W. – *Marine Mining*, **4**, No. 1, 123–137, New York 1983.
- MARCHIG, V.: 2 Hydrothermale Aktivität am Ostpazifischen Rücken. – *Geol. Jb.*, **D 93**, "Forschungsschiff Sonne – 50 Fahrten im Dienst der geowissenschaftlichen Meeresforschung", Commemorative Volume, 125–140, Hannover 1991.
- MARCHIG, V. & GUNDLACH, H.: Did we observe recent ophiolites on the sea bottom? – *Terra cognita*, **7**, 188, 1987 a.
- MARCHIG, V. & GUNDLACH, H.: Ore Formation at Rapidly Diverging Plate Margins – Results of Cruise GEOMETEP 4. – *BGR Circular* **4**, Hannover 1987 b.
- MARCHIG, V., GUNDLACH, H., HOLLER, G. & WILKE, M.: New discoveries of massive sulfides on the East Pacific Rise. – *Marine Geology*, **84**, 179–190, Amsterdam 1988(a).
- MARCHIG, V. & H. RÖSCH, H.: Massivsulfide aus der Divergenzzone des Ostpazifischen Rückens zwischen 18 und 22 Grad Süd. – In: BUNDESANSTALT FÜR GEOWISSENSCHAFTEN UND ROHSTOFFE HANNOVER – REEDEREIGEMEINSCHAFT FORSCHUNGSSCHIFFFAHRT GMBH BREMEN: Abschlußbericht SO 40 – der 4. Fahrt mit FS Sonne im Rahmen des Geometep-Programms, 361–372, Hannover 1987.
- MARCHIG, V., RÖSCH, H., LALOU, C., BRICHET, E. & OUDIN, E.: Mineralogical zonation and radiochronological Relations in a large sulfide chimney from the East Pacific Rise at 18° 25' S. – *Canadian Mineralogist*, **26**, 541–554, 1988 (b).
- MOTTL, M.J.: Metabasalts, axial hot springs, and the structure of hydrothermal systems at mid-ocean ridges. – *Geol. Soc. Amer. Bull.*, **94**, 161–180, Boulder, Colorado 1983.
- MOTTL, M.J. & HOLLAND, H.D.: Chemical exchange during hydrothermal alteration of basalt by seawater – I. Experimental results for major and minor components of seawater. – *Geochim. Cosmochim. Acta*, **42**, 1103–1115, Elmsford, New York 1978.
- MOTTL, M.J., HOLLAND, H.D. & CORR, R.F.: Chemical exchange during hydrothermal alteration of basalt by seawater – II. Experimental results for Fe, Mn and sulfur species. – *Geochim. Cosmochim. Acta*, **43**, 869–884, Elmsford, New York 1979.
- MOTTL, M.J. & SEYFRIED, W.E.: Sub-seafloor hydrothermal systems: rock-versus seawater-dominated. – In: RONA, P.A. & LOWELL, R.P.: Seafloor Spreading Centers: Hydrothermal Systems. – *Benchmark Papers in Geology*, **56**, 66–82, London 1980, Dowden, Hutchinson and Ross Inc., Stroudsburg, Pennsylvania 1980.
- OUDIN, E.: Hydrothermal Sulfide Deposits of the East Pacific Rise (21° N), Part I: Descriptive Mineralogy. – *Marine Mining*, **4**, No. 1, 39–72, New York 1983.
- PFEIFFER, L., KURZE, M. & MATHÉ, G.: Einführung in die Petrologie. – 2nd edition, Berlin (Akademie-Verlag) 1985.
- RAMDOHR, P.: Die Erzminerale und ihre Verwachsungen. – 4th edition, Akademie-Verlag Berlin 1975.
- RAMDOHR, P.: The ore minerals and their intergrowths. – 2nd edition (International series in earth sciences, 35, editor: D. E. INGERSON), 1–2, Pergamon Press, Oxford, New York, Toronto, Sydney, Paris, Frankfurt 1981.
- RAST, H.: Vulkane und Vulkanismus. – BSB B. G. Teubner Verlagsgesellschaft, Leipzig 1980.
- RENARD, V., HEKINIAN, R., FRANCHETEAU, J., BALLARD, R.D. & BÄCKER, H.: Submersible observations at the axis of the ultrafast-spreading East Pacific Rise (17° 30' to 21° 30' S). – *Earth and Planet. Sci. Letters*, **75**, 339–353, Amsterdam 1985.
- RONA, P.A.: Exploration for Hydrothermal Mineral Deposits at Seafloor Spreading Centers. – *Marine Mining*, **4**, No. 1, 7–38, New York 1983.
- ROSENBAUER, R.J. & BISCHOFF, J.L.: Uptake and transport of heavy metals by heated seawater: A summary of the experimental results. – In: RONA, P.A., BOSTRÖM, K., LAUBIER, L. & SMITH, K.L.: Hydrothermal Processes at Seafloor Spreading Centers. – *NATO Conference Series, Series IV: Marine Sciences*, **12**, 177–197, Plenum Press, New York 1983.
- SEYFRIED, W.E.: Seawater-basalt interaction from 25°–300°C and 1–500 bars: Implications for the origin of submarine metal-bearing hydrothermal solutions and regulation of ocean chemistry. – Doctoral thesis, University of South California, 1977.
- SPIESS, F.N., MACDONALD, K.C., ATTWATER, T., BALLARD, R., CARRANZA, A., CORDOBA, D., COX, C., DIAZ GARCIA, V.M., FRANCHETEAU, J., GUERRERO, J.T., HAWKINS, J., HAYMON, R.M., HESSLER, R., JUTEAU, T., KASTNER, M., LARSON, R., LUYDENDYK, B., MACDOUGALL, J.D., MILLER, S., NORMARK, W.R., ORCUTT, J. & RANGIN, C.: East Pacific Rise: Hot springs and geophysical experiments. – *Science*, **207**, 1421–1433, Washington 1980.
- STYRT, M.M., BRACKMANN, A.J., HOLLAND, H.D., CLARK, B.C., PISUTHA-ARNOND, V., ELDRIDGE, C.S. & OHMOTO, H.: The mineralogy and the isotopic composition of sulfur in hydrothermal sulfide/sulfate deposits on the East Pacific Rise, 21° N latitude. – *Earth Planet. Sci. Lett.*, **53**, 382–390, Amsterdam 1981.
- TUFAR, W.: Lagerstättenkundliche und erzpetrographische Untersuchungen an (sub-) rezenten komplexen massiven Sulfiderzen („Schwarze Raucher“) und sulfiderzhaltigen Proben des Ostpazifischen Rückens: Fahrt „Geometep 4“ – „Sonne 40“, Leg 3 – Schlußbericht. – In: BUNDESANSTALT FÜR GEOWISSENSCHAFTEN UND ROHSTOFFE HANNOVER – REEDEREIGEMEINSCHAFT FORSCHUNGSSCHIFFFAHRT GMBH BREMEN: Abschlußbericht SO 40 – der 4. Fahrt mit FS Sonne im Rahmen des Geometep-Programms, 223–356, Hannover 1987.
- TUFAR, W.: Recent Complex Massive Sulfide Deposits ("Black Smokers") and Hydrothermal Metallogenesis at Actively Spreading Plate Boundaries in the Pacific (East Pacific Rise, Galápagos Rift): Potential Marine Mineral Resources and a

- Future Field of Activity for Deep-sea Mining. – Journal of Engineering, Islamic Republic of Iran, National Center for Scientific Research, **1**, Nr. 4, 219–241, Teheran 1988.
- TUFAR, W.: Recent Complex Massive Sulfide Deposits (“Black Smokers”) and Hydrothermal Metallogenesis at Actively Spreading Plate Boundaries in the Pacific (East Pacific Rise, Galápagos Rift): Potential Marine Mineral Resources and a Future Field of Activity for Deep-sea Mining. – Second Mining Symposium Iran, Kerman 1988, Ministry of Mines and Metals, University of Teheran, **3**, Proceedings, 1–47, Teheran 1989.
- TUFAR, W.: Modern Hydrothermal Activity, Formation of Complex Massive Sulfide Deposits and Associated Vent Communities in the Manus Back-Arc Basin (Bismarck Sea, Papua New Guinea). – Mitt. österr. geol. Ges., **82**, 1989, 183–210, Vienna 1990.
- TUFAR, W.: Hydrothermale Aktivität auf dem Meeresboden – 3 Ostpazifischer Rücken, Galápagos-Rift, Rotes Meer, Tyrrhenisches Meer. – Geol. Jb., **D 93**, „Forschungsschiff Sonne – 50 Fahrten im Dienst der geowissenschaftlichen Meeresforschung“. – Commemorative Volume, 140–153, 169–193, Hannover 1991.
- TUFAR, W., GUNDLACH, H. & MARCHIG, V.: Zur Erzparagenese rezenter Sulfid-Vorkommen aus dem südlichen Pazifik. – Mitt. österr. geol. Ges., **77**, 1984, 185–245, Vienna 1984.
- TUFAR, W., GUNDLACH, H. & MARCHIG, V.: Ore Paragenesis of Recent Sulfide Formations from the East Pacific Rise. – Monograph Series on Mineral Deposits, **25**, H.-J. Schneider-Commemorative Volume (editor: K. GERMAN), 75–93, Berlin – Stuttgart 1985.
- TUFAR, W. & JULLMANN, H.: Mit OLGA in den “Wienerwald” – Geowissenschaftliches Großprojekt zur Untersuchung von Lagerstätten in den Ozeanen. – Spiegel der Forschung, **8**, No. 1, 39–45, Gießen 1991.
- TUFAR, W., TUFAR, E. & LANGE, J.: Zur Paragenese von rezenten Hydrothermalprodukten an der Cocos-Nazca-Plattengrenze bei 85° 50' W: Komplexe massive Sulfiderze („Schwarze Raucher“), Basaltvererzungen und -Alterationen, postgenetische Veränderungen. – In: LANGE, J. & PROBST, U.: Schlußbericht Mineralische Rohstoffe–GARIMAS 1–Galápagos Rift Massiv-sulfide. – Preussag AG Meerestechnik, Schlußbericht Bundesminister für Forschung und Technologie, 1–34, Hannover 1986 a.
- TUFAR, W., TUFAR, E. & LANGE, J.: Relationships between Recent Hydrothermal Metallogenesis (“Black Smokers”) and Deep-sea Organisms in the Pacific (East Pacific Rise, Galápagos Rift). – Biology and Geology of Coral Reefs, Annual Meeting of the International Society for Reef Studies, **52**, Marburg 1986 b.
- TUFAR, W., TUFAR, E. & LANGE, J.: Ore paragenesis of recent hydrothermal deposits at the Cocos-Nazca plate boundary (Galápagos Rift) at 85° 51' and 85° 55' W: complex massive sulfide mineralizations, non-sulfidic mineralizations and mineralized basalts. – Geol. Rdsch. **75**, No. 3, Hans Cloos-Commemorative Volume, 829–861, Stuttgart 1986 c.
- WILLIAMS, H., TURNER, F. & GILBERT, C.: Petrography – An Introduction to the Study of Rocks in Thin Sections. – 2nd edition, W. H. Freeman and Company, San Francisco 1982.
- ZIERENBERG, R.A., SHANKS III, W.C. & BISCHOFF, J.L.: Massive sulfide deposits at 21° N, East Pacific Rise: Chemical composition, stable isotopes, and phase equilibria. – Geol. Soc. Amer. Bull., **95**, 922–929, Colorado 1984.

Manuscript submitted October 14th, 1992
Accepted October 14th, 1992

ZOBODAT - www.zobodat.at

Zoologisch-Botanische Datenbank/Zoological-Botanical Database

Digitale Literatur/Digital Literature

Zeitschrift/Journal: [Archiv für Lagerstättenforschung der Geologischen Bundesanstalt](#)

Jahr/Year: 1993

Band/Volume: [16](#)

Autor(en)/Author(s): Tufar Werner

Artikel/Article: [Recent Complex Massive Sulfide Mineralizations \(Black Smokers\) from the Southern Part of the East Pacific Rise 109-145](#)